Investigation of Linear and Nonlinear Torsional Guided Waves in Hollow Circular Cylinders for Damage Detection

By

Carman Yeung

Thesis submitted for the degree of

Doctor of Philosophy

The University of Adelaide

School of Civil, Environmental and Mining Engineering

Faculty of Engineering, Computer and Mathematical Sciences

September 2020

Abstract

Non-destructive testing plays an important role in structural health monitoring. One of the promising options is the use of guided wave for damage detection in engineering applications, such as pipeline and truss system. Common types of damage in the structures include cracks and corrosion. Guided wave is sensitive to cracks up to micro scale. Long range inspection is the other benefit of using guided wave. The overall aim of this thesis is to present a systematic investigation of guided wave in pipe-like structures to gain physical insights into linear and nonlinear features associated with torsional guided wave interaction with damage.

This thesis includes a number of published and prepared journal papers under the same topic. The overview of linear and nonlinear guided wave, and guided wave mixing is introduced in Chapter 1. A computational model using one-dimensional time-domain spectral finite element with cracked element is presented in Chapter 2. This chapter mainly focuses on linear features of guided wave, such as scattering and mode conversion phenomena. The results show that the proposed cracked model has good agreement between the experimental results and three-dimensional (3D) finite element (FE) simulations.

Nonlinear guided wave is highly sensitive to early stage of micro cracks. Material nonlinearity is one of the nonlinear phenomena in the presence of the micro cracks. It can induce higher-order harmonics of guided wave. Guided wave mixing is the advanced version of nonlinear guided wave since the generation of combinational harmonics at sum and difference frequencies can minimise the effect due to the nonlinearity generated by equipment. Chapter 3 analyses the nonlinear characteristics of two interacting fundamental torsional guided wave modes numerically and experimentally.

Chapter 4 and Chapter 5 are the extension parts based on the work in Chapter 3 since pipe-like structures are commonly used in many circumstances, for example embedded pipes and pre-stressed hollow structures. Comprehensive studies in this thesis can gain more understanding for the real applications. In Chapter 4, a 3D FE embedded pipe model with the implementation of nonlinear strain energy function is established to simulate the energy leakage of guided wave propagation due to the existence of soil media. The use of 3D laser scanning system receives guided wave signals from the surface of the pipe for verification. Both numerical and experimental results indicate a significant decline in the interested harmonics at mixed frequency and single frequency. On the other hand, acoustoelastic effect is studied in Chapter 5. A series of case studies are carried out to observe the group velocity change with respect to different levels of loading. The nonlinear features, such as combinational harmonics and second harmonics, are also investigated numerically and experimentally.

Declaration

I, Carman Yeung, certify that this work contains no material which has been accepted for the award of any other degree or diploma in my name, in any university or other tertiary institution and, to the best of my knowledge and belief, contains no material previously published or written by another person, except where due reference has been made in the text. In addition, I certify that no part of this work will, in the future, be used in a submission in my name, for any other degree or diploma in any university or other tertiary institution without the prior approval of the University of Adelaide and where applicable, any partner institution responsible for the joint-award of this degree.

I acknowledge that copyright of published works contained within this thesis resides with the copyright holder(s) of those works.

I also give permission for the digital version of my thesis to be made available on the web, via the University's digital research repository, the Library Search and also through web search engines, unless permission has been granted by the University to restrict access for a period of time.

I acknowledge the support I have received for my research through the provision of Hong Kong Scholarship for Excellence Scheme and Divisional Scholarship provided by the University of Adelaide.

Signature: _____ Date: 30 September 2020

List of Publications

The following directory presents a list of published and prepared journal and conference papers authored by the candidate.

Journal papers in the main research included in this thesis

1. **Yeung, C.**, & Ng, C. T. (2019). Time-domain spectral finite element method for analysis of torsional guided waves scattering and mode conversion by cracks in pipes. *Mechanical Systems and Signal Processing*, *128*, 305-317.
2. **Yeung, C.**, & Ng, C. T. (2020). Nonlinear guided wave mixing in pipes for detection of material nonlinearity. *Journal of Sound and Vibration*, 115541.
3. **Yeung, C.**, Ng, C. T. & He, Y. (2020). Investigation of nonlinear features of torsional guided wave mixing in pipes embedded in soils. (under preparation)
4. **Yeung, C.**, & Ng, C. T. (2020). Torsional guided wave mixing with acoustoelastic effect in tubular structures with weakly material nonlinearity. (under preparation)

Relevant journal and conference papers in the main research topic excluded in this thesis

1. **Yeung, C.**, & Ng, C. T. (2019). Analysis of scattering and mode conversion of torsional guided waves by cracks in pipes using time-domain spectral element method. In *16th East Asia-Pacific Conference on Structural Engineering & Construction*. Brisbane, Australia.
2. He, S., Ng, C. T & **Yeung, C**. (2020). Time-domain spectral finite element method for modelling second harmonics generation of guided waves induced by material, geometric and contact nonlinearities in beams. *Journal of Structural Dynamics and Stability*. https://doi.org/10.1142/S0219455420420055

Acknowledgements

PhD study is undeniably one of the milestones in my life. Support and encouragement from others are crucial. I am grateful to be supervised by A/Prof Alex Ching-Tai Ng. His mentorship guided me to explore the new territories in the field of civil and structural engineering. He has been encouraging me to think independently when I came across with difficulties. I would also like to thank for the support given by my co-supervisor Dr Paul Heung-Fai Lam.

I would like to acknowledge the laboratory support from my technicians in the Faculty of Engineering, Computer and Mathematical Science. My research basically links with experiments which I knew nothing at the beginning. They taught me a lot of things and we became friends afterwards.

Life does not always work out as we think, especially when we experience obstacles which affect our emotions. I am glad that I have a group of friends to be companied with. Some of them are under the same department and some are the members in the Civil Engineering Postgraduate Liaison Committee. I would like to say thank you to them as they went through my ups and downs. I always make a joke on the word PhD so called as “permanent head damage”. When I felt powerless and frustrated, their encouragement rescued me from the hard time in my PhD. Finally, I would also like to show my heartfelt appreciation to my family.

Table of Contents

List of Figures

List of Tables

Chapter 1

Introduction

1.1 Background knowledge

Cylindrical structures have many applications in our daily life, such as underground pipelines and hollow sections in truss systems. It is necessary to carry out damage detection for this type of structure. Assigning workers for inspection is the easiest way, yet restrictions usually emerge during the interrogation. Thus, structural health monitoring (SHM) has been widely used for damage diagnosis in different engineering fields. This is a process to identify damage due to material and geometric changes in structures. The damage include cracks, composite delamination and corrosion, etc [1]-[4]. SHM can constantly update the performance of in-service structures and ensure their integrity [5]. It is also used as a fast screening tool when small flaws are induced by a sudden impact.

Figure 1.1 Release of flammable gas due to the damage of a butane oil pipeline [6]

The importance of SHM has attracted increasing attention in extending the life of existing buildings or structures. There were some catastrophic failure examples in the last decade. In 2012, a gas plant was exploded and caused 26 people dead in Mexico. Rupture of a

butane oil pipeline in 2018 released flammable gas [6], which affected dozens of homes to be evacuated (Figure 1.1). Because of those miseries, it is necessary to advocate the development of efficient and cost-effective damage detection systems in SHM which includes many aspects (Figure 1.2). The major elements of SHM [7] are shown in the chart

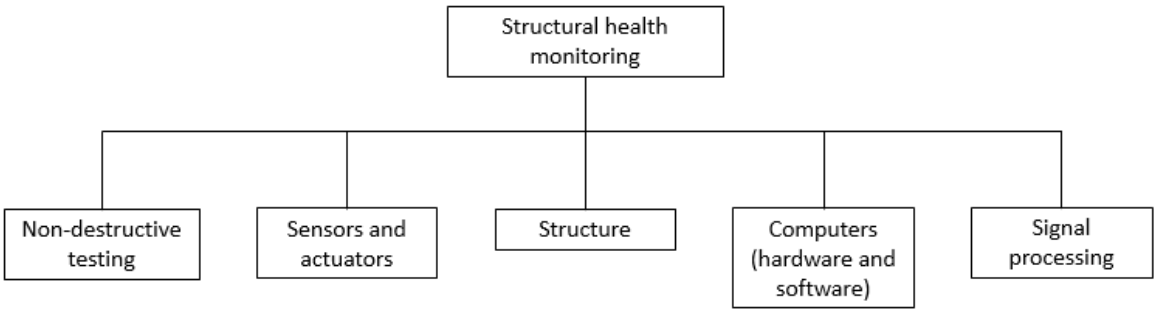

Figure 1.2 Major elements of SHM

Non-destructive testing (NDT) is considered as a method for inspecting and evaluating the severity of a material. In other words, it provides early warnings to failure for different kind of structures, such as pipelines and concrete structures. Different techniques for NDT have been used in the literature [8]-[10]. The existing techniques used in the industry are visual inspection, eddy current and ultrasonic guided wave. Visual inspection simply uses our bare eyes to check the existence of cracks. However, it is impractical to be used in a larger inspection area. Eddy current testing can only apply to electrically conductive materials. On the contrary, the advantage of using guided wave far outweigh the benefits of the other applications.

Guided wave is recognised as a prominent technique for damage detection. It is defined as mechanical stress wave travelling with boundaries in various structures [11], such as plates, bars and pipes. It initially starts with analysing scattered wave in time domain signals, which is named as linear guided waves. From Rayleigh waves [12] along the surface of solids to Lamb waves [13] in plate-like structures, the research on guided waves for damage detection has been

carried out in the last two decades. The investigation has also conducted in pipe-like structures [14] due to its nondispersive feature in the fundamental torsional guided wave. Another attractive advantage is the long propagation distance available in pipe-like structures. It is noted that the utilisation of low frequency (i.e. below 250 kHz) is more preferable in experimental studies since a relatively less wave modes are made from the excitation of torsional guided waves [15].

The generation of higher harmonics has attracted significant research interests in the development of guided wave [16]. It is categorised as nonlinear guided wave as the time domain signals are distorted due to the appearance of micro-cracks. High sensitivity of nonlinear guided wave to microscale cracks provides early warning for structural failure. However, second harmonic generation from material nonlinearity can possibility be contaminated by transmitting or receiving systems, such as amplifiers and transducers [17].

As compared with nonlinear guided wave, guided wave mixing technique is more attractive since it can eliminate undesired harmonics from the equipment. It is because mixing two guided waves can generate combinational harmonics at sum and difference frequencies, which are purely from material nonlinearity itself. Therefore, even without analysing the second harmonics generated by a material, the combinational harmonics can be used to detect small damages. In the literature, wave mixing has been studied for different structures, such as polymers [18], concrete structures [19] and plates [20]. However, the use of torsional guided wave mixing in pipes has not been fully discussed and investigated.

The study of combinational harmonic generation is extensive, which can be employed in different situations. Guided wave experiences tremendous energy leakage when it propagates in embedded pipes [21]. Such effect weakens the strength of the received time domain signals and thus damage information cannot be obviously observed. On the other hand, mechanical

stress and thermally-induced stress are not preventable which can potentially generate flaws in structures. It causes a phenomenon called acoustoelasticity in guided wave. While the acoustoelastic effect has the influence on the wave speed [22], limited research studied the pre-stress effect on the nonlinear features of guided wave. With the aid of guided wave mixing, micro cracks induced in cylindrical structures can be quantified promisingly.

1.2 Objective and aims of the research

This PhD research comprehensively studies different circumstances in cylindrical structures. It initially focuses on the wave propagation of linear guided waves in pipes, such as wave scattering and mode conversion effect. It then focuses on torsional guided wave mixing to investigate the nonlinear features, combinational harmonic generation, in detail. The following aims help to achieve the objective:

- To propose spectral finite element method (SFEM) to the simulation of linear guided wave propagation in pipes for macro scale damage
- To gain insight into the effect of material nonlinearity experimentally and numerically in nonlinear torsional wave mixing approach for hidden damage
- To develop a FE pipe model assembling with soil for the investigation of nonlinear features of torsional guided waves due to material nonlinearity
- To study the acoustoelastic effect on nonlinear torsional guided wave mixing in cylindrical structures under different levels of loading

1.3 Thesis structure

Chapter 1 gives a general background for SHM and the importance of SHM is highlighted. Different NDT methods are discussed in this chapter. Among those, guided wave techniques

are more preferential for damage identification. The use of linear guided wave, nonlinear guided wave and guided wave mixing are then discussed.

Chapter 2 proposes a one-dimensional time domain SFEM model with cracked element to predict the torsional wave propagation, which deals with visible cracks. In this chapter, the proposed method can accurately and efficiently simulate the scattering and mode conversion effect with the presence of an asymmetric crack in pipes and is validated by experiments.

Chapter 3 investigates the generation of the combinational harmonics at sum and difference frequencies in low frequency range using wave mixing technique in pipes for micro scale damage. The experimentally data measured by a three-dimensional (3D) scanning laser is validated by numerical results from a 3D FE model with the inclusion of strain energy function. Fast Fourier Transform (FFT) is implemented to analyse the frequency response of the combinational harmonics in pipe-like structures and demonstrate the existence of material nonlinearity.

Chapter 4 extends the finding in Chapter 3, which is the effect of material nonlinearity using two interacting guided waves, to the response under a certain soil condition. Pipes, in practice, usually embedded in soil or covered by materials, such as high temperature pipes. An embedded pipe model is developed to gain physical insight into the energy leakage of the guided wave signals due to the partial energy transmission to an external media, e.g. soil. The nonlinear characteristics of the combinational harmonics with the effect of soil are discussed in this chapter.

Chapter 5 is based on the study in Chapter 3 and further investigates the effect of acoustoelasticity in hollow structures, such as members of truss systems. Experiments are conducted to validate the 3D FE model under the pre-stressed condition where the results in terms of nonlinear features are compared with the values obtained from the FE models. A series

of case scenarios using the FE simulations are presented in order to study the effect on material nonlinearity with different pre-stressed loadings.

1.4 References

1. Maalej, M., Ahmed, S. F. U., Kuang, K. S. C., & Paramasivam, P. (2004). Fiber optic sensing for monitoring corrosion-induced damage. *Structural Health Monitoring*, *3*(2), 165-176.
2. Haggag, F. M. (2001). In-Situ Nondestructive Measurements of Key Mechanical Properties of Oil and Gas Pipelines. *ASME-PUBLICATIONS-PVP*, *429*, 99-104.
3. Yeung, C., & Ng, C. T. (2019). Time-domain spectral finite element method for analysis of torsional guided waves scattering and mode conversion by cracks in pipes. *Mechanical Systems and Signal Processing*, *128*, 305-317.
4. Quaegebeur, N., Micheau, P., Masson, P., & Maslouhi, A. (2010). Structural health monitoring strategy for detection of interlaminar delamination in composite plates. *Smart materials and structures*, *19*(8), 085005.
5. Farrar, C. R., & Worden, K. (2007). An introduction to structural health monitoring. *Philosophical Transactions of the Royal Society A: Mathematical, Physical and Engineering Sciences*, *365*(1851), 303-315.
6. MacKinnon, B. (2018 May 9). Irving oil butane leak lasted about 17 hours, board finds. CBC News. Retrieved from https://www.cbc.ca/news/canada/new-brunswick/butane-leak-irving-oil-saint-john-eub-1.4655324
7. Stepinski, T., Uhl, T., & Staszewski, W. (Eds.). (2013). *Advanced structural damage detection: from theory to engineering applications*. John Wiley & Sons.
8. Adams, R. D., & Cawley, P. D. R. D. (1988). A review of defect types and nondestructive testing techniques for composites and bonded joints. *NDT international*, *21*(4), 208-222.
9. Tian, G. Y., & Sophian, A. (2005). Reduction of lift-off effects for pulsed eddy current NDT. *NDT & E International*, *38*(4), 319-324.
10. Ng, C. T., & Veidt, M. (2011). Scattering of the fundamental anti-symmetric Lamb wave at delaminations in composite laminates. *The Journal of the Acoustical Society of America*, *129*(3), 1288-1296.

11. Ostachowicz, W., Kudela, P., Krawczuk, M., & Zak, A. (2011). *Guided waves in structures for SHM: the time-domain spectral element method*. John Wiley & Sons.
12. Rayleigh, L. (1885). On waves propagated along the plane surface of an elastic solid. *Proceedings of the London mathematical Society*, *1*(1), 4-11.
13. Lamb, H. (1917). On waves in an elastic plate. *Proceedings of the Royal Society of London. Series A, Containing papers of a mathematical and physical character*, *93*(648), 114-128.
14. Lowe, M. J., Alleyne, D. N., & Cawley, P. (1998). Defect detection in pipes using guided waves. *Ultrasonics*, *36*(1-5), 147-154.
15. Cawley, P., & Alleyne, D. (1996). The use of Lamb waves for the long range inspection of large structures. *Ultrasonics*, *34*(2-5), 287-290.
16. Soleimanpour, R., Ng, C. T., & Wang, C. H. (2017). Higher harmonic generation of guided waves at delaminations in laminated composite beams. *Structural Health Monitoring*, *16*(4), 400-417.
17. Metya, A. K., Tarafder, S., & Balasubramaniam, K. (2018). Nonlinear Lamb wave mixing for assessing localized deformation during creep. *NDT & E International*, *98*, 89-94.
18. Demčenko, A., Koissin, V., & Korneev, V. A. (2014). Noncollinear wave mixing for measurement of dynamic processes in polymers: Physical ageing in thermoplastics and epoxy cure. *Ultrasonics*, *54*(2), 684-693.
19. McGovern, M. E., Buttlar, W. G., & Reis, H. (2015). Estimation of oxidative ageing in asphalt concrete pavements using non-collinear wave mixing of critically-refracted longitudinal waves. *Insight-Non-Destructive Testing and Condition Monitoring*, *57*(1), 25-34.
20. Cho, H., Hasanian, M., Shan, S., & Lissenden, C. J. (2019). Nonlinear guided wave technique for localized damage detection in plates with surface-bonded sensors to receive Lamb waves generated by shear-horizontal wave mixing. *NDT & E International*, *102*, 35-46.
21. Leinov, E., Lowe, M. J., & Cawley, P. (2016). Ultrasonic isolation of buried pipes. *Journal of Sound and Vibration*, *363*, 225-239.
22. Pau, A., & Lanza di Scalea, F. (2015). Nonlinear guided wave propagation in prestressed plates. *The Journal of the Acoustical Society of America*, *137*(3), 1529-1540

Chapter 2

Time-domain Spectral Finite Element Method for Analysis of Torsional Guided Waves Scattering and Mode Conversion by Cracks in Pipes

(Paper 1, Published)

Carman Yeung and Ching Tai Ng

School of Civil, Environmental and Mining Engineering

The University of Adelaide, SA 5005, Australia

Publication:

Yeung, C., & Ng, C. T. (2019). Time-domain spectral finite element method for analysis of torsional guided waves scattering and mode conversion by cracks in pipes. Mechanical Systems and Signal Processing, 128, 305-317.

Statement of Authorship

Title of Paper	Time-domain spectral finite element method for analysis of torsional guided waves scattering and mode conversion by cracks in pipes
Publication Status	☑ Published ☐ Accepted for Publication ☐ Submitted for Publication ☐ Unpublished and Unsubmitted w ork w ritten in manuscript style
Publication Details	Yeung, C., & Ng, C. T. (2019). Time-domain spectral finite element method for analysis of torsional guided waves scattering and mode conversion by cracks in pipes. Mechanical Systems and Signal Processing, 128, 305-317.

Principal Author

Name of Principal Author (Candidate)	Carman Yeung		
Contribution to the Paper	Undertook literature review, developed and validated numerical models, designed experimental tests, performed data analysis and prepared manuscript		
Overall percentage (%)	80%		
Certification:	This paper reports on original research I conducted during the period of my Higher Degree by Research candidature and is not subject to any obligations or contractual agreements with a third party that would constrain its inclusion in this thesis. I am the primary author of this paper.		
Signature		Date	10 Sep 2020

Co-Author Contributions

By signing the Statement of Authorship, each author certifies that:

i. the candidate's stated contribution to the publication is accurate (as detailed above);

ii. permission is granted for the candidate in include the publication in the thesis; and

iii. the sum of all co-author contributions is equal to 100% less the candidate's stated contribution.

Name of Co-Author	Ching-Tai Ng		
Contribution to the Paper	Supervised development of numerical model, reviewed manuscript and prepared for submission		
Signature		Date	9 Sep 2020

Abstract

This paper presents a computationally efficient time-domain spectral finite element method (SFEM) and a crack model to take into account guided wave propagation, scattering and mode conversion in pipes. The proposed SFEM couples torsional and flexural motions of guided waves. A cracked element is proposed to predict the scattering and mode conversion effect of guided wave interaction with the crack in the pipes. The proposed SFEM and cracked element are verified by 3D finite element and experimental data. The results show that the proposed SFEM is able to predict the torsional guided wave propagation, scattering and mode conversion accurately. A series of numerical and experimental case studies are carried out to investigate the effect of the crack size on the scattering and mode converted guided waves. The findings of the study provide physical insights into the guided wave scattering and mode conversion and further advance the development of damage detection using guided waves.

Keywords: Guided waves, spectral finite element method, scattering, mode conversion, crack, pipe, torsional wave, circular waveguide

2.1 Introduction

Structural health monitoring (SHM) plays an important role in assessing condition of structures in many engineering fields, such as civil, mechanical and, oil and gas industry. Successful applications of SHM could help engineers achieve cost-effective management of infrastructure and avoid catastrophic failure by providing an early detection of defects. This improves the safety and sustainability of the infrastructures. In the last two decades, different damage detection techniques have been developed [1,2], for example, non-destructive evaluation (NDE) techniques, such as conventional ultrasonic techniques, eddy current, infrared thermography, vibration-based techniques [3], and guided wave techniques [4-6].

2.1.1 Damage detection in circular waveguides

Guided waves are elastic waves travelling in solid materials and the wave propagation characteristics depend on the boundary conditions of structures. Based on the wave propagation characteristics, guided waves can be categorized as different types of waves, e.g. shear horizontal wave [7], torsional wave [8], Rayleigh wave [9] and Lamb wave [10], etc. The shear horizontal wave refers to the wave with propagation direction perpendicular to the particle motion. The torsional wave is a shear horizontal wave in pipes with propagation direction aligning with the longitudinal axis [11]. The Rayleigh wave is a type of surface wave and has been commonly used in the literature [12]. The Lamb wave are elastic waves propagating in thin-walled structures, such as plates [13,14]. There are two common types of waveguides, one-dimensional (1D) waveguides, such as beams, rods and pipes [15,16], and two-dimensional (2D) waveguides, such as plates and shells [17-19].

2.1.2 Damage detection in circular waveguides

Pipelines are commonly used in different industrial sectors and pipes are usually treated as circular waveguide in the context of wave propagation. Defects in a pipe are a considerable problem for oil, chemical or other industries [20]. When pitting defects and corrosion appear in the structures, there is higher chance of structural failure. The safety inspection becomes more difficult if external surface of the pipes has a layer of protective material, such as bitumen. For example, if flawed pipelines are buried as underground utilities, this will cause a significant inconvenience to the public. The study of Ahmad *et al.* [21] showed that pipes were frequently embedded in the soil with insulated coatings. Angani *et al*. [22] studied the use of eddy current to inspect the defects in pipelines but the inspection can be carried out in a limited area only. It is impractical to use inspection methods that require direct access to the pipes since the associated cost of removing the insulation is unpredictably high.

Damage detection using torsional guided waves in circular waveguide has been demonstrated that it can provide long-range inspection. Due to the non-dispersive characteristic of the fundamental torsional wave T(0,1), the use of this wave mode has practical significance in structural integrity assessment [23,24]. Løvstad and Cawley [25] proposed to use torsional guided waves to detect defects in pipes. They concluded that the damage inspection can cover ten meters of pipe section and the long-range testing is not affected by the pipe coatings. Eybpoosh *et al*. [26] further investigated the application of guided waves for damage detection of pipelines under varying environmental and operational conditions. The study of circular waveguides can further advance damage detection techniques for the pipes using guided waves.

2.1.3. Numerical method for wave propagation simulations

Different methods for modelling wave propagation phenomena in structures have been developed in the literature. Numerical methods have been used for simulating guided wave

propagation in different types of structures [27]. The finite difference method (FDM) is defined on regular grids, which is efficient for large scale simulations. But it is not capable of handling wave simulation when there are changes in material property and geometry of the structures [28]. The boundary element method (BEM) is capable for modelling small surface/volume ratio. By contrast, it is not computational efficient for modelling large structures [29]. The finite strip element method (FSE) requires a low discretisation level, but it is not suitable to model geometrically complex structures [30]. The finite element method (FEM) is extensively used in modelling complex geometries. However, it is computationally expensive for wave propagation simulations [31,32].

The main difference of the spectral finite element method (SFEM) and FEM is that SFEM uses a higher-order interpolation with specific quadrature formulae [33,34]. Less arithmetic operations can be achieved since the mass matrix is diagonalized by using particular formulations. The computation time can be enhanced when SFEM is applied due to the mass matrix diagonalization. With the use of this higher-order numerical simulation method, the number of degrees of freedom (DoFs) can be minimized significantly [37]. SFEM is capable of simulating wave propagation and has better convergent rate than FEM. The research on SFEM for wave propagation has been conducted since 1984 [35]. Most of the studies in the early stage started by employing Chebyshev–Gauss–Lobatto (CGL) nodes to simulate acoustic waves [36]. Gauss–Lobatto-Legendre (GLL) nodes, which have similar capability of CGL, were then introduced to model elastic waves.

Other higher-order schemes, such as SFEM, p-version of FEM (p-FEM) and isogeometric analysis (IGA) [37-39], have been applied for wave propagation analysis in order to reduce the computational costs. The selection of basis functions is the difference between these three numerical methods. The SFEM uses the Lagrange interpolation polynomials. The normalized integrals of the Legendre polynomials are deployed as the basis functions of the p-

FEM. The IGA employs NURBS-based (Nonuniform Rational B-splines) basis functions. Among these numerical simulation methods, the main advantage of SFEM is the diagonal mass matrix due to the Kronecker delta property of the shape functions and the GLL quadrature.

This paper presents a cracked element to take into account the mode conversion effect of guided waves in pipe using time-domain SFEM. A comprehensive study of guided waves in pipes using time-domain SFEM is conducted and the results are verified by 3D FEM and experimental data. The findings of this study gain physical insights into the guided wave scattering and mode conversion at the crack in pipes and can further advance the development of damage detection methods using guided wave.

The structure of this paper is as follow. Section 2.2 presents the time-domain SFEM and the proposed crack model. The properties and selection of the guided wave mode are discussion in Section 2.3. Section 2.4 presents a comparison of the results between SFEM and 3D FEM. This section validates the proposed cracked model for the time-domain SFEM, and also investigates the scattering and mode conversion effect of guided waves at the crack in pipes. The proposed time-domain SFEM is then validated by experimental data in Section 2.5. Finally, conclusions are drawn in Section 2.6.

2.2 Methodology

2.2.1 Coupling of torsional and flexural motions for circular waveguide

In this study, the time-domain SFEM for a pipe is developed based on the elementary rod theory [40] and Timoshenko beam theory [15]. Figure 2.1 shows a schematic diagram of a pipe element with a crack. Timoshenko beam theory considers the vertical/horizontal direction and the corresponding shear deformation defect. The torsional motion is modelled by the

elementary rod theory based on Saint-Venant principle. The governing equations for coupling torsional and flexural motions of circular waveguide are [41]

$$GJ\frac{\partial^2\theta}{\partial x^2} + F_\theta(x,t) = \rho I_o\ddot{\theta} \tag{2.1}$$

$$K_1^{Tim}GA\frac{\partial}{\partial x}\left(\frac{\partial v}{\partial x} - \varphi\right) = \rho A\ddot{v} - F_V(x,t)$$

$$EI\frac{\partial^2\varphi}{\partial x^2} + K_1^{Tim}GA\left(\frac{\partial v}{\partial x} - \varphi\right) = K_2^{Tim}\rho I\ddot{\varphi} \tag{2.2}$$

where θ is the rotation about x-axis, v is the displacement along y-axis, and φ is the rotation about z-axis (Fig. 2.1). The mass density and cross-section area of the pipe are denoted by ρ and A, respectively. I, J and I_o are the second moment of inertia about z-axis, the polar moment of inertia, and the second moment of inertia about x-axis, respectively. E is Young's modulus and G is shear modulus. The influence of group velocity is controlled by K_1^{Tim} and K_2^{Tim} [42]. The parameters for torsional guided waves are $K_1^{Tim} = 0.28$ and $K_2^{Tim} = 45K_1^{Tim}/\pi^2$. F_θ and F_v represent the function for the external torsional and vertical excitation, respectively.

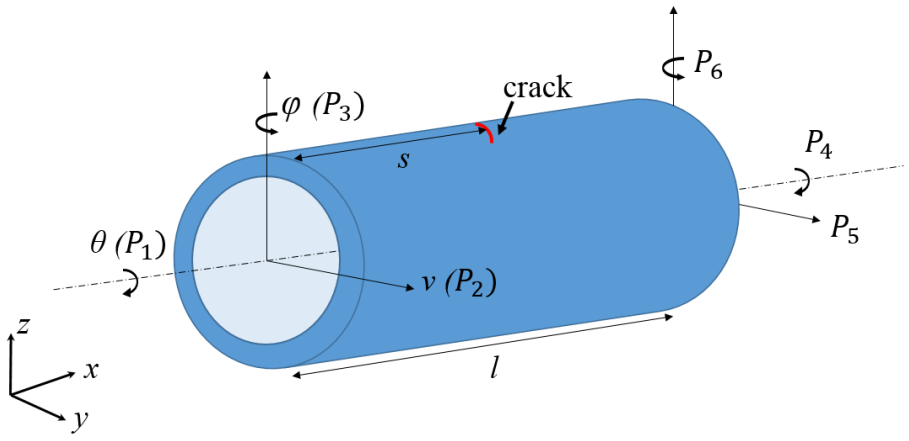

Figure 2.1 Schematic diagram of a pipe with a surface crack

2.2.2. Time-domain spectral finite element method

The wave propagation can be represented by ordinary differential equation [43]

$$\mathbf{M\ddot{u}} + \mathbf{C\dot{u}} + \mathbf{Ku} = \mathbf{F}(t) \tag{2.3}$$

where **M** is the global mass matrix, **C**=η**M** is the global damping matrix with damping parameter η [44,45]. **K** is the global stiffness matrix and **F**(*t*) is the global force vector. **u**, **u̇** and **ü** denote the displacement, velocity and acceleration vector, respectively. The local mass matrix **m**, local stiffness matrix **k**, and local load vector **f** are

$$\mathbf{m} \approx \sum_{i=1}^{n} \mathrm{w_i} \mathbf{N_e}(\xi_\mathrm{i})^{\mathrm{T}} \boldsymbol{\mu} \mathbf{N_e}(\xi_\mathrm{i}) \det(\boldsymbol{J}(\xi_\mathrm{i})) \tag{2.4}$$

$$\mathbf{k} \approx \sum_{i=1}^{n} \mathrm{w_i} \mathbf{B_e}(\xi_\mathrm{i})^{\mathrm{T}} \mathbf{D} \mathbf{B_e}(\xi_\mathrm{i}) \det(\boldsymbol{J}(\xi_\mathrm{i})) \tag{2.5}$$

$$\mathbf{f} \approx \sum_{i=1}^{n} \mathrm{w_i} \mathbf{N_e}(\xi_\mathrm{i})^{\mathrm{T}} \mathbf{f}(\xi_\mathrm{i}) \det(\boldsymbol{J}(\xi_\mathrm{i})) \tag{2.6}$$

where *n* is the node number in the element. $\boldsymbol{J} = \frac{\partial x}{\partial \xi}$ is the Jacobian function used to assign the local coordinate to the global domain. $\mathbf{f}(\xi_\mathrm{i})$ is the external force and ξ_i is the local coordinate of node *i* in the element.

In this study, completed Lobatto polynomial is applied [46]. The derivatives of the Legendre polynomials are the Lobatto polynomials. GLL nodes are used in each element [47]. The nodes are taken as roots of the equation

$$(1-\xi_i^2)L'_{n-1}(\xi_i) = 0 \quad \text{for} \quad \xi_i \in [-1,1] \text{ and } i \in 1,\dots,n \tag{2.7}$$

where L'_{n-1} denotes the first derivative of the (*n*-1)th order Legendre polynomial. The weighting function of the corresponding GLL point ξ_i is

$$w_i = \frac{2}{n(n-1)(L_{n-1}(\xi_i))^2} \tag{2.8}$$

The diagonal form of mass matrix is achieved due to the Kronecker property of the shape function in conjunction with the use of the (p+1)-point GLL integration scheme. Equation (2.3) can be solved by the central difference scheme. The shape function matrix $\mathbf{N_e}$ in equation (2.4) is defined as

$$\mathbf{N_e} = \mathbf{N} \otimes \mathbf{I} \tag{2.9}$$

where $\otimes$ is the Kronecker product, $\mathbf{I}$ is a 3×3 identity matrix, and $\mathbf{N} = [N_1(\xi), \dots, N_n(\xi)]$. The spectral shape function $N_i(\xi)$ for node *i* is defined as

$$N_i(\xi) = \prod_{k=1, k\neq i}^{n} \frac{\xi - \xi_k}{\xi_i - \xi_k} \tag{2.10}$$

In the SFEM, each node consists of three DoFs which are presented in the following matrix

$$\begin{bmatrix} \theta^e \\ v^e \\ \varphi^e \end{bmatrix} = \sum_{i=1}^{n} \begin{bmatrix} N_i(\xi) & 0 & 0 \\ 0 & N_i(\xi) & 0 \\ 0 & 0 & N_i(\xi) \end{bmatrix} \begin{bmatrix} q_\theta^e(\xi_i) \\ q_v^e(\xi_i) \\ q_\varphi^e(\xi_i) \end{bmatrix} \tag{2.11}$$

The strain-displacement operator $\mathbf{B}$ is a 3×3 matrix and is defined as

$$\mathbf{B} = \begin{bmatrix} E_{Tor} & 0 \\ 0 & E_{Tim} \end{bmatrix} \mathbf{N} \tag{2.12}$$

where $E_{Tor} = \left[\frac{1}{J}\frac{\partial}{\partial \xi}\right]$, $E_{Tim} = \begin{bmatrix} \frac{1}{J}\frac{\partial}{\partial \xi} & -1 \\ 0 & \frac{1}{J}\frac{\partial}{\partial \xi} \end{bmatrix}$ (2.13)

E_{Tor} and E_{Tim} are differential operator for elementary rod theory and Timoshenko beam theory, respectively. **D** and **μ** are 3×3 stress-strain matrix and 3×3 mass density matrix, respectively. They are defined as

$$\mathbf{D} = \begin{bmatrix} D_{Tor} & 0 \\ 0 & D_{Tim} \end{bmatrix} \tag{2.14}$$

$$\text{where } D_{Tor} = [GJ] \ , D_{Tim} = \begin{bmatrix} K_1^{Tim} GA & 0 \\ 0 & EI \end{bmatrix} \tag{2.15}$$

$$\boldsymbol{\mu} = \begin{bmatrix} \mu_{Tor} & 0 \\ 0 & \mu_{Tim} \end{bmatrix} \tag{2.16}$$

$$\mu_{Tor} = [\rho I_o], \mu_{Tim} = \begin{bmatrix} \rho A & 0 \\ 0 & K_2^{Tim} \rho I \end{bmatrix} \tag{2.17}$$

2.2.3 Cracked element modelling

This section presents the formulation for the cracked element for pipes in SFEM. The analysis of cracks in circular shape structural elements has been reported in the literature [48,49]. The following derivation of the cracked element is an extension of the work of Darpe *et al*. [50]. Consider a circular waveguide with hollow cross-section at the crack location as shown in Fig. 2. *D* and *d* are outer and inner diameter of the pipe, respectively, and *a* is crack depth.

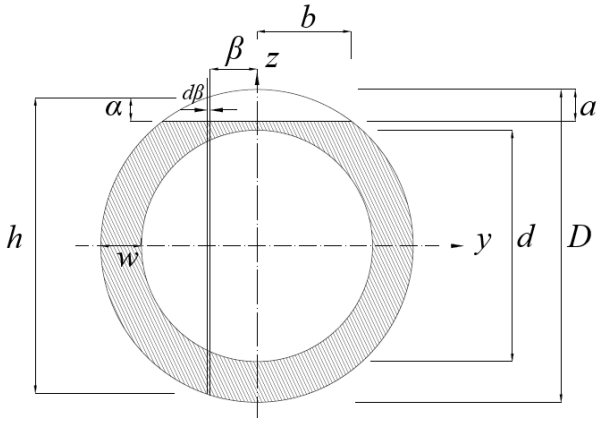

Figure 2.2 Cross-section of circular waveguide at the crack location

The notations h, β and α in Fig. 2.2 are for calculating the flexibility matrix and are used in equation (2.31). h and α in equations (2.18) and (2.19) are linked by D, a and y.

$$h = 2\sqrt{(\frac{D}{2})^2 - y^2} \tag{2.18}$$

$$\alpha = \frac{h}{2} - (\frac{D}{2}) + \mathrm{a} \tag{2.19}$$

The proposed cracked element is a two-node element having three DoFs (θ, v and φ) at each node. Figure 2.3 shows the discretization of a circular waveguide with a two-node cracked element. Due to the existence of crack, the stiffness properties in the cracked element are different to the uncracked element. The modified stiffness matrix takes into account the mode coupling effect. So the guided wave scattering and mode conversion effect can be simulated by the time-domain SFEM.

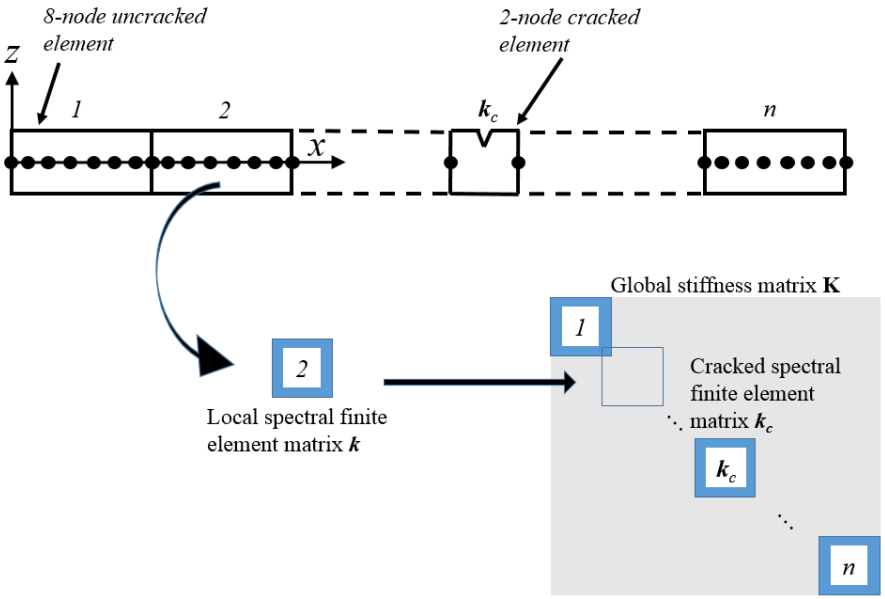

Figure 2.3 Discretization of a circular waveguide with a cracked element and general outline of assembling global stiffness matrix by local stiffness matrices

The modified stiffness matrix can be obtained from the local flexibility matrix since they are interrelated to each other. By using Castingliano's theorem,

$$Q_i = \frac{\partial U}{\partial P_i} \qquad \text{for} \qquad i \in 1,2,3 \tag{2.20}$$

where Q_i and P_i are the displacement and load along the *i*th coordinate at the first node, respectively. P_1, P_2 *and* P_3 are torsional moment, shear force and bending moment, respectively. U is the total strain energy, which can be separated from the strain energy of the uncracked (U^u) and cracked (U^c) elements. Equation (2.20) can be expressed as

$$Q_i = Q_i^u + Q_i^c = \frac{\partial U^u}{\partial P_i} + \frac{\partial U^c}{\partial P_i} \tag{2.21}$$

The strain energy with the uncracked element is written as

$$U^U = \frac{1}{2}\int [\frac{{P_1}^2}{GI_o} + \frac{k{P_2}^2}{GA} + \frac{(sP_2 + P_3)^2}{EI}]\, dx \tag{2.22}$$

where k is the shear coefficient [51]. The individual displacement of the uncracked elements is given by the following expression

$$Q_1^u = \frac{lP_1}{GI_o}$$

$$Q_2^u = \left(\frac{kl}{GA} + \frac{l^3}{3EI}\right)P_2 + \frac{l^2}{2EI}P_3$$

$$Q_3^u = \frac{l}{EI}P_3 + \frac{l^2}{2EI}P_2 \tag{2.23}$$

The strain energy due to crack U^c can be calculated by fracture mechanics, which is defined in the form

$$U^c = \int_A R(A)dA \tag{2.24}$$

where $R(A)$ is the strain energy density function. The function is defined as

$$R(A) = \frac{1}{E}\left[\left(\sum_{i=1}^{3} K_{Ii}\right)^2 + \left(\sum_{i=1}^{3} K_{IIi}\right)^2 + m\left(\sum_{i=1}^{3} K_{IIIi}\right)^2\right] \tag{2.25}$$

where $m = 1 + \upsilon$. υ is the Poisson ratio. K_{Ii}, K_{IIi} and K_{IIIi} are the stress intensity factors (SIF) for opening mode, sliding mode and shearing mode of crack displacement, respectively. The stress intensity factors for different opening modes are

SIF for opening mode,

$$K_{I3} = \frac{(P_3 + sP_2)\beta}{\pi/64(D^4 - d^4)}\sqrt{\pi\alpha}F_1$$

$$K_{I1} = K_{I2} = 0 \tag{2.26}$$

SIF for sliding mode,

$$K_{II1} = \frac{P_1\beta}{\pi/32(D^4 - d^4)}\sqrt{\pi\alpha}F_{II}$$

$$K_{II2} = K_{II3} = 0 \tag{2.27}$$

SIF for shearing mode,

$$K_{III1} = \frac{2P_1h}{\pi/32(D^4 - d^4)}\sqrt{\pi\alpha}F_{III}$$

$$K_{III2} = \frac{P_2k}{\pi\left({}^{D}/_{2}{}^{2} - {}^{d}/_{2}{}^{2}\right)}\sqrt{\pi\alpha}F_{III}$$

$$K_{III3} = 0 \tag{2.28}$$

The calculations of F_1, F_{II} and F_{III} are depicted as

$$F_1 = \sqrt{\frac{2h}{\pi\alpha}\tan\left(\frac{\pi\alpha}{2h}\right)}\,\frac{0.752 + 2.02\left(\frac{\alpha}{h}\right) + 0.37\left[1 - \sin\left(\frac{\pi\alpha}{2h}\right)\right]^3}{\cos\left(\frac{\pi\alpha}{2h}\right)}$$

$$F_{II} = \frac{1.122 - 0.561\left(\frac{\alpha}{h}\right) + 0.085\left(\frac{\alpha}{h}\right)^2 + 0.18\left(\frac{\alpha}{h}\right)^3}{\sqrt{1 - \left(\frac{\alpha}{h}\right)}} \tag{2.29}$$

$$F_{III} = \sqrt{\frac{2h}{\pi\alpha}\tan\left(\frac{\pi\alpha}{2h}\right)}$$

Substitute the equations (2.26)-(2.29) into equations (2.24) and (2.25), Q_i^c is simplified to

$$Q_1^c = \left(I_{g_1} + I_{g_2}\right)P_1 + I_{g_5}P_2$$

$$Q_2^c = I_{g_5}P_1 + s(sP_2 + P_3)I_{g_3} + I_{g_4}P_2$$

$$Q_3^c = (sP_2 + P_3)I_{g_3} \tag{2.30}$$

where I_{g_1}, I_{g_2}, I_{g_3}, I_{g_4} and I_{g_5} in equation (2.30) are defined as

$$I_{g_1} = \int_A \frac{8\alpha\beta^2 {F_{II}}^2}{\pi E\left({D/_2}^4 - {d/_2}^4\right)^2}\,dA \qquad I_{g_4} = \int_A \frac{2mk^2\alpha\left({D/_2}^2 + {d/_2}^2\right)^2 {F_{III}}^2}{\pi E\left({D/_2}^4 - {d/_2}^4\right)^2}\,dA$$

$$I_{g_2} = \int_A \frac{2m\alpha h^2 {F_{III}}^2}{\pi E\left({D/_2}^4 - {d/_2}^4\right)^2}\,dA \qquad I_{g_5} = \int_A \frac{2mk\alpha h\left({D/_2}^2 + {d/_2}^2\right){F_{III}}^2}{\pi E\left({D/_2}^4 - {d/_2}^4\right)^2}\,dA$$

$$I_{g_3} = \int_A \frac{32\alpha\beta^2 {F_1}^2}{\pi E\left({D/_2}^4 - {d/_2}^4\right)^2}\,dA \tag{2.31}$$

By combining equations (2.23) and (2.30), the total displacement Q_i from equation (2.21) can be expressed in a matrix from as

$$[Q_i] = \boldsymbol{G}[P_i] \qquad \text{for} \qquad i \in 1, \ldots, 6 \tag{2.32}$$

The flexibility matrix ***G*** is defined as

$$\boldsymbol{G} = \begin{bmatrix} g_{11} & g_{12} & g_{13} \\ g_{21} & g_{22} & g_{23} \\ g_{31} & g_{32} & g_{33} \end{bmatrix} \tag{2.33}$$

where

$$g_{11} = \frac{l}{GI_o} + I_{g_1} + I_{g_2} \qquad g_{12} = g_{21} = I_{g_5}$$

$$g_{22} = \frac{kl}{GA} + \frac{l^3}{3EI} + I_{g_4} + s^2 I_{g_3} \qquad g_{13} = g_{31} = 0$$

$$g_{33} = \frac{l}{EI} + I_{g_3} \qquad g_{23} = g_{32} = \frac{l^2}{2EI} + s\, I_{g_3}$$

Considering the static equilibrium of the cracked element, the flexibility matrix G can be converted to the stiffness matrix by transformation matrix $\boldsymbol{T}$. The orders of the DoFs in this two-node element are presented by the subscripts q.

$$\{q_i\}^T = \boldsymbol{T}\{q_j\}^T \quad \text{for} \qquad i \in 1,\dots,6 \;\; \& \;\; j \in 1,2,3 \tag{2.34}$$

$$\boldsymbol{T}^T = \begin{bmatrix} 1 & 0 & 0 & -1 & 0 & 0 \\ 0 & 1 & 0 & 0 & -1 & -l \\ 0 & 0 & 1 & 0 & 0 & -1 \end{bmatrix} \tag{2.35}$$

The stiffness matrix for the cracked element can be calculated by flexibility matrix as

$$\boldsymbol{k_c} = \boldsymbol{T}\boldsymbol{G}^{-1}\boldsymbol{T}^T \tag{2.36}$$

It should be noted that the global stiffness matrix **K** in equation (2.3) is assembled by the local uncracked stiffness matrix $\boldsymbol{k}$ and the local cracked stiffness matrix $\boldsymbol{k_c}$. Figure 2.3 illustrates the assembly procedure of how k and kc form K. So the proposed time-domain SFEM can take into account the torsional-flexural coupling effect in modelling the guided waves scattering and mode conversion at the crack on pipes.

2.3 Wave Mode Selection

Dispersion curves are a fundamental indication for the selection of optimal excitation mode and excitation frequency in damage detection. Figure 2.4(a) shows the group velocity dispersion curves of longitudinal, torsional and flexural modes in pipes, which are marked as L(*m*,*n*), T(*m*,*n*) and F(*m*,*n*), respectively. '*m*' and '*n*' are integers, which represent the harmonic order of circumferential variation and a sequential number of modes of each category, respectively [52]. Torsional modes are axially symmetric, while the flexural modes are non-axisymmetric. Most of the wave modes are dispersive, which limits the wave propagation distance. But the fundamental torsional mode T(0,1) is non-dispersive, which is useful for damage detection in pipes. So torsional T(0,1) mode is adopted as incident wave in this study. Figure 2.4(b) indicates the detail view of the dashed red region in Fig. 2.4(a). The group velocity calculated by SFEM and DISPERSE. Red dashed line and blue solid line denote the group velocities of T(0,1) mode and F(1,1) mode from a commercial software DISPERSE [53]. The markers represent the group velocities calculated from the proposed SFEM.

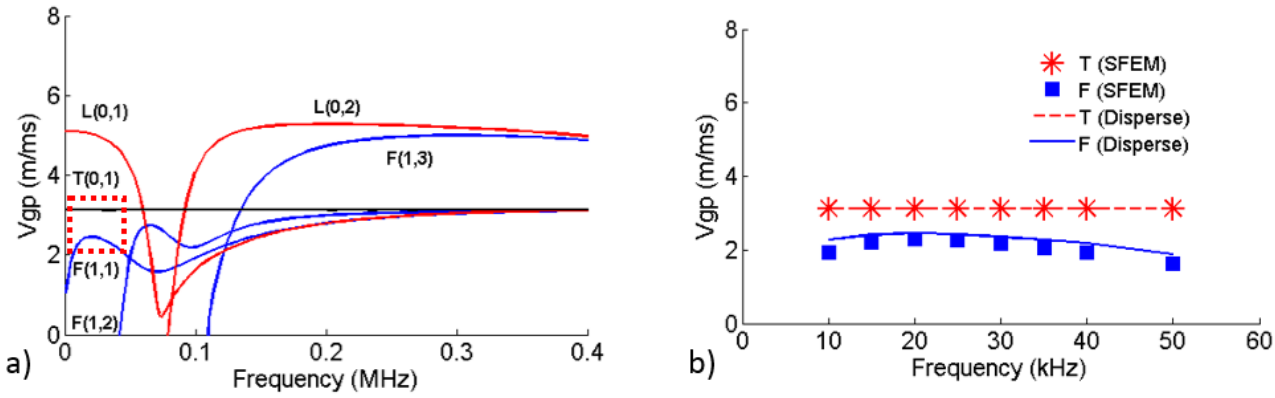

Figure 2.4 (a) Group velocity dispersion curves obtained from DISPERSE and (b) group velocities calculated by the proposed SFEM and DISPERSE

A 1m long aluminium pipe is modelled using the proposed time-domain SFEM method. The density and Poisson's ratio are 2700kg/m^3 and 0.3, respectively. The wall thickness and outer diameter of the pipe are 3mm and 25mm, respectively. A crack is modelled at the middle of the pipe using the proposed cracked element. Polynomial degree (p=7) with 0.01m long spectral elements were used to model the pipe. The central difference method was applied to solve the semi-discrete equation of motion (Eq. 2.3). The time step was 1×10^{-7} s to ensure the solution to be converged. The torsional guided wave T(0,1) was generated by applying nodal rotation about x-axis at the left end of the pipe to generate the torsional guided waves. The excitation signal was a 50kHz 5-cycle sinusoidal tone burst modulated by a Hann window.

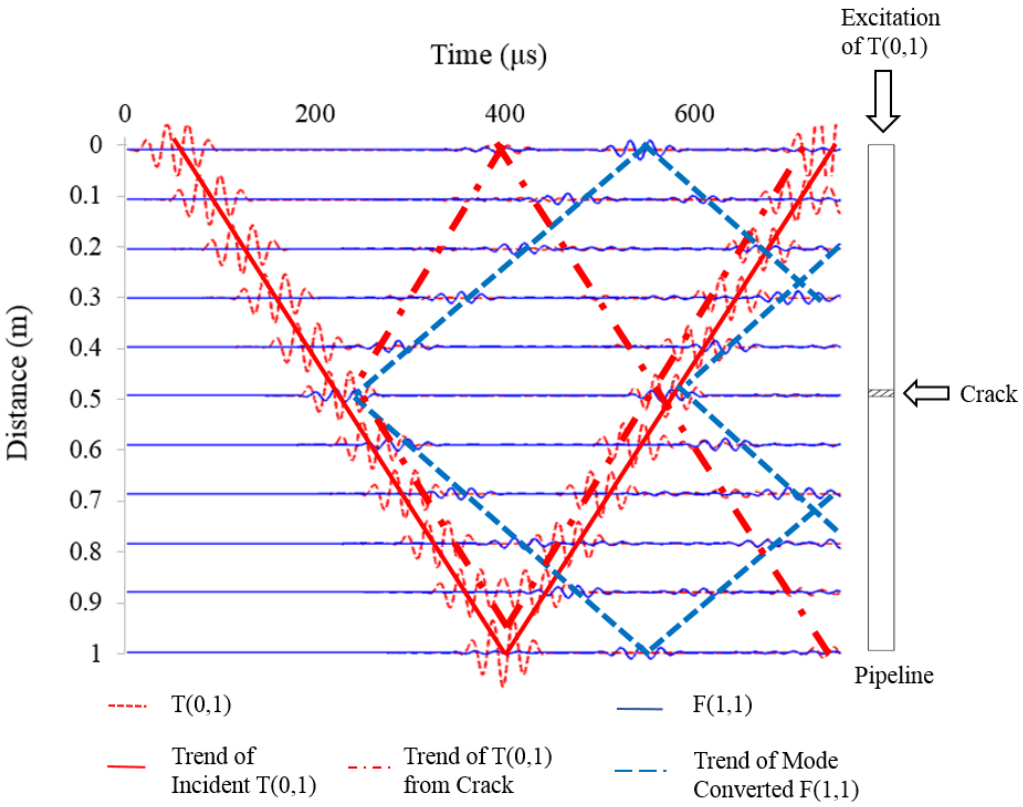

Figure 2.5 Wave propagation of torsional wave and mode converted flexural wave

The propagation of the T(0,1) wave and mode converted F(1,1) wave due to the crack is shown in Fig. 2.5. Torsional wave and flexural wave are indicated by red dashed line and

blue solid line, respectively. The trend lines for different wave modes are shown in Fig. 2.5. The propagation velocities for T(0,1) wave and F(1,1) wave are different. The group velocity for the T(0,1) and F(1,1) wave are 3130 *m/s* and 1900 *m/s*, respectively. The mode converted F(1,1) wave first appears at the middle of the pipe because of the presence of the crack. Since the incident T(0,1) and the T(0,1) reflected from the crack have the same group velocity, the slopes of their trend lines are in parallel as shown in Fig. 2.5.

2.4. Verification by Three-dimensional finite element model

A 3D finite element model of the same aluminium pipe with the same crack and incident wave used in Section 2.4 was created by ABAQUS and used to verify the accuracy of the proposed SFEM. 3D eight-node brick elements (C3D8R) [54] were used to model the pipe and the maximum size of the element used in the model is 0.8mm, which ensures there are at least 20 elements per wavelength for both T(0,1) and F(1,1) modes [55]. The thickness of the elements is 0.6mm so that there are five elements across the thickness of pipe wall. A notch having 1mm width and different depths was modelled at the middle of the pipe by removing the elements. Crack dimensions a and b, which were used in the numerical and experimental case studies, are listed in Table 2.1. The excitation of the T(0,1) mode was achieved by applying a tangential force at four nodes in circumferential direction. The excitation signal is the same as the signal used in Section 2.3. Figure 2.6 shows the notch modelled at the middle of the pipe, which is modelled asymmetrically about the longitudinal axis.

Crack dimensions	a (mm)	1.05	1.26	1.50	1.60	1.73	1.94	2.01	2.20	2.41	2.60	2.81
	b (mm)	4.93	5.48	5.94	6.12	6.35	6.69	6.80	7.00	7.38	7.87	7.89

Table 2.1. Crack dimensions a and b according to Figure 2.2

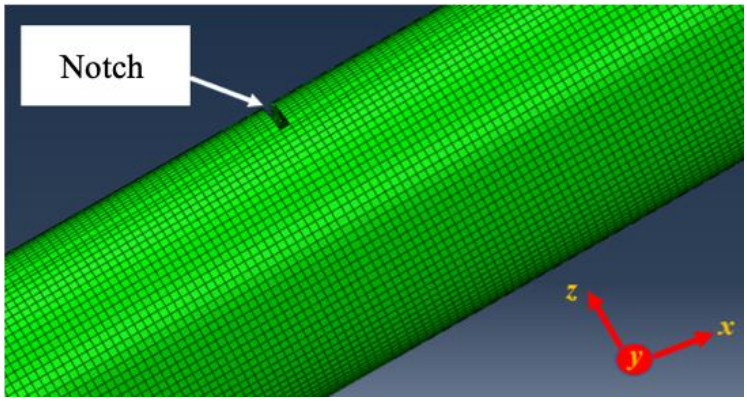

Figure 2.6 Notch at the middle of the pipe in the 3D finite element model

Figure 2.7 compares the wave signals simulated by SFEM and 3D FEM. The signals were obtained at 0.3m away from the excitation location and the crack depth is 2.01mm. Figure 2.7a shows the deformation in torsional DoF (θ), which contains the information of the incident wave T(0,1) wave and T(0,1) wave due to the crack (T-T wave). Figure 2.7b shows that the deformation in vertical DoF (v), which is the mode converted F(1,1) wave due to the crack (T-F wave). There is good agreement between the results calculated by SFEM and 3D FEM. The incident T(0,1), T-T wave from the crack and the mode converted T-F wave from the crack are labelled in Fig. 2.7.

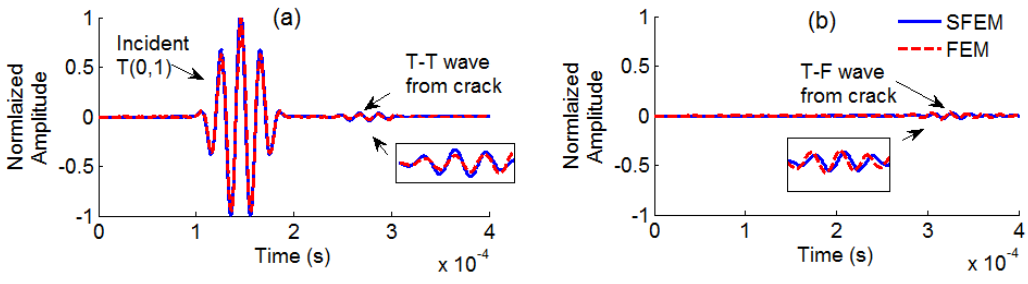

Figure 2.7 Signals simulated by SFEM and 3D FEM (a) torsional DoF and (b) vertical DoF

A series of parametric studies were carried out using the SFEM and 3D FEM to investigate the characteristics of T-T wave and mode converted T-F wave due to the crack. Different crack depths were simulated using the SFEM and 3D FEM the results are shown in Figs. 2.8 and 2.9. These two figures show the relationship between the wave amplitudes and the crack depth against pipe wall thickness ratios. Figure 2.8 shows the reflected T-T wave and the reflected T-F wave due to mode conversion effect at the crack and Fig. 2.9 shows the corresponding transmitted waves.

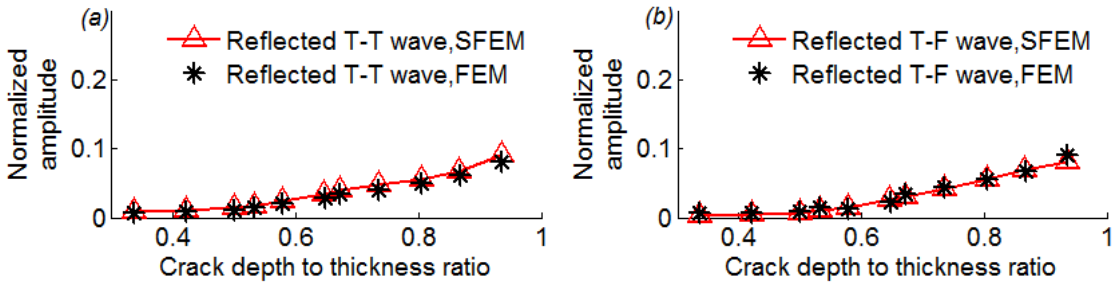

Figure 2.8 Normalized amplitude of (a) the reflected T-T wave and (b) the reflected T-F wave as a function of crack depth to thickness ratio for the results simulated by SFEM and 3D FEM

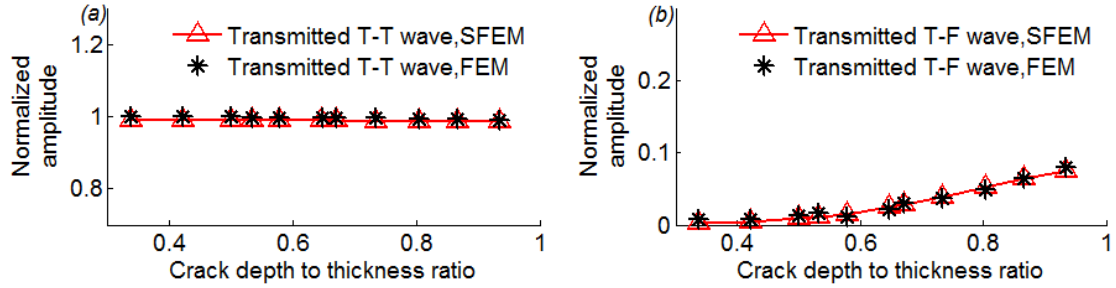

Figure 2.9 Normalized amplitude of (a) the transmitted T-T wave and (b) the transmitted T-F wave as a function of crack depth to thickness ratio for the results simulated by SFEM and 3D FEM

The transmitted and reflected waves are generated due to the interaction of the incident guided wave at the crack. The transmitted guided wave propagates toward the measurement point located at $x = 0.7m$. Meanwhile, the reflected wave travels back from the crack to the measurement point located at $x = 0.3m$. The amplitude of the measured data was normalized to allow comparison. The generation of mode converted waves is due to the asymmetric crack. The transmitted wave is the superposition of scattered wave and incident wave, while the reflected waves only contain scattered waves. This explains why the transmission signal is much larger than the wave reflected from the crack. The amplitude of transmitted T-T wave slightly decreases with crack depth to thickness ratio because part of the energy is transferred to the other wave mode. As shown in Figs. 2.8 and 2.9, there is good agreement between the results simulated by SFEM and 3D FEM.

2.5 Experimental Setup for Actuating and Sensing Torsional Guided Wave

A 1m long aluminium pipe with an outer diameter of 25mm and pipe wall thickness of 3mm was used to further validate the accuracy of the proposed time-domain SFEM. A slot cut of 1mm width was created at the middle of the pipe. Three different depths of the slot cut, a = 1.94, 2.20 and 2.81, were considered in the experiment. Figure 2.10 shows the aluminium pipe with piezoceramic transducers and the location of the slot cut. Four equally-spaced Ferroperm Pz27 piezoceramic shear plates were bonded on the outer diameter surface at the left end of the pipe using conductive epoxy adhesive (Fig. 2.10). These piezoceramic shear plates generate shear forces in torsional direction of the pipe to induce the T(0,1) incident wave. In this study, it has been found that four piezoceramic shear plates are enough to generate the T(0,1) incident wave. The other piezoceramic shear plate was bonded at 0.3m away from the excitation location and it is used to measure the guided waves. The dimensions of each piezoceramic

transducer are $6\times6\times1mm^3$. The density, Possion's ratio and relative dielectric constant of the piezoceramic transducers are 7700 kg/m^3, 0.39 and 1800, respectively. The incident wave is excited by applying the equivalent torque generated by the piezoceramic transducers to the node of torsional motion (θ) in the SFEM model.

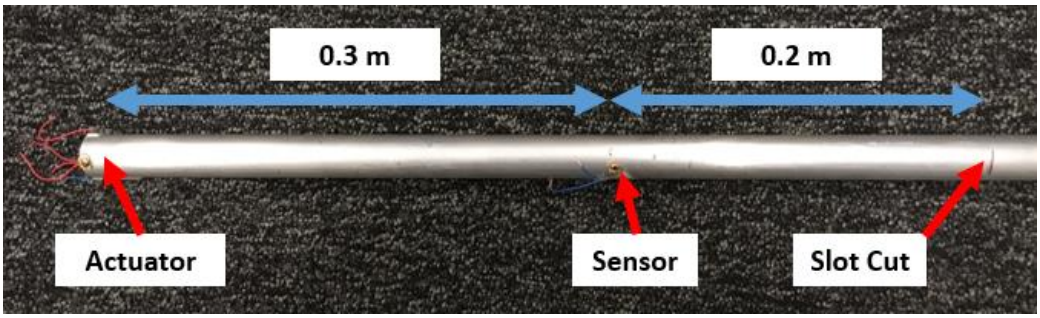

Figure 2.10 Piezoceramic transducers for generating incident T(0,1) wave and measurement, and the location of the slot cut in the aluminium pipe

A 5-cycle Hann windowed tone burst with centre frequency of 50kHz was generated by a computer-controlled function generator NI PIX-5412. A power amplifier (KROHN-HITE 7500) was used to amplify the signal from the function generator. The signal measured by the piezoceramic transducers was digitized by a data acquisition system (NI PIXe-5105). The sampling rate was 60MHz and the quality of the received signals was improved by averaging the measurements 500 times. A schematic diagram of the experiment setup is shown in Fig. 2.11.

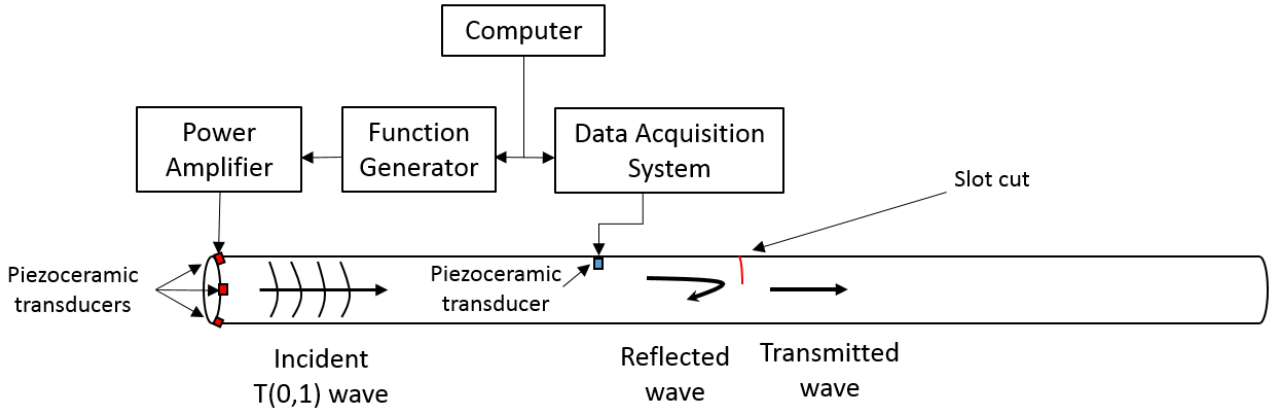

Figure 2.11 Schematic diagram of the experiment setup

The guided wave signals simulated by the proposed time-domain SFEM was compared with the experimentally measured data. Fig. 2.12 shows the guided wave simulated by SFEM and the experimental data measured at a distance of 0.3m from the excitation location. The red dashed line indicates the experimentally measured data, while the blue solid line presents the data simulated by the proposed SFEM. The incident wave T(0,1) interacts with the slot cut and generates T-T wave and mode converted T-F wave. The first captured wave packet is incident T(0,1). The second and third wave packets with small amplitude are T-T wave reflected from the slot cut and T-F wave induced due to mode conversion effect at the slot cut. The fourth wave packet is the T-T wave generated from the slot cut. It propagates to the left pipe end and then reflects back to the measurement point. The last wave packet is the incident T(0,1) wave reflected back from the right pipe end. There is good agreement between the results simulated by the SFEM and experimental data for all three different depths of slot cuts. This shows the proposed time-domain SFEM and the cracked element are able to accurately predict the

incident torsional wave, and scattered waves and mode converted wave due to the slot cut.

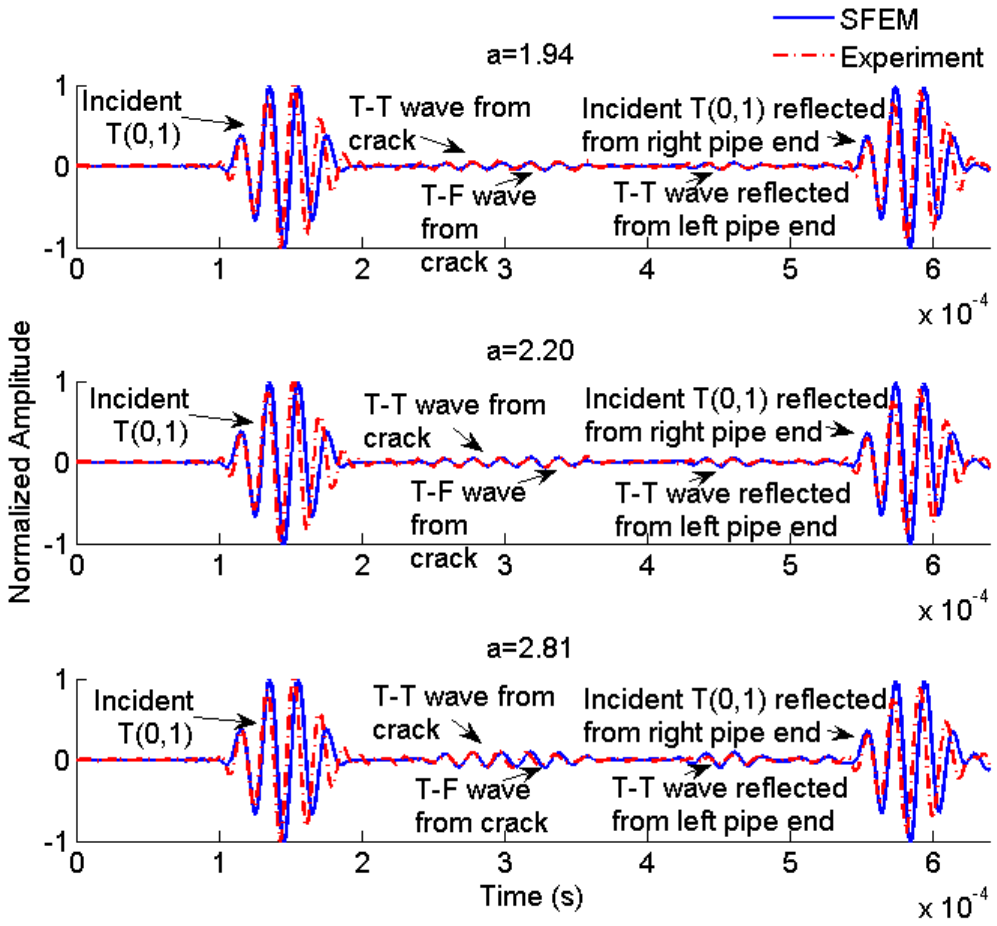

Figure 2.12 Guided wave signals simulated by time-domain SFEM and measured in experiment

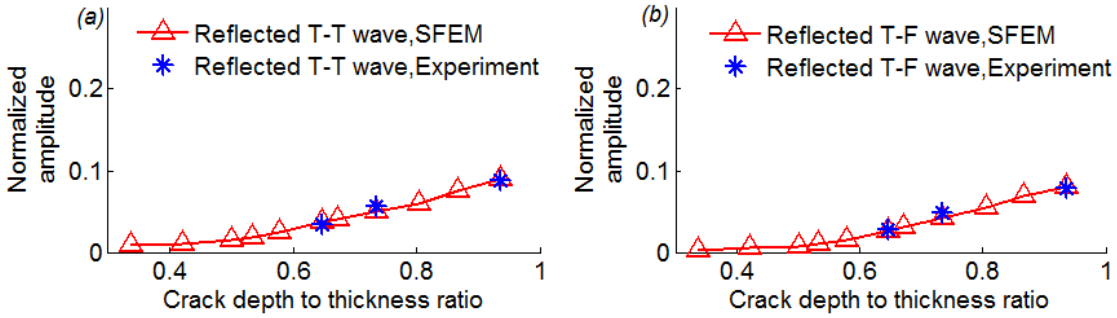

Figure 2.13 Normalized amplitude of SFEM simulated and experimentally measured wave signals as a function of crack depth to thickness ratio for (a) reflected T-T wave, and (b) reflected T-F wave.

The amplitudes of the reflected T-T wave and T-F wave are extracted from the measured time-domain signals shown Fig. 2.12 and they are plotted in Fig. 2.13. The SFEM results of the parametric studies with different crack depth to thickness ratios are shown in the same figure. Figure 2.13 shows that there is good agreement between the amplitudes obtained by SFEM and experiment for different crack depths to thickness ratios.

2.6 Conclusions

A time-domain SFEM has been presented to simulate the torsional guided wave propagation, scattering and mode conversion at cracks in pipes. The proposed time-domain SFEM has three DoFs at each node, which is developed based on elementary rod theory and Timoshenko beam theory. A cracked element has been proposed to simulate the scattering and mode conversion when the guided wave interacts with the cracks in pipes. 3D finite element model has been used to validate the proposed time-domain SFEM and the cracked element. A series of parametric studies has been carried out to investigate the scattering and mode conversion effect of the torsional guided waves at different depths of the cracks. Experimental studies have been carried out to further verify the proposed SFEM method and the cracked element. The results have shown that the time-domain SFEM with the proposed cracked element is able to accurately predict the torsional wave propagation, scattering and mode conversion effect at the cracks in pipes. The reflected and transmitted wave amplitudes are sensitive to the change of the crack depth. The results of this study have gained physical insights into the torsional guided wave propagation, scattering and mode conversion at the cracks in pipes. The findings can further support the developments of damage detection techniques using torsional guided wave. Future research can extend the study to bent pipe and buried pipe.

Acknowledgement

This work was supported by the Australian Research Council (ARC) under Grant No. DP160102233. Their support is greatly appreciated.

2.7 References

1. Clarke T, Cawley P. (2011). Enhancing the defect localization capability of a guided wave SHM system applied to a complex structure. *Structural Health Monitoring*, *10*(3):247-259.
2. Mohseni, H., & Ng, C. T. (2019). Rayleigh wave propagation and scattering characteristics at debondings in fibre-reinforced polymer-retrofitted concrete structures. *Structural Health Monitoring*, *18*(1), 303-317.
3. Carden, E. P. &Fanning, P. (2004). Vibration based condition monitoring: a review. *Structural Health Monitoring*, *3*(4):355-377.
4. Ng, C. T. (2015). A two-stage approach for quantitative damage imaging in metallic plates using Lamb waves. *Earthquakes and Structures, 8*(4):821-841.
5. Zhou, C., Zhang, C., Su, Z., Yue, X., Xiang, J. & Li, G. (2017) Health monitoring of rail structures using guided waves and three-dimensional diagnostic image. *Structural Control and Health Monitoring*, *24*:e1966.
6. Soleimanpour, R. & Ng, C. T. (2017). Locating delaminations in laminated composite beams using nonlinear guided wave. *Engineering Structures, 131*:207-219.
7. Zhou, W., Li, H., & Yuan, F. G. (2013). Guided wave generation, sensing and damage detection using in-plane shear piezoelectric wafers. *Smart Materials and Structures*, *23*(1), 015014.
8. Miao, H., Huan, Q., Wang, Q., & Li, F. (2017). Excitation and reception of single torsional wave T (0, 1) mode in pipes using face-shear d24 piezoelectric ring array. *Smart Materials and Structures*, *26*(2), 025021.
9. Mohseni, H., & Ng, C. (2017). Rayleigh wave for detecting debonding in FRP-retrofitted concrete structures using piezoelectric transducers. *Computers and Concrete*, *20*(5):583-593.

10. Ng, C. T. (2015). On accuracy of analytical modeling of Lamb wave scattering at delaminations in multilayered isotropic plates. *International Journal of Structural Stability and Dynamics*, *15*(08), 1540010.
11. Sun, F., Sun, Z., Chen, Q., Murayama, R., & Nishino H (2016). Mode conversion behavior of guided wave in a pipe inspection system based on a long waveguide. *Sensors*, *16*(10):1737.
12. Ng, C. T., Mohseni, H., & Lam, H. F. (2018). Debonding detection in CFRP-retrofitted reinforced concrete structures using nonlinear Rayleigh wave. *Mechanical Systems and Signal Processing*. https://doi.org/10.1016/j.ymssp.2018.02.027
13. Mohabuth, M., Kotousov, A., & Ng C. T. (2016). Effect of uniaxial stress on the propagation of higher-order Lamb wave modes. *International Journal of Nonlinear Mechanics*, *86*:104-111.
14. Kudela, P., Radzienski, M., Ostachowicz, W., & Yang, Z. (2018). Structural health monitoring system based on a concept of Lamb wave focusing by the piezoelectric array. *Mechanical Systems and Signal Processing*, *108*:21-32
15. He, S., & Ng, C. T. (2017). Guided wave-based identification of multiple cracks in beams using a Bayesian approach. *Mechanical Systems and Signal Processing*, *84*:324-345.
16. Galvagni, A., & Cawley, P. (2011). The reflection of guided waves from simple supports in pipes. *The Journal of the Acoustical Society of America*, *129*(4):1869-1880.
17. Cho, H., & Lissenden, C. (2012). Structural health monitoring of fatique crack growth in plate structures with ultrasonic guided waves. *Structural Health Monitoring* , *11*(4):393-404.
18. Yang, Y., Ng, C. T., Kotousov, A., Sohn, H., & Lim, H. J. (2018). Second harmonic generation at fatigue cracks by low-frequency Lamb waves: experimental and numerical studies. *Mechanical Systems and Signal Processing*, *99*:760-773.
19. Yang, Y., Ng, C. T. & Kotousov, A. (2018). Influence of crack opening and incident wave angle on second harmonic generation of Lamb waves. *Smart Materials and Structures*, *27*:055013.
20. Nagy, P. B., Simonetti, F., & Instanes, G. (2014). Corrosion and erosion monitoring in plates and pipes using constant group velocity Lamb wave inspection. *Ultrasonics*, *54*(7):1832-1841.
21. Ahmad, R., Banerjee, S., & Kundu, T. (2008). Pipe Wall Damage Detection in Buried Pipes Using Guided Waves. *Journal of Pressure Vessel Technology*, *131*(1):011501.

22. Angani, C., Park, D., Kim, C., Leela, P., Kishore, M. & Cheong, Y. (2011). Pulsed eddy current differential probe to detect the defects in a stainless steel pipe. *Journal of Applied Physics*, *109*(7):07D348.
23. Rose, J. L., Sun, Z., Mudge, P. J., & Avioli, M. J. (2003). Guided Wave Flexural Mode Tuning cand Focusing for Pipe Testing. *Materials Evaluation, 61*: 162-167.
24. Niu, X., Duan, W., Chen, H. P., & Marques, H. R. (2019). Excitation and propagation of torsional T (0, 1) mode for guided wave testing of pipeline integrity. *Measurement*, *131*:341-348.
25. Løvstad, A. & Cawley, P. (2011). The reflection of the fundamental torsional guided wave from multiple circular holes in pipes. *NDT and E International, 44*:553-562.
26. Eybpoosh, M., Berges, M. & Noh, H. (2017). An energy-based sparse representation of ultrasonic guided-waves for online damage detection of pipelines under varying environmental and operational conditions. *Mechanical Systems and Signal Processing, 82*:260-278.
27. Willberg, C., Duczek, S., Vivar-Perez, J. M., & Ahmad, Z. A. B. (2015). Simulation methods for guided wave-based structural health monitoring: a review. *Applied Mechanics Reviews*, *67*(1):010803.
28. Xu, F., Zhang, Y., Hong, W., Wu, K., & Cui, T. J. (2003). Finite-difference frequency-domain algorithm for modeling guided-wave properties of substrate integrated waveguide. *IEEE Transactions on Microwave Theory and Techniques*, *51*(11):2221-2227.
29. Zhao, X. & Rose, J. (2003). Boundary element modeling for defect characterization potential in a wave guide. *International Journal of Solids and Structures , 40*:2645-2658.
30. Liu, G. (2002). A combined finite element/ strip element method for analyzing elastic wave scattering by cracks and inclusions in laminates. *Computayional Mechanics, 28*:76-82.
31. Aryan, P., Kotousov, A., Ng, C. T., & Cazzolato, B. (2017). A model-based method for damage detection with guided waves. *Structural Control & Health Monitoring*, *24*(3):e1884
32. Soleimanpour, R, & Ng, C. T. (2017). Higher harmonic generation of guided waves at delaminations in laminated composite beams. *Structural Health Monitoring*, *16*(4):400-417.

33. Kim, Y., Ha, S., & Chang, F. K. (2008). Time-domain spectral element method for built-in piezoelectric-actuator-induced lamb wave propagation analysis. *AIAA journal*, *46*(3), 591-600.
34. He, S, & Ng, C. T. (2016). A probabilistic approach for quantitative identification of multiple delaminations in laminated composite beams using guided waves. *Engineering Structures*, *127*(15):602-614.
35. Patera, A. T. (1984). A spectral element method for fluid dynamics: laminar flow in a channel expansion. *Journal of computational Physics*, *54*(3), 468-488.
36. Dauksher, W., & Emery, A. F. (1999). An evaluation of the cost effectiveness of Chebyshev spectral and p-finite element solutions to the scalar wave equation. *International journal for numerical methods in engineering*, *45*(8):1099-1113.
37. Willberg, C., Duczek, S., Perez, J. V., Schmicker, D., & Gabbert, U. (2012). Comparison of different higher order finite element schemes for the simulation of Lamb waves. *Computer Methods in Applied Mechanics and Engineering*, *241*:246-261.
38. Duczek, S., Willberg, C., Schmicker, D., & Gabbert, U. (2012). Development, validation and comparison of higher order finite element approaches to compute the propagation of Lamb waves efficiently. *Key Engineering Materials, 518*:95-105.
39. Ostachowicz, W., Kudela, P., Krawczuk, M., & Zak, A. (2011). *Guided waves in structures for SHM: the time-domain spectral element method*. John Wiley & Sons.
40. Petyt, M. (2010). *Introduction to finite element vibration analysis*. Cambridge: Cambridge University Press.
41. Rucka, M. (2010). Experimental and numerical study on damage detection in an L-joint using guided wave propagation. *Journal of Sound and Vibration, 329*:1760-1779.
42. Doyle, J. F. (1989). *Wave propagation in structures*. Springer, New York, NY.
43. Reddy, J. N. (2006). *An introduction to the infinite element method*. New York: McGraw-Hill.
44. Rucka, M. (2010). Experimental and numerical studies of guided wave damage detection in bars with structural discontinuities. *Archive Applied Mechanics, 80*:1371-1390.
45. He, S., & Ng, C. T. (2017). Modelling and analysis of nonlinear guided waves interaction at a breathing crack using time-domain spectral finite element method. *Smart Materials and Structures, 26*:085002.

46. Pozrikidis, C. (2005). *Introduction to finite and spectral element methods using MATLAB*. CRC Press.
47. Kudela, P., Krawczuk, M. & Ostachowicz, W. (2006). Wave propagation modelling in 1D structures using spectral finite elements. *Journal of Sound and Vibration*, *300*:88-100.
48. Tada, H., Paris, P., & Irwin, G. (2000). The analysis of cracks handbook. *New York: ASME Press*, *2*, 1.
49. Ostachowicz, W., & Krawczuk, M. (1992). Coupled torsional and bending vibrations of a rotor with an open crack. *Archive of Applied Mechanics*, 62(3):191-2001.
50. Darpe, A. K., Gupta, K., & Chawla, A. (2004). Coupled bending, longitudinal and torsional vibrations of a cracked rotor. *Journal of Sound and Vibration*, *269*(1-2):33-60.
51. Cowper, G. R. (1966). The shear coefficient in Timoshenko's beam theory. *Journal of Applied Mechanics*, *33*(2):335-340.
52. Alleyne, D. N., Vogt, T. & Cawley, P. (2009). The choice of torsional or longitudinal excitation in guided wave pipe inspection. *Insight-Non-Destructive Testing and Condition Monitoring*, *51*(7):373-377.
53. Pavlakovic, B Lowe, M. J. S. (2003). DISPERSE: *A System for Generating Dispersion Curves, User's Manual Version 2.0.16B*, Imperial College.
54. Yang, Y., Ng, C. T., Kotousov, A. (2019). Second harmonic generation of guided wave at crack-induced debonding in FRP-strengthened metallic plates. *International Journal of Structural Stability and Dynamics*, *19*(1):1940006.
55. Aryan, P., Kotousov, A., Ng, C. T., & Widly, S. (2016). Reconstruction of baseline time-trace under changing environmental and operational conditions. *Smart Materials and Structures*, *25*:035018.

Chapter 3

Nonlinear Guided Wave Mixing in Pipes for Detection of Material Nonlinearity

(Paper 2, Published)

Carman Yeung and Ching Tai Ng

School of Civil, Environmental and Mining Engineering

The University of Adelaide, SA 5005, Australia

Publication:

Yeung, C., & Ng, C. T. (2020). Nonlinear guided wave mixing in pipes for detection of material nonlinearity. Journal of Sound and Vibration, 115541.

Statement of Authorship

Title of Paper	Nonlinear guided wave mixing in pipes for detection of material nonlinearity.
Publication Status	☑ Published ☐ Accepted for Publication ☐ Submitted for Publication ☐ Unpublished and Unsubmitted w ork w ritten in manuscript style
Publication Details	Yeung, C., & Ng, C. T. (2020). Nonlinear guided wave mixing in pipes for detection of material nonlinearity. Journal of Sound and Vibration, 115541.

Principal Author

Name of Principal Author (Candidate)	Carman Yeung		
Contribution to the Paper	Undertook literature review, developed numerical models, designed experimental tests, performed data analysis and prepared manuscript		
Overall percentage (%)	80%		
Certification:	This paper reports on original research I conducted during the period of my Higher Degree by Research candidature and is not subject to any obligations or contractual agreements with a third party that would constrain its inclusion in this thesis. I am the primary author of this paper.		
Signature		Date	10 Sep 2020

Co-Author Contributions

By signing the Statement of Authorship, each author certifies that:

i. the candidate's stated contribution to the publication is accurate (as detailed above);

ii. permission is granted for the candidate in include the publication in the thesis; and

iii. the sum of all co-author contributions is equal to 100% less the candidate's stated contribution.

Name of Co-Author	Ching-Tai Ng		
Contribution to the Paper	Supervised development of numerical model, reviewed manuscript and prepared for submission		
Signature		Date	9 Sep 2020

Abstract

Pipes have multiple applications in daily life and they are subjected to different types of defects. Nonlinear guided wave has attracted significant attention in detecting microstructural change at early stage of material deterioration. Extensive research using wave mixing with different wave modes has focused on plate-like structures. However, limited experimental studies have been conducted on the detection of material nonlinearity in pipes using two interacting guided waves. This study investigates nonlinear features generated due to mixing of torsional guided waves and material nonlinearity in pipes at low frequency range. The nonlinear theory of elasticity is implemented in a three-dimensional (3D) finite element (FE) method to simulate the effect of material nonlinearity on torsional guided wave mixing. The phenomenon of nonlinear features generated due to torsional guided wave mixing is investigated by 3D FE models. There is good agreement between the data obtained in the laboratory and numerical simulation results. This study demonstrates the existence of the combinational harmonic generation experimentally and provides physical insight into the phenomenon of nonlinear wave mixing. The findings of this study can further advance the damage detection techniques based on material nonlinearity in wave mixing.

Keywords: Guided wave, wave mixing, material nonlinearity, finite element simulation, pipe, torsional wave, circular waveguide

3.1 Introduction

Non-destructive evaluation (NDE) and damage detection techniques are important for safety-critical structures [1]. Time-dependent loads result in material degradation in metallic structures. Cracks developed in degrading materials may cause catastrophic failures if proper structural investigation has not been done to identify damage at early stage. Studies focused on using ultrasonic guided wave have been carried out in the literature [2]. Ultrasonic guided waves are one of the reliable NDE techniques. The benefits includes the high sensitivity to small defects and a relatively large inspection area [3-5]. Linear ultrasonic guided waves can also interrogate inaccessible location of structures and provide online condition monitoring of in-service structures [6].

Torsional guided wave has an advantage of long-range damage detection in pipelines. Fundamental axisymmetric torsional mode of guided wave T(0,1) has attracted increasing attention due to its nondispersive characteristic [7-8]. The use of low frequency is preferential for actuating torsional waves experimentally since less wave modes are generated at low frequency range. Carandente and Cawley [9] carried out an experimental study on the T(0,1) mode in a frequency range around 100kHz. Geometrical change due to various defects in pipes, such as corrosion [10], notch [11] and delamination [12], can be identified using linear guided wave scattered from the damage. In most of the situations, baseline measurement is essential [13-14] to extract the damage information which is limited to macro-scale. To address these restrictions of linear guided wave methods, research has focused on adopting nonlinear features of guided waves because this approach is highly sensitive to micro-scale damage [15].

Many studies on nonlinear guided waves have focused on contact and material nonlinearity [16-18]. Examples of contact nonlinearity have fatigue cracks and loosening [19-21]. Material nonlinearity is primarily induced by the interaction with discontinuities at lattice level, such as

micro-cracks and voids. In the time-domain signals, the nonlinear features do not show significant difference compared to linear guided wave responses in terms of scattering and mode conversion. However, the distortion due to the nonlinear elastic wave behaviours of a material has a significant change after the transformation to frequency-domain [22]. By studying material nonlinearity, nonlinear guided wave provides damage information at higher order harmonics in frequency-domain. They are always the integral multiples of the incident wave frequency. In most of the cases, higher harmonic generation [23] caused by the contact and/or material nonlinearity can be applied to baseline-free damage detection because baseline data from pristine condition of the structure is not necessary for this approach. Liu *et al.* [24] conducted a study on shear horizontal wave for the generation of Rayleigh-Lamb secondary mode in plates. Ideally, primary Rayleigh-Lamb mode should not appear if shear horizontal wave is generated. However, due to finite width transducers, they concluded that non-planar wavefront leads to the generation of both primary and secondary harmonics in Rayleigh-Lamb wave.

Research focused on harmonic generation in cylindrical waveguide has been conducted theoretically and experimentally [25-27] using single frequency guided wave. Liu *et al.* [17] carried out analytical studies for the second harmonics generation from different modes which were applicable to simple pipe-like structures. Chillara and Lissenden [28] used longitudinal mode of guided wave to study the nonlinear features in pipes. Li and Cho [29] measured second harmonics with thermal fatigue damage in pipes. Choi *et al.* [30] applied the fundamental torsional mode of guided wave in pipe-like structures and measured the higher harmonic generation. Li *et al.* [31] investigated the generation of second harmonics due to material nonlinearity in tube-like structures. However, it is potentially difficult to distinguish the cause of nonlinearity between weakly material nonlinearity and instrumentation nonlinearity. The

nonlinear distortion can be induced by measurement systems, such as amplifiers and transducers [32].

Due to the generation of undesired higher harmonic from equipment, relevant research work has been focused on the feasibility of combinational harmonic generation induced by the mix of two incident waves at different frequencies [33-34]. It has been demonstrated that guided wave mixing is sensitive to material degradation [35]. The harmonics are generated at sum and difference of the excitation frequencies due to guided wave mixing for damage detection. Early development of the guided wave mixing focused on bulk waves [36]. It can be used to detect contact acoustic nonlinearity (CAN) induced by imperfect bond interfaces in structures [37]. Alston *et al.* [38] investigated CAN in aluminium specimens using two incident waves propagating in different directions. The wave mixing technique can also be applied to different materials. Demčenko *et al.* [39] implemented bulk wave mixing method to study different dynamic processes in polymers, such as ageing problem. McGovern *et al.* [40] used the mixing of two bulk waves in non-collinear direction to study the nonlinear response in concrete structures. However, the use of bulk wave is ineffective as the inspection area is very limited, which is much smaller than Rayleigh wave and Lamb wave.

Research on wave mixing has been gradually extended to Lamb waves [41-42] because they are capable of selecting multiple wave modes for damage detection and able to provide large inspection area. Jingpin *et al.* [32] mixed two Lamb waves with different excitation frequencies in plates using collinear interaction approach. They investigated the generation of combinational harmonics due to the Lamb wave mixing phenomenon. Hassanian and Lissenden [35] studied the generation of secondary combinational harmonics at sum and difference of excitation frequencies in plate-like structures due to wave mixing. They demonstrated that material defects appeared in plates can be characterised by studying material nonlinearity. Extensive studies have been done on bulk wave mixing and Lamb wave mixing

to study the phenomenon of combinational harmonic generation. However, a very limited experimental investigation has been carried out on combinational harmonic generation due to torsional wave mixing in pipes. The purpose of this study is to carry out experimental validation for the existence of the combinational harmonics generated by torsional guided wave mixing in pipe-like structures and the measured results are also compared with three-dimensional (3D) finite element (FE) simulations.

The paper is organised as follows. Section 3.2 introduces the guided wave mixing approach and the theory of elasticity for material nonlinearity. The 3D scanning laser vibrometer is used to collect experimental data in Section 3.3. Section 3.4 applies the weakly nonlinear elasticity in FE method. The development of the FE model can confirm the experiment conducted in this study and provide the framework for more complex studies in future. In Section 3.5, the 3D FE model of a pipe is described and validated using experimentally measured data. This section also studies the sensitivity of the combinational harmonic generation due to torsional wave mixing in relation to different levels of fatigue damage. Finally, conclusions are drawn in Section 3.6.

3.2 Nonlinear guided wave mixing techniques

3.2.1 Generation of combinational harmonics

The generation of combinational harmonics requires the interaction of two or more wave sources. Using two wave sources as an example, mixed frequency (f_1 & f_2) is composed by two incident waves at frequencies f_1 and f_2, where $f_2 > f_1$. It not only induces their corresponding second order harmonics (i.e. $2f_1$ and $2f_2$), but also generates the combinational harmonics at their sum and difference frequencies when mixing the waves. Figure 3.1a shows a schematic

frequency spectrum which indicates the interaction of fundamental waves and the combinational second harmonic generation due to wave mixing. For more practical application, a single excitation point of two individual wave sources has the advantage to provide convenient access because it only requires one-side access to implement the ultrasonic guided wave mixing. The wave mixing zone indicated in Figure 3.1b represents the interaction of the wave mixing.

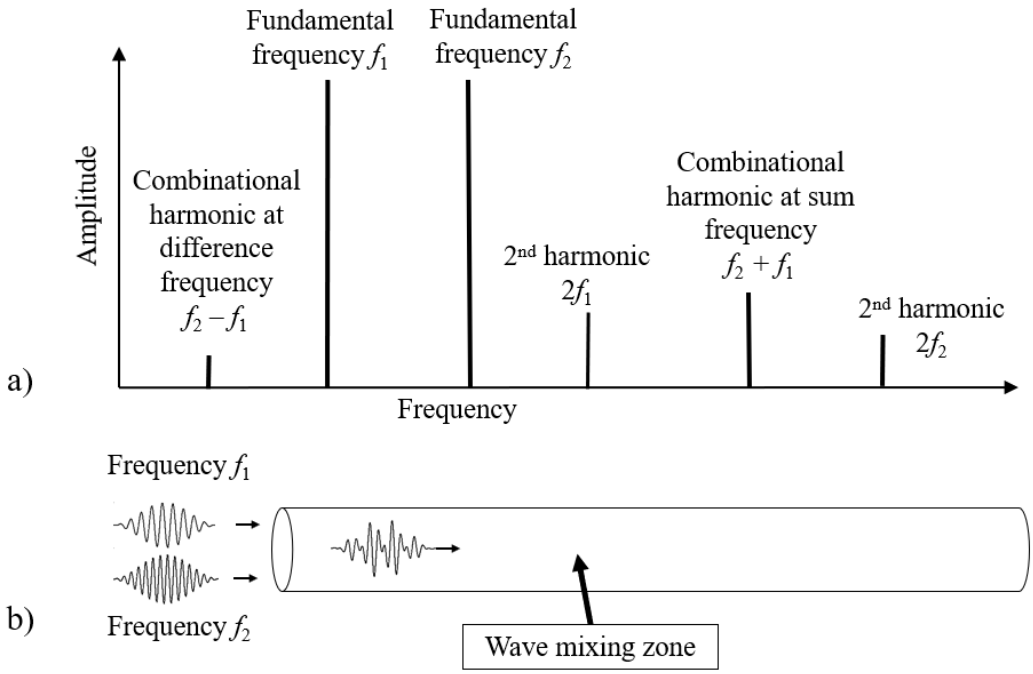

Figure 3.1 Schematic diagram of a) frequency spectrum for ultrasonic guided wave mixing, and b) wave mixing zone in pipe

3.2.2 Theoretical framework for weakly nonlinear elasticity

The following FE modelling framework for material nonlinearity not only can be used in simple structures, but also can apply to complicated configurations. In order to gain physical insights of combinational harmonic generation for wave mixing in pipes, this study aims to

have experimental validation by a FE model with the aid of nonlinear strain energy function. The derivation of nonlinear guided wave equation is based on continuum mechanics. The interaction of wave propagation is regarded as an infinitesimal deformation. The deformation gradient **F** (Figure 3.2) can quantify the change of a shape and the rigid rotation of a material. [16]

$$\mathrm{d}\mathbf{s} = \mathbf{F}\mathrm{d}\mathbf{S} = \frac{\partial \mathbf{s}}{\partial \mathbf{S}}\mathrm{d}\mathbf{S} \tag{3.1}$$

where **S** is the position of the material particle in the stress-free reference configuration located at **s** in the current configuration.

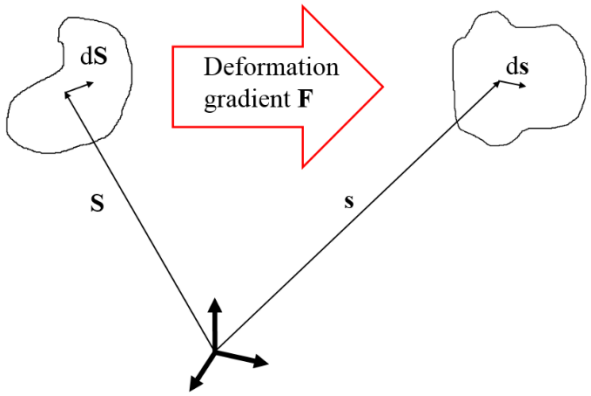

Figure 3.2 Illustration of deformation gradient

The right Cauchy-Green strain tensor **C** considers the rigid body translation between configurations. This strain tensor is symmetric and can be related to **F** as below

$$\mathbf{C} = \mathbf{U}^2 = \mathbf{F}^{\mathrm{T}}\mathbf{F} \tag{3.2}$$

where **U** is the right stretch tensor for local stretching at **S**. It is noted that **C** and **U** are the material tensors. The Green-Lagrange strain tensor **E** is used in the nonlinear strain energy function.

$$\mathbf{E} = \frac{1}{2}(\mathbf{F}^{\mathrm{T}}\mathbf{F} - \mathbf{I}) \tag{3.3}$$

where **I** is the identity tensor. It is noted that **E** is also symmetric. Polar decomposition is a way to separate the deformation gradient into the rotation tensor and the stretch tensor.

$$\mathbf{F} = \mathbf{RU} \tag{3.4}$$

R is an orthogonal tensor for local rotation of the material at **S**.

$$\mathbf{R}^{-1} = \mathbf{R}^{\mathrm{T}} \tag{3.5}$$

where det **R**=1

The governing equation used in the theory of elasticity (Eq. (3.6)) refers to the strain energy function *W*, where the strain is in the second order terms. To perform a small amplitude wave motion in an elastic object, the function *W* is presented in the Green-Lagrange strain tensor **E**. This particular form of strain tensor allows the expansion of the strain energy function to the third order. The equations are capable of studying nonlinear guided waves since they take material nonlinearity into consideration due to the inclusion of the third order terms. Based on the study of Murnaghan [44] , the expansion of the nonlinear strain energy function *W* can be written as

$$W(\mathbf{E}) = \frac{1}{2}(\lambda + 2\mu)i_1^2 + \frac{1}{3}(l + 2m)i_1^3 - 2\mu i_2 - 2m i_1 i_2 + n i_3 \tag{3.6}$$

where λ and μ are the Lamé elastic constants; *l*, *m* and *n* are the third order elastic constants. The principal invariants of **E** (i_1, i_2 and i_3) are given by

$$i_1 = tr\mathbf{E}$$

$$i_2 = \frac{1}{2}[i_1^2 - tr(\mathbf{E})^2]$$

$$i_3 = det\mathbf{E} \tag{3.7}$$

The second Piola-Kirchhoff (PK2) stress is obtained by the partial derivation of $W(\mathbf{E})$ with respect to **E**, i.e. $\frac{\partial W(\mathrm{E})}{\partial \mathrm{E}}$. The Cauchy stress can be written in terms of the PK2 stress and the deformation gradient as below

$$\boldsymbol{\sigma} = \mathrm{J}^{-1}\mathbf{F}\frac{\partial W(\mathbf{E})}{\partial \mathbf{E}}\mathbf{F}^{\mathrm{T}} \tag{3.8}$$

where $\mathrm{J}^{-1}$is the Jacobian determinant and equals to $\det(\mathbf{F})$.

3.3 Excitation using piezoceramic transducers and measurements using 3D scanning laser Doppler vibrometer

This section illustrates the mixing of torsional waves at two different excitation frequencies and the details of the excitation using piezoceramic transducers and measurements using 3D scanning laser Doppler vibrometer [46] to investigate the material nonlinearity of torsional wave mixing phenomenon in an aluminium pipe. Figure 3.3 is a schematic diagram of the experimental setup used in this study. The outer diameter of the pipe is r = 25 mm with wall thickness of 1.5 mm. The excitation of torsional guided wave was achieved by four square-shaped piezoceramic shear transducers (Ferroperm Pz27) with dimensions of 6 mm × 6 mm × 1 mm. Reflective spray was coated on the surface of the pipe specimen to improve the signal-to-noise ratio of the signals measured by the 3D scanning laser vibrometer.

Two excitation signals with low frequencies at f_1 = 70 kHz and f_2 = 110 kHz were used in the laboratory test to avoid less complication of multi-modes. The combined frequency excitation signal was achieved by merging the two single frequency excitation signals together. The signal at frequency f_1 lagged behind the signal at frequency f_2 for 22 μs in the pre-mixing procedure. Hann-windowed tone burst pulses [45] of 6 and 13 cycles at f_1 and f_2 were employed, respectively. The actual excitation from the actuators in time-domain was measured by the laser Doppler vibrometer and is shown in Figure 3.4a. The Fast Fourier Transform (FFT) was employed to transform the time-domain data to the frequency-domain data for analysis. Figure 3.4b shows the corresponding response in frequency-domain. The excitation signal was generated by a computer-controlled signal generator. The peak-to-peak output voltage was amplified by a power amplifier to 120 V.

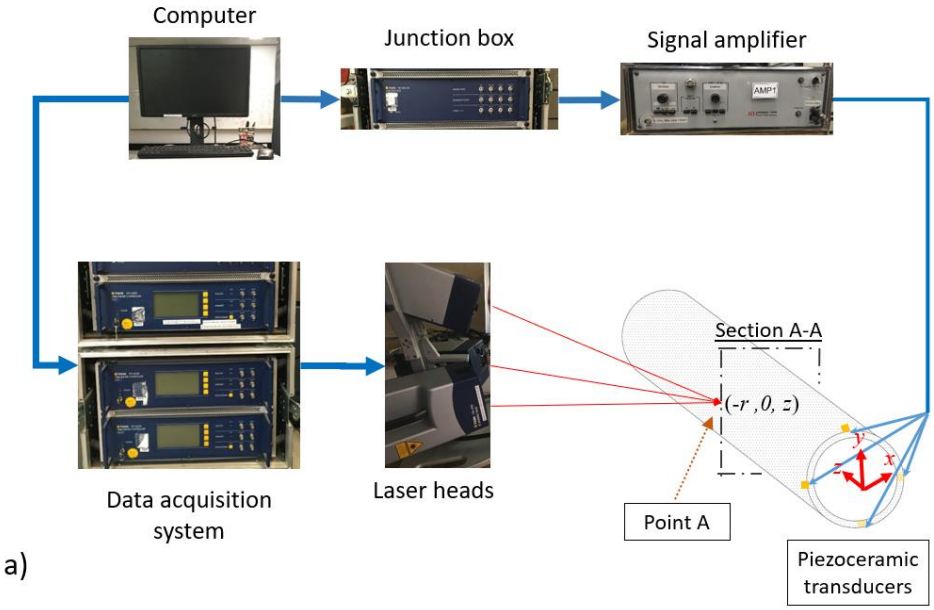

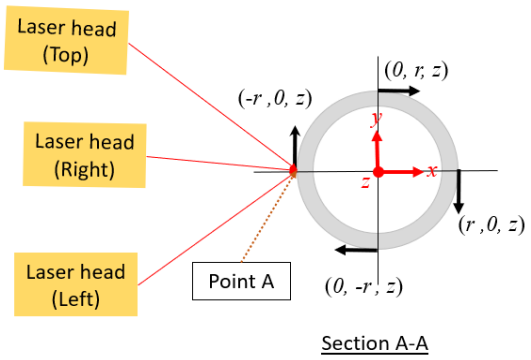

b)

Figure 3.3 (a) Experimental setup of piezoceramic shear transducers, 3D laser Doppler vibrometer and the pipe specimen, (b) cross-section of the pipe specimen

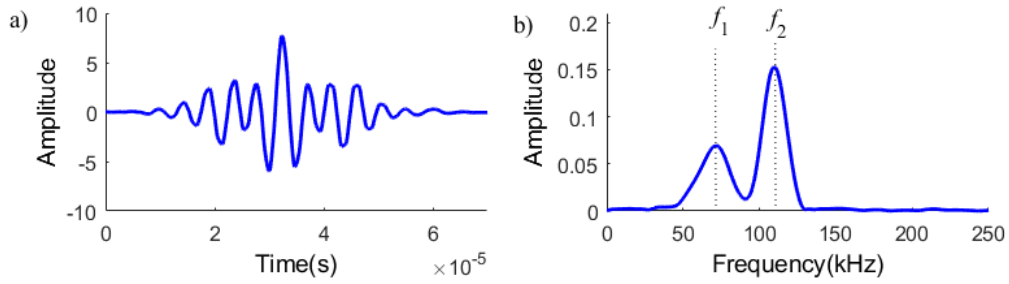

Figure 3.4 Actual mixed frequency excitation from actuators measured by laser Doppler vibrometer, a) time-domain and b) frequency-domain

The experimental data was collected using Polytec high-frequency 3D scanning laser Doppler vibrometer (PSV-400-3D-M). Low-pass filter with the cut-off frequency of 600 kHz and signal averaging with 2000 acquisitions were applied to enhance the signal-to-noise ratio of the measured data. This 3D laser scanning system is for non-contact optical vibration measurement. It consists of three spatially independent laser scanning heads. Figure 3.3b indicates the measurement locations in Cartesian coordinate system (i.e. in-plane horizontal *x*, in-plane vertical *y* and out-of-plane *z*). The measurements were done by using the three heads at the measurement point. The intersection point of the laser beams measures the velocity fields.

Section A-A in the same figure illustrates that the velocities in tangential and longitudinal directions were measured simultaneously at Point A. The torsional wave has the maximum signal magnitude in tangential direction.

Figures 3.5a and 3.5b present the time-domain experimentally measured mixed frequency waves in torsional (tangential) and longitudinal direction, respectively. Figures 3.5c and 3.5d show the corresponding signals in frequency-domain. The measurement point is at 450 mm away from the excitation location. The time-domain signals are normalised by the maximum signal amplitude so that the harmonics are comparable for the subsequent sections.

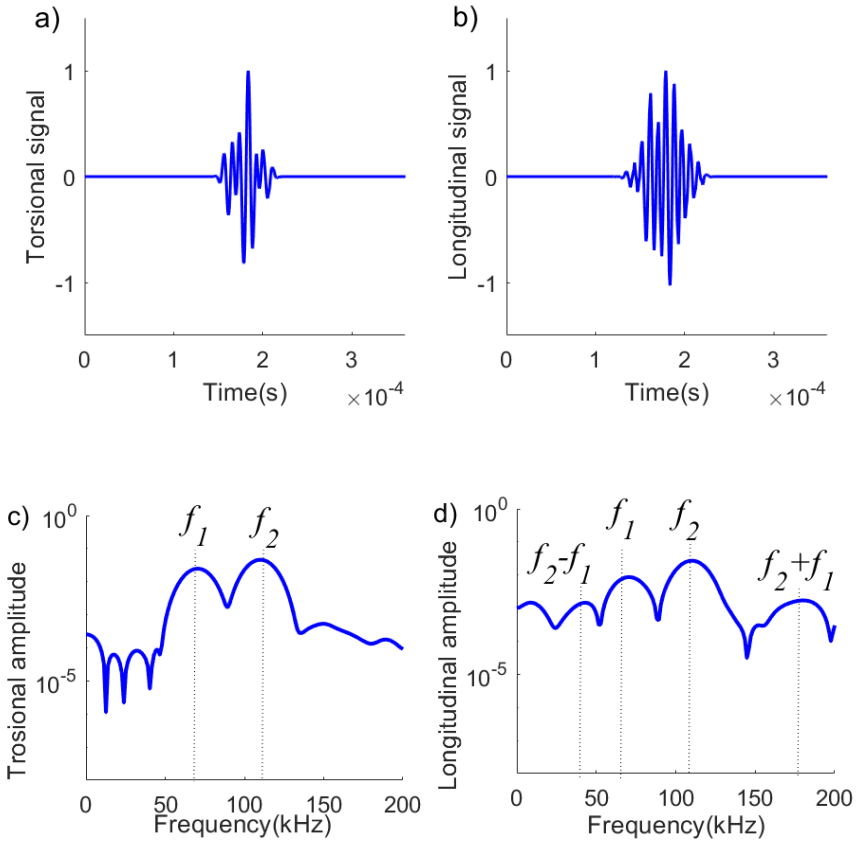

Figure 3.5 Experimentally measured of time-domain signal in (a) torsional direction and (b) longitudinal direction, and (c)-(d) corresponding signals in frequency-domain

Figure 3.6 compares the experimentally obtained single and mixed frequency responses in frequency-domain. In this experimental study, the generation of combinational harmonics are the main focus which are highlighted in Figure 3.6b. Three different tests were carried out in the study. The first test used the fundamental frequency f_1 excitation signal. The second test used the fundamental frequency f_2 excitation signal. The third test used the mixed frequencies (f_1 & f_2) excitation signal. They are indicated using black dotted line, red solid line and blue solid line in Figure 3.6, respectively. The tangential motion of the fundamental torsional guided wave mode shall not give second harmonics in wave mixing. Previous study [17] used analytical method and stated this point of view at single frequency. However, very limited research was carried out to experimentally confirm the generation of combination harmonics in torsional wave mixing for material nonlinearity. Therefore, the current study focuses on the combinational harmonics generation due to guided wave mixing and experimentally validates this phenomenon.

It is expected that no higher harmonics appear in the torsional direction when the two incident waves interact with each other in Figure 3.6. Apart from the fundamental frequency at f_1 and f_2, the combinational harmonics at difference frequency ($f_2 - f_1$ = 40 kHz) and sum frequency ($f_2 + f_1$ = 180 kHz) have obvious peaks in the longitudinal measurement, which are highlighted by dotted vertical lines.

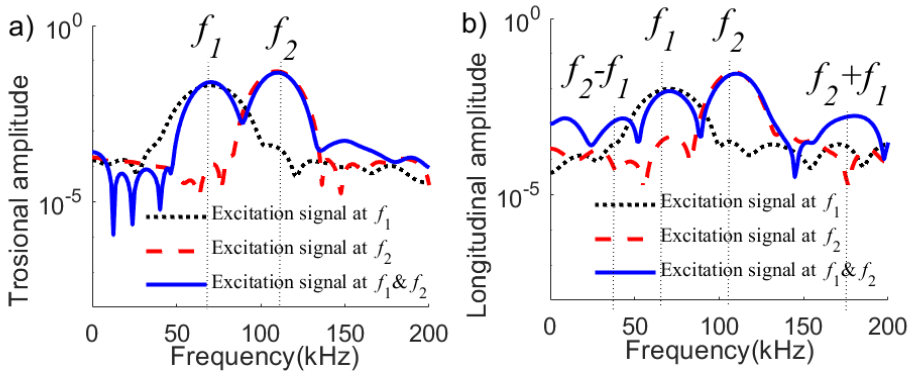

Figure 3.6 Experimentally measured single and mixed frequency velocity responses in frequency-domain, (a) torsional and (b) longitudinal directions

3.4 Three-dimensional finite element model of pipes

In this study, a 3D FE model was used to simulate guided wave mixing for the phenomenon of material nonlinearity. The excitation location was the same excitation position in the pipe specimen using in the experiment. The geometry of the pipe model was created and meshed in ABAQUS. The pipe is modelled by eight-node linear brick elements with hourglass control and reduced integration (C3D8R). The in-plane dimension of the element is approximately 0.25 mm × 0.25 mm to ensure the simulation is stable. This ensures that there are at least 20 and 25 FE nodes per wavelength for torsional wave and longitudinal wave. The thickness of the elements is 0.25 mm so there are six layers of elements in the thickness direction (Figure 3.7a). The dynamic simulation is solved by ABAQUS/Explicit. The density and Young's modulus of the aluminium are 2700 kg/m^3 and 69 GPa, respectively. The Lame's and third order elastic constants used in the user-defined subroutine are listed in Table 3.1.

Table 3.1 Lame's and third order elastic constants of aluminium used in the FE simulations (in GPa)

Lame's constants		Third order elastic constants		
λ	μ	l	m	n
54.9	26.5	-252.2	-325	-351.2

A layout of the pipe modelled using FE method is shown in Figure 3.7. As shown in Figure 3.7a, the incident T(0,1) waves at f_1 and f_2 excitation frequencies were excited by applying tangential point loads at four edges of the circumference located at the pipe end. The coordinate of Point B is (r,0,0), which has the measured velocity in v_y. This is the maximum signal magnitude of the torsional wave in y direction. The longitudinal wave signal can be

obtained from the nodal displacement in *z* direction. The study used the same frequencies and number of cycles Hann-windowed tone burst pulses used in experiment as the excitation signals. This study considered three different situations in the excitation signals at low frequency range, which are fundamental frequency f_1 excitation signal, fundamental frequency f_2, excitation signal, and pre-mixed frequencies (f_1 & f_2) excitation signal. The three situations considered in FE are the same as in the experimental study. The existence of combinational harmonics at the sum and difference frequencies can be associated with the induction of shear coupling from the fundamental torsional waves to longitudinal waves at the combinational harmonic frequencies. Thus, the data in the FE simulations were extracted in both the torsional and longitudinal directions. Figures 3.8a and 3.8b show the numerically simulated time-domain signals in tangential and longitudinal directions at the location of 500 mm from the excitation location. The corresponding data in frequency domain are shown in Figures 3.8c and 3.8d. The FE model includes the nonlinear strain function (Section 3.2.2) to simulate the effect of material nonlinearity.

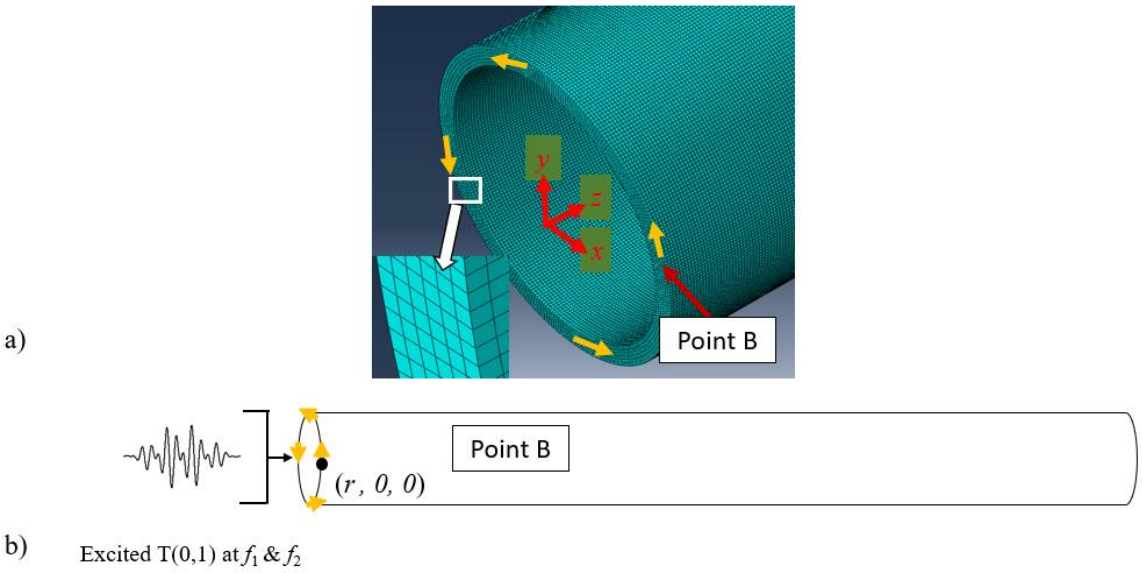

Figure 3.7 (a) 3D FE model and T(0,1) mode excitation (b) schematic diagram of the configuration used in the FE model

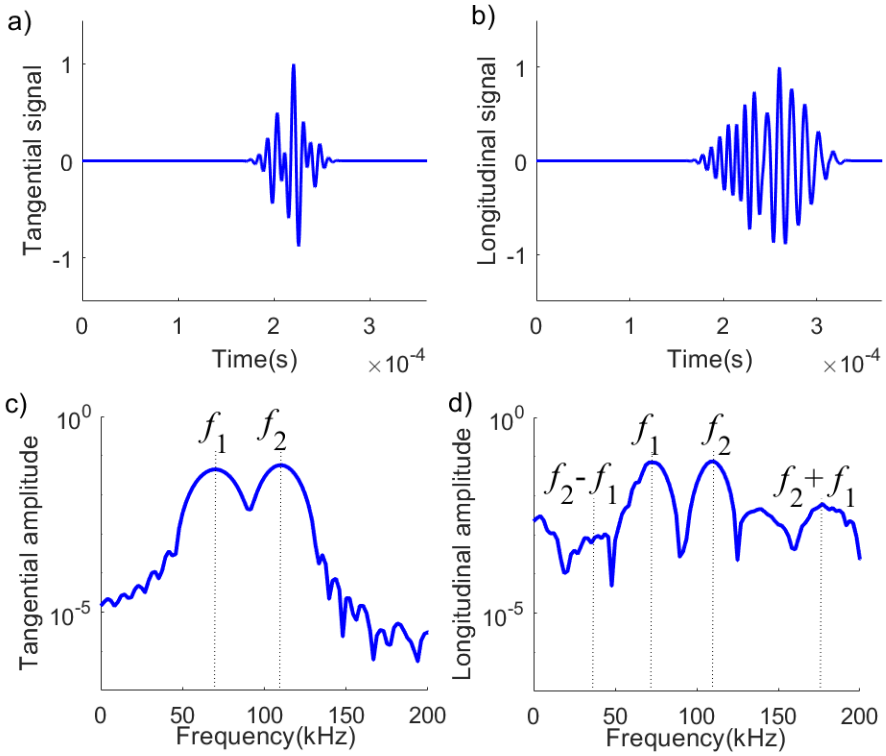

Figure 3.8 Numerical simulated time-domain signals in (a) tangential direction and (b) longitudinal direction, and (c)-(d) the corresponding signals in frequency-domain

Figure 3.9 shows the phase velocity dispersion curves for the torsional and longitudinal wave modes from 50 kHz to 330 kHz in steps of 20 kHz. The signals at five measurement points were recorded and used to calculate the averaged phase velocity at each excitation frequency. The first measurement is located at 300 mm from the excitation signal and the distance between two consecutive measuring points is 1 mm. Therefore, the separation of two measurement points is less than one half of the incident wave wavelength. The following equation is used to calculate the phase velocity

$$c_p = \frac{2\pi f \Delta y}{\Delta \varphi} \tag{3.9}$$

where f is the central frequency of the incident wave, Δy is the distance between the two measurements and $\Delta \varphi$ is the change in phase angle.

Results calculated by a software DISPERSE [47] is used to compare with the results calculated from FE simulation data in Figure 3.9. The theoretical calculation is indicated by dashed lines while the FE data is indicated by square markers. The T(0,1) mode and L(0,1) mode are represented by blue and red colours, respectively. The FE calculations are in agreement with the theoretical values. Thus, the FE model can accurately predict both the torsional and longitudinal wave propagations.

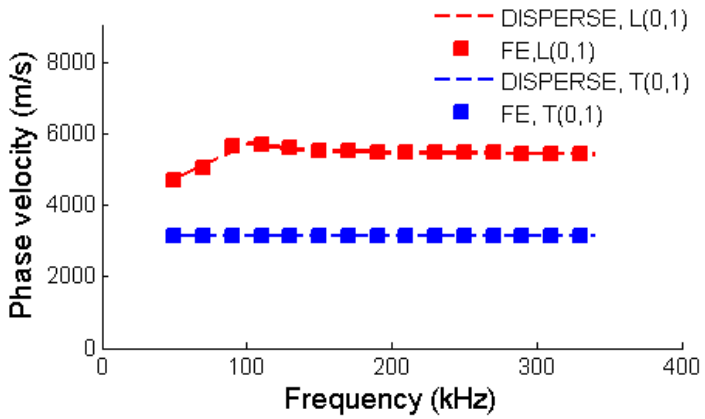

Figure 3.9 Phase velocity dispersion obtained from DISPERSE and FE simulation

3.5 Experimental validation 3D FE model with nonlinear elasticity

Figure 3.10 is the comparison between the data from the FE model with the consideration of material nonlinearity and the experimentally measured mixed frequency response. FFT was used for the conversion in experimental and numerical data. The results from the experiment and the FE model were normalised to allow direct comparison. The blue solid line and the red dotted line refer to the FE simulated frequency spectra and the experimentally measured frequency spectra, respectively. The corresponding frequencies are labelled in Figure 3.10. The

FFT signals simulated by the nonlinear FE model in the tangential and longitudinal directions generally share the same pattern with those signals in the experiment. It implies that the direction of torsional force for the nonlinear FE model does not generate any combinational harmonics.

The generation of primary and combinational harmonics at sum and difference frequencies (i.e. $f_2 \pm f_1$) can be observed in the longitudinal motion (Figure 3.10b). It should be noted that the primary harmonics at f_1 and f_2 in the longitudinal direction are induced because of the non-planar wavefront generated by finite width transducers [24]. In the current study, the excitations in the experiments and simulations were four individual piezoceramic transducers at the end of the pipe. This produces non-planar wavefront, and hence, it induces the primary harmonics at f_1 and f_2 in the longitudinal direction. Therefore, the longitudinal signal contains both primary and combinational harmonic frequencies when mixed frequency torsional wave is generated.

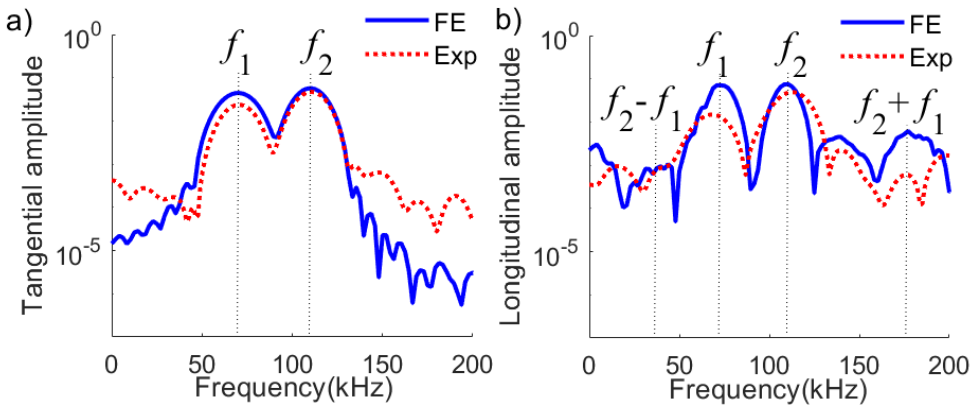

Figure 3.10 Mixed frequency response of FE simulation and experimentally measured data in (a) tangential and (b) longitudinal directions

3.5.1 Simulation results and discussion

In this section, two FE models were used to simulate the guided wave responses. The FE model with the use of the material subroutine VUMAT [48] which implemented extended Murnaghan's strain energy equation in Section 3.2.2 is labelled as nonlinear FE (blue solid line) in the figure. The other model is a benchmark simulation which does not take into account the material nonlinearity. The corresponding FFT response is labelled as linear FE (black dashed line) in the figure. Figures 3.11 and 3.12 show the measured data in both directions for individual excitation frequencies f_1 and f_2. The linear and nonlinear signals do not have much difference in the tangential direction (Figures 3.11a and 3.12a).

Since the primary fundamental torsional waves cannot generate second harmonic torsional waves, the second harmonic does not appear in those plots. Only the peaks at the excitation frequencies, which are the fundamental frequency components, appear in the tangential direction. Instead, there are additional peaks at $2f_1$ and $2f_2$ in nonlinear FE. It is demonstrated that the modified strain energy function with third order terms in Eq. (3.6) can effectively model the nonlinear guided wave behaviours through the utilisation of user subroutine. The second harmonics at $2f_1$ and $2f_2$ appear in the data measured in longitudinal direction (Figures 3.11b and 3.12b). In the meantime, no harmonic appears in the linear response (black dashed lines) at the double frequency of the excitation signals.

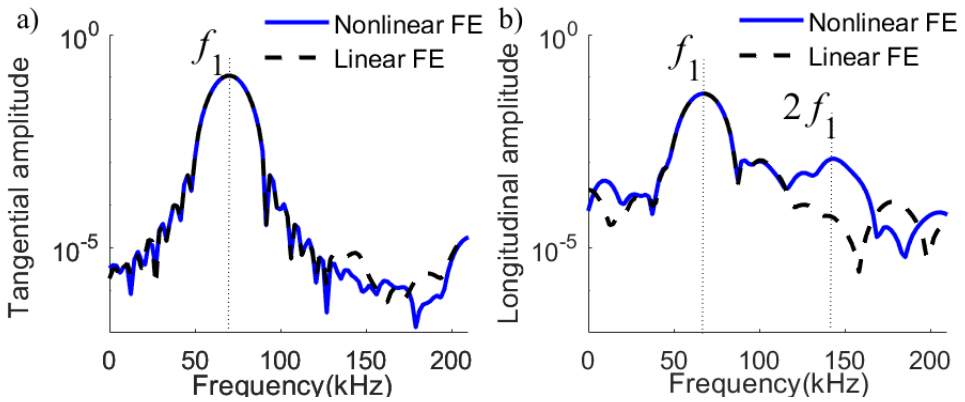

Figure 3.11 FE model verification of single frequency at f_1 in (a) tangential and (b) longitudinal directions

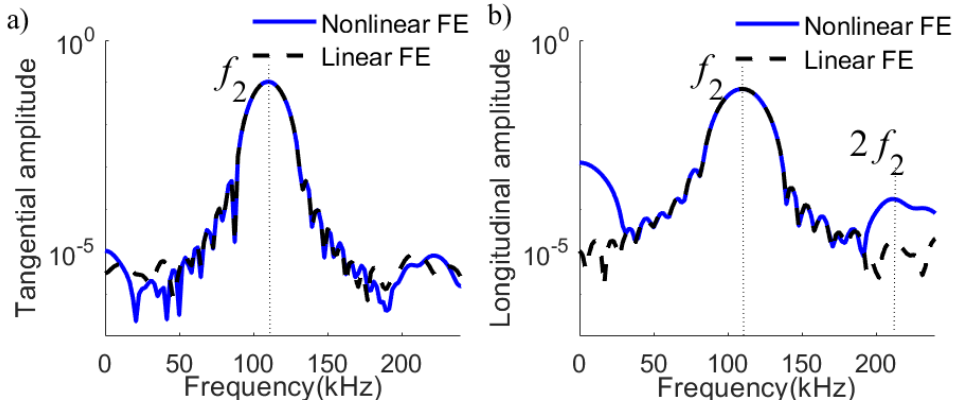

Figure 3.12 FE model verification of single frequency at f_2 in (a) tangential and (b) longitudinal directions

Similarly, Figure 3.13a shows that the signal does not contain any second harmonic components in the data calculated in the tangential direction. In Figure 3.13b, the combinational harmonic at the sum frequency ($f_2 + f_1$) is approximately 20 % higher than at the difference frequency ($f_2 – f_1$). Due to the mutual wave interaction [28], the combinational harmonics at the sum and difference frequencies can be observed in the mixed frequency response. It is noticeable that single frequency excitation does not generate the combination harmonics at sum and different frequencies since they are originally from the mutual interaction

of two waves. Therefore, none of these combinational harmonic components can be observed in the measured data using single frequency excitation at f_1 and f_2, respectively.

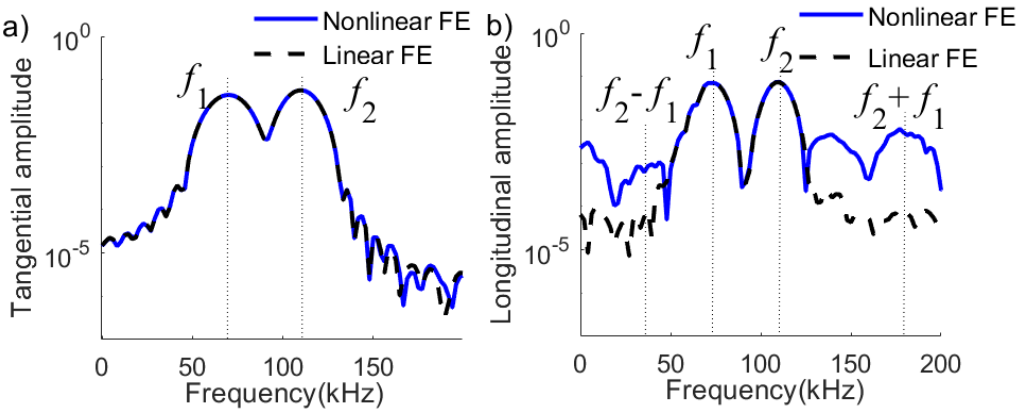

Figure 3.13 Mixed frequency response in frequency domain for FE models in (a) tangential and (b) longitudinal directions

3.5.2 Effect on relative nonlinear parameter in material nonlinearity at different fatigue stages

This section presents a study to relate the relative nonlinear parameter with the several stages of evenly distributed fatigue damage growth using FE simulations. A material with various fatigue states subjected to the accumulation of dislocation substructures leads to the change in the value of higher harmonics. This can be applied to the combinational harmonics in nonlinear guided wave mixing in pipes to characterise the fatigue damage of a material quantitatively. The relative nonlinear parameter β' is defined as [43]

$$\beta' = \frac{A_3}{A_1 A_2} \tag{3.10}$$

where A_3 is the amplitude of the harmonic wave and A_1, A_2 are the amplitudes of the two incident waves. The parameter β' can used as an indicator as the term A_3 is the generation of combinational harmonic frequencies in the incident wave frequency signal. It can monitor the material nonlinearity quantitatively prior to the initiation of micro-cracks. An accurate

experimental study about the fatigue damage of aluminium was carried out in the previous research [49] which provided convincible data at different stages in an evenly distributed fatigue damage cycle. The relevant data is shown in Table 3.2.

Table 3.2 Material properties of aluminium at three different stages in a fatigue life cycle (in GPa)[49]

Third elastic constants \ Fatigue life (%) order	0	40	80
l	-149.4	-153.7	-155.9
m	-102.8	-113.2	-115.3
n	-351.2	-358.3	-359.8

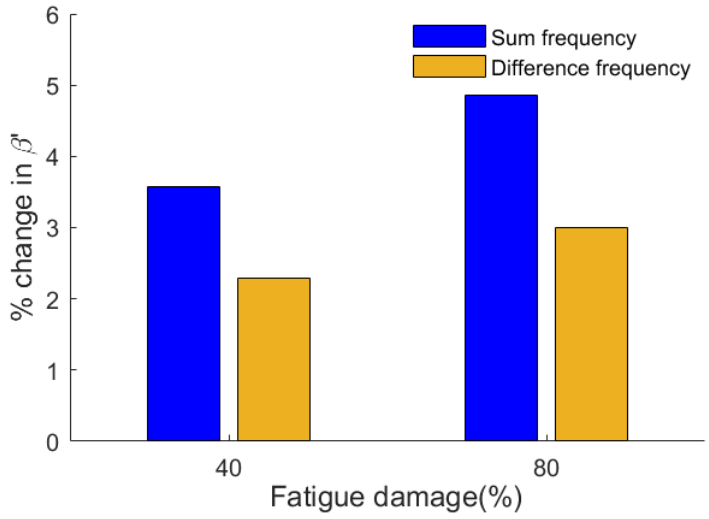

Figure 3.14 Percentage change in the nonlinear parameter calculated from the FE simulation against the fatigue damage

In order to allow direct comparison between the sum and difference harmonics, the data is expressed in percentage change for the relative nonlinear parameter *β'* when the fatigue life is at 40 % and 80 %. As shown in Figure 3.14, the combinational harmonics at sum and difference frequencies are indicated by blue colour and yellow colour, respectively. The measurement points are at the distance of 450 mm away from the excitation points. The

increase in β' at sum frequency is more obvious than that at difference frequency. The overall value of β' at difference frequency is about a half of the value of β' at sum frequency.

3.6 Conclusions

The study of guided wave mixing of two fundamental torsional waves in pipe-like structures has been investigated numerically and experimentally. The 3D scanning laser Doppler vibrometer was used in the experiment. The generation of combinational harmonics due to guided wave mixing in pipes has been measured in experiment. They were induced at the sum and difference frequencies of the incident waves in longitudinal direction when the two T(0,1) mode waves interact with each other. The modified Murnaghan's energy equation to third order terms was implemented in the 3D FE model to capture the combinational harmonic generation in guided wave mixing. There is good agreement between the frequency responses of experimental measurements and numerical simulations. The experimentally validated 3D FE model has been used to investigate the generation of combinational harmonics with increasing percentage of fatigue damage level. Current investigations are focusing on extending the study to higher order harmonic generation due to material nonlinearity using guided wave mixing.

Acknowledgement

This work was funded by the Australian Research Council (ARC) under the grant number DP200102300. The authors are grateful to this support.

3.7 Appendix

In this study, the material nonlinearity is taken into account in the 3D FE model. A set of equations are implemented through a user subroutine VUMAT in ABAQUS/Explicit to analyse the effect of material nonlinearity on guided wave mixing in pipes. The stress in ABAQUS is the Cauchy stress tensor $\boldsymbol{\sigma}$ in the basis of Green-Naghdi rate.

$$\hat{\boldsymbol{\sigma}} = \mathbf{R}^{\mathrm{T}}\boldsymbol{\sigma}\mathbf{R} \tag{A.1}$$

Using Eq. (3.4), (3.6), (3.8) and (A.1), the stress in ABAQUS can be interpreted as

$$\hat{\boldsymbol{\sigma}} = \mathrm{J}^{-1}\mathbf{R}^{\mathrm{T}}\mathbf{F}\frac{\partial W(\mathbf{E})}{\partial \mathbf{E}}\mathbf{F}^{\mathrm{T}}\mathbf{R}$$

$$= \mathrm{J}^{-1}\mathbf{R}^{\mathrm{T}}\mathbf{R}\mathbf{U}\frac{\partial W(\mathbf{E})}{\partial \mathbf{E}}\mathbf{U}^{\mathrm{T}}\mathbf{R}^{\mathrm{T}}\mathbf{R}$$

$$= \mathrm{J}^{-1}\mathbf{U}\frac{\partial W(\mathbf{E})}{\partial \mathbf{E}}\mathbf{U}^{\mathrm{T}} \tag{A.2}$$

The values of **U** and **F** at the end of final time step (t) will be updated in the stress equations at the end of an integration step ($t + \Delta t$) and renewed in stressNew(i).

3.8 References

1. Pan, J., Zhang, Z., Wu, J., Ramakrishnan, K. R., & Singh, H. K. (2019). A novel method of vibration modes selection for improving accuracy of frequency-based damage detection. *Composites Part B: Engineering*, *159*, 437-446.
2. Chakraborty, N., Rathod, V. T., Mahapatra, D. R., & Gopalakrishnan, S. (2012). Guided wave based detection of damage in honeycomb core sandwich structures. *Ndt & E International*, *49*, 27-33.

3. Pudipeddi, G. T., Ng, C. T., & Kotousov, A. (2019). Mode conversion and scattering of Lamb waves at delaminations in composite laminates. *Journal of Aerospace Engineering*, *32*(5), 04019067.
4. Mariani, S., Nguyen, T., Phillips, R. R., Kijanka, P., Lanza di Scalea, F., Staszewski, W. J., ... & Carr, G. (2013). Noncontact ultrasonic guided wave inspection of rails. *Structural Health Monitoring*, *12*(5-6), 539-548.
5. Mohseni, H., & Ng, C. T. (2019). Rayleigh wave propagation and scattering characteristics at debondings in fibre-reinforced polymer-retrofitted concrete structures. *Structural Health Monitoring*, *18*(1), 303-317.
6. Hughes, J. M., Vidler, J., Ng, C. T., Khanna, A., Mohabuth, M., Rose, L. F., & Kotousov, A. (2019). Comparative evaluation of in situ stress monitoring with Rayleigh waves. *Structural Health Monitoring*, *18*(1), 205-215.
7. Kwun, H., Kim, S. Y., Choi, M. S., & Walker, S. M. (2004). Torsional guided-wave attenuation in coal-tar-enamel-coated, buried piping. *Ndt & E International*, *37*(8), 663-665.
8. Wu, B., Su, Y., Liu, D., Chen, W., & Zhang, C. (2018). On propagation of axisymmetric waves in pressurized functionally graded elastomeric hollow cylinders. *Journal of Sound and Vibration*, *421*, 17-47.
9. Carandente, R., & Cawley, P. (2012). The effect of complex defect profiles on the reflection of the fundamental torsional mode in pipes. *NDT & E International*, *46*, 41-47.
10. Nagy, P. B., Simonetti, F., & Instanes, G. (2014). Corrosion and erosion monitoring in plates and pipes using constant group velocity Lamb wave inspection. *Ultrasonics*, *54*(7), 1832-1841.
11. Yeung, C., & Ng, C. T. (2019). Time-domain spectral finite element method for analysis of torsional guided waves scattering and mode conversion by cracks in pipes. *Mechanical Systems and Signal Processing*, *128*, 305-317.
12. Bingham, J., & Hinders, M. (2009). Lamb wave detection of delaminations in large diameter pipe coatings. *The Open Acoustics Journal*, *2*(1).
13. Jhang, K. Y. (2009). Nonlinear ultrasonic techniques for nondestructive assessment of micro damage in material: a review. *International journal of precision engineering and manufacturing*, *10*(1), 123-135.
14. Rose, J. L. (2002). A baseline and vision of ultrasonic guided wave inspection potential. *J. Pressure Vessel Technol.*, *124*(3), 273-282.2

15. Shen, Y., & Cesnik, C. E. (2017). Modeling of nonlinear interactions between guided waves and fatigue cracks using local interaction simulation approach. *Ultrasonics*, *74*, 106-123.
16. Yang, Y., Ng, C. T., Mohabuth, M., & Kotousov, A. (2019). Finite element prediction of acoustoelastic effect associated with Lamb wave propagation in pre-stressed plates. *Smart Materials and Structures*, *28*(9), 095007.
17. Liu, Y., Khajeh, E., Lissenden, C. J., & Rose, J. L. (2013). Interaction of torsional and longitudinal guided waves in weakly nonlinear circular cylinders. *The Journal of the Acoustical Society of America*, *133*(5), 2541-2553.
18. Sohn, H., Lim, H. J., DeSimio, M. P., Brown, K., & Derriso, M. (2014). Nonlinear ultrasonic wave modulation for online fatigue crack detection. *Journal of Sound and Vibration*, *333*(5), 1473-1484.
19. Yang, Y., Ng, C. T., & Kotousov, A. (2019). Bolted joint integrity monitoring with second harmonic generated by guided waves. *Structural Health Monitoring*, *18*(1), 193-204.
20. Pruell, C., Kim, J. Y., Qu, J., & Jacobs, L. J. (2009). Evaluation of fatigue damage using nonlinear guided waves. *Smart Materials and Structures*, *18*(3), 035003.
21. Yang, Y., Ng, C. T., & Kotousov, A. (2018). Influence of crack opening and incident wave angle on second harmonic generation of Lamb waves. *Smart Materials and Structures*, *27*(5), 055013.
22. Pau, A., & Lanza di Scalea, F. (2015). Nonlinear guided wave propagation in prestressed plates. *The Journal of the Acoustical Society of America*, *137*(3), 1529-1540.
23. Ng, C. T., Mohseni, H., & Lam, H. F. (2019). Debonding detection in CFRP-retrofitted reinforced concrete structures using nonlinear Rayleigh wave. *Mechanical Systems and Signal Processing*, *125*, 245-256.
24. Liu, Y., Chillara, V. K., & Lissenden, C. J. (2013). On selection of primary modes for generation of strong internally resonant second harmonics in plate. *Journal of sound and vibration*, *332*(19), 4517-4528.
25. Liu, Z., Xu, Q., Gong, Y., He, C., & Wu, B. (2014). A new multichannel time reversal focusing method for circumferential Lamb waves and its applications for defect detection in thick-walled pipe with large-diameter. *Ultrasonics*, *54*(7), 1967-1976.
26. Wang, Y., & Achenbach, J. D. (2016). The effect of cubic material nonlinearity on the propagation of torsional wave modes in a pipe. *The Journal of the Acoustical Society of America*, *140*(5), 3874-3883.

27. X. Guo, D. Zhang, J. Zhang, Detection of fatigue-induced micro-cracks in a pipe by using time-reversed nonlinear guided waves: A three-dimensional model study, *Ultrasonics* **52** (2012) 912-919
28. V.K. Chillara, C.J. Lissenden, Analysis of second harmonic guided waves in pipes using a large-radius asymptotic approximation for axis-symmetric longitudinal modes, *Ultrasonics* **53** (2013) 862-869
29. Li, W., & Cho, Y. (2014). Thermal fatigue damage assessment in an isotropic pipe using nonlinear ultrasonic guided waves. *Experimental Mechanics*, *54*(8), 1309-1318.
30. Choi, G., Liu, Y., & Lissenden, C. J. (2015, July). Nonlinear guided waves for monitoring microstructural changes in metal structures. In *Pressure Vessels and Piping Conference* (Vol. 57021, p. V007T07A002). American Society of Mechanical Engineers.
31. Li, W., Deng, M., & Cho, Y. (2016). Cumulative second harmonic generation of ultrasonic guided waves propagation in tube-like structure. *Journal of Computational Acoustics*, *24*(03), 1650011.
32. Jingpin, J., Xiangji, M., Cunfu, H., & Bin, W. (2017). Nonlinear Lamb wave-mixing technique for micro-crack detection in plates. *Ndt & E International*, *85*, 63-71.
33. Ishii, Y., Biwa, S., & Adachi, T. (2018). Non-collinear interaction of guided elastic waves in an isotropic plate. *Journal of Sound and Vibration*, *419*, 390-404.
34. Li, N., Sun, J., Jiao, J., Wu, B., & He, C. (2016). Quantitative evaluation of micro-cracks using nonlinear ultrasonic modulation method. *Ndt & E International*, *79*, 63-72.
35. Hasanian, M., & Lissenden, C. J. (2018). Second order ultrasonic guided wave mutual interactions in plate: Arbitrary angles, internal resonance, and finite interaction region. *Journal of Applied Physics*, *124*(16), 164904.
36. Chen, Z., Tang, G., Zhao, Y., Jacobs, L. J., & Qu, J. (2014). Mixing of collinear plane wave pulses in elastic solids with quadratic nonlinearity. *The Journal of the Acoustical society of America*, *136*(5), 2389-2404.
37. Jiao, J., Lv, H., He, C., & Wu, B. (2017). Fatigue crack evaluation using the non-collinear wave mixing technique. *Smart Materials and Structures*, *26*(6), 065005.
38. Alston, J., Croxford, A., Potter, J., & Blanloeuil, P. (2018). Nonlinear non-collinear ultrasonic detection and characterisation of kissing bonds. *NDT & E International*, *99*, 105-116.

39. Demčenko, A., Koissin, V., & Korneev, V. A. (2014). Noncollinear wave mixing for measurement of dynamic processes in polymers: Physical ageing in thermoplastics and epoxy cure. *Ultrasonics*, *54*(2), 684-693.
40. McGovern, M. E., Buttlar, W. G., & Reis, H. (2014). Characterisation of oxidative ageing in asphalt concrete using a non-collinear ultrasonic wave mixing approach. *Insight-Non-Destructive Testing and Condition Monitoring*, *56*(7), 367-374.
41. Li, F., Zhao, Y., Cao, P., & Hu, N. (2018). Mixing of ultrasonic Lamb waves in thin plates with quadratic nonlinearity. *Ultrasonics*, *87*, 33-43.
42. Metya, A. K., Tarafder, S., & Balasubramaniam, K. (2018). Nonlinear Lamb wave mixing for assessing localized deformation during creep. *NDT & E International*, *98*, 89-94.
43. Croxford, A. J., Wilcox, P. D., Drinkwater, B. W., & Nagy, P. B. (2009). The use of non-collinear mixing for nonlinear ultrasonic detection of plasticity and fatigue. *The Journal of the Acoustical Society of America*, *126*(5), EL117-EL122.
44. Murnaghan, F. D. (1937). Finite deformations of an elastic solid. *American Journal of Mathematics*, *59*(2), 235-260.
45. He, S., & Ng, C. T. (2017). Modelling and analysis of nonlinear guided waves interaction at a breathing crack using time-domain spectral finite element method. *Smart Materials and Structures*, *26*(8), 085002.
46. Staszewski, W. J., Lee, B. C., & Traynor, R. (2007). Fatigue crack detection in metallic structures with Lamb waves and 3D laser vibrometry. *Measurement Science and Technology*, *18*(3), 727.
47. Pavlakovic, B., & Lowe, M. J. S. (2000). DISPERSE: A system for generating dispersion curves, User's Manual. *Imperial College London*.
48. Yang, Y., Ng, C. T., & Kotousov, A. (2019). Second-order harmonic generation of Lamb wave in prestressed plates. *Journal of Sound and Vibration*, *460*, 114903.
49. Wan, X., Tse, P. W., Xu, G. H., Tao, T. F., & Zhang, Q. (2016). Analytical and numerical studies of approximate phase velocity matching based nonlinear S0 mode Lamb waves for the detection of evenly distributed microstructural changes. *Smart Materials and Structures*, *25*(4), 045023.

Chapter 4

Nonlinear Torsional Guided-Wave Mixing in Pipes Buried in Soil

(Paper 3, Manuscript)

Carman Yeung[a] , Ching Tai Ng[a], Yuncheng He[b]

[a] School of Civil, Environmental and Mining Engineering, The University of Adelaide, SA 5005, Australia

[b] Joint Research Centre for Engineering Structure Disaster Prevention and Control, Guangzhou University, Guangdong 510006, China

Publication:

Yeung, C., Ng, C. T & He, Y. (2020). Nonlinear torsional guided-wave mixing in pipes buried in soil.

Statement of Authorship

Title of Paper	Nonlinear torsional guided wave mixing in pipes buried in soil
Publication Status	☐ Published ☐ Accepted for Publication ☐ Submitted for Publication ☑ Unpublished and Unsubmitted work written in manuscript style
Publication Details	Yeung, C., Ng, C. T. & He, Y. (2020). Nonlinear torsional guided wave mixing in pipes buried in soil.

Principal Author

Name of Principal Author (Candidate)	Carman Yeung		
Contribution to the Paper	Undertook literature review, developed numerical models, designed experimental tests, performed data analysis and prepared manuscript		
Overall percentage (%)	80%		
Certification:	This paper reports on original research I conducted during the period of my Higher Degree by Research candidature and is not subject to any obligations or contractual agreements with a third party that would constrain its inclusion in this thesis. I am the primary author of this paper.		
Signature		Date	10 Sep 2020

Co-Author Contributions

By signing the Statement of Authorship, each author certifies that:

I. the candidate's stated contribution to the publication is accurate (as detailed above);
II. permission is granted for the candidate in include the publication in the thesis; and
III. the sum of all co-author contributions is equal to 100% less the candidate's stated contribution.

Name of Co-Author	Ching-Tai Ng		
Contribution to the Paper	Supervised development of numerical model, reviewed manuscript and prepared for submission		
Signature	1	Date	9 Sep 2020

Name of Co-Author	Yuncheng He		
Contribution to the Paper	Helped evaluate, edit and review the manuscript		
Signature		Date	10 Sep 2020

Abstract

Pipes have widespread applications, such as drainage and the conveyance of chemical products. Pipelines are usually installed underground, which increases the difficulty in structural integrity inspection. Numerous studies have investigated the phenomenon of guided wave propagation in buried pipes and its interaction with different types of damage, e.g. corrosion and thermal damage. However, very limited studies focused on utilising guided-wave mixing techniques for embedded pipes. This study develops a three-dimensional (3D) finite element (FE) model incorporating strain energy function to analyse wave-mixing phenomena in pipes embedded in soil. To characterise nonlinear features due to guided-wave mixing, combinational harmonic generation, the 3D FE model is used when two torsional guided waves interact with each other. The numerical results are then verified by experimentally measured data which show that the amplitude in frequency-domain exhibits sharp drop due to the energy leakage in the existence of soil medium at fundamental frequencies, second and combinational harmonics.

Keywords: Guided-wave mixing; material nonlinearity; finite element; buried pipes; combinational harmonic; second harmonic

4.1 Introduction

Reliable non-destructive testing (NDT) provides early precaution for failure of underground structures, for example gas pipe leakage. The current commonly used practice is to send labours to manholes for pipeline integrity inspection. This approach is time consuming and unreliable. Moreover, it disturbs the normal operation of pipelines. Cost effective pipe inspection techniques can be developed using ultrasonic guided waves. This kind of techniques can inspect the internal conditions of pipeline with less manpower. The use of guided wave in damage detection has attracted significant interest due to its high sensitivity to small and different types of damage, and long inspection distance [1]. In the last decade, the study of guided wave mainly paid attention on linear features [2], for example time-of-flight information and amplitudes of scattered wave from damage, to detect damage in composite laminates [3], concrete [4], metallic plates [5] and pipes [6]. Different guided wave-based inspection systems were also developed for in-service integrity inspection and structural health monitoring.

4.1.1 Pipes embedded in soil

Detection of underground burst pipeline is a challenging issue. The use of guided waves for inspecting cylindrical structures covered by other materials were investigated in the literature [7-8]. Compared with bare pipes, the performance of wave propagation in pipes embedded in soil becomes more unpredictable since the energy propagated by guided waves can be radiated to the surrounding materials [9]. The amount of energy leakage is determined by the material properties from two sources: the pipeline itself and the surrounding medium. Ahmad *et al.* [10] investigated whether guided wave signals would be weakened when pipes were buried in soil. They compared the received signals with and without soil surrounded. The results showed that

the embedded pipes have weaker signals due to energy leakage. Muggleton *et al.* [11] derived and extended equations for guided wave propagation with the consideration of the ambient soil behaviour. They used a numerical model to validate assumptions in their analytical model for studying the effect of soil. Leinov *et al.* [12] studied the energy leakage of guided wave in buried pipes. They also investigated the effect of soil properties in the cases of loose sand, compacted sand, saturated sand and drained sand. They demonstrated that soil condition has direct influence on the amplitude of propagating waves. Therefore, one of the purposes of this study is to further elaborate the application of guided wave in embedded pipes.

4.1.2 Linear and nonlinear features of guided waves in pipes

Linear features of guided waves have been widely used to detect and characterise different types of macro-scale defects [13-14]. Most of the linear guided wave methods rely on baseline subtraction method to extract the scattered wave from damage for damage detection and identification in plate-like and pipe-like structures [6]. Sun *et al.* [15] used torsional guided wave to detect damage in pipes. The nondispersive nature is one of the advantages of using the torsional guided wave. Related studies focusing on torsional wave were carried out because it is applicable for long range damage detection in pipelines [16]. The preferential frequency range for exciting the fundamental mode of torsional wave is about 100kHz [17]. The reason is that higher excitation frequency generates many unwanted wave modes, which make the analysis of wave signals become very challenging. Different studies were carried out to investigate the propagation and scattering of the torsional guided wave because it is sensitive to different types of defects, e.g. corrosion [18] and delamination [19]. However, the use of linear guided wave approach is limited to investigate micro-scale defects. The deficiency of recognising small damage in structures through linear guided waves can be overcome by using

nonlinear features, for example higher harmonic and combinational harmonic generation of guided waves. These nonlinear features of guided wave are sensitive to micro-scale damage. Waveform distortion in time-domain response is not noticeable to identify micro-scale defects. In the literature, studies focused on analysing higher harmonic generation in frequency-domain provided an aid to scrutinise the nonlinear characteristics of the guided wave signals [20,21], which can potentially be a baseline free approach.

Material nonlinearity [22-23] detects material imperfections which is distributed along the entire structure. The microstructural change results in the generation of second harmonic which is an important indicator for damage detection. The nonlinear behaviour of the material is the focus of this paper since the amplitudes of the harmonic waves provide information for revealing the nonlinearity at the early stage of health status of the structure. Nonlinear features of guided wave propagation in pipes have been studied in the literature. The second harmonic generation of longitudinal wave in pipes was studied by Chillara and Lissenden [24] theoretically. The criteria for generating higher harmonics in cylinders using different wave modes were investigated [25]. Li and Cho [26] carried out fatigue tests to experimentally demonstrate the cumulative effect of second harmonic in pipes. It was demonstrated that laboratory equipment, such as signal amplifiers, data acquisition systems and transducers, can potentially generate non-damage related higher harmonics, which can contaminate the damage related higher harmonics [27].

4.1.3 Wave mixing technique

The method of mixing distinct frequencies of ultrasonic waves can effectively rule out the nonlinearities generated by the equipment [27]. When the waves interact with each other, combinational harmonics at sum or difference excitation frequencies are generated if micro-

scale defects exist in the materials [28-29]. Wave mixing technique is applicable to different types of guided waves and can be used for damage interrogation. Bulk wave is one of the popular used waves for NDT. It was studied in the early development of guided-wave mixing in the literature [30-32]. The strategy of sending two wave sources into a structure is utilised to identify imperfect bonds for localised nonlinear behaviour in different materials [33-34]. Nevertheless, bulk waves are only applicable for inspecting a relatively small area compared to other types of guided wave, such as Lamb waves and shear horizontal (SH) waves.

As compensation, Lamb waves provide larger inspection area while they have multiple wave modes to be selected for damage prognosis [35]. Metya *et al.* [36] investigated nonlinear characteristics of two nonlinear Lamb waves interaction during creeping. They also studied the material nonlinearity experimentally to predict the structural failure. The other study of Shan *et al.* [37] carried out a wave mixing analysis subjected to material nonlinearity in plates by exciting two SH waves using collinear interaction approach. A recent study [38] on guided wave mixing associated with thermal aging has been carried out to measure the nonlinear parameter at adhesive joints. The aforementioned research demonstrated that wave mixing technique is a good candidate for the development of damage detection in solid blocks and plate-like structures. However, the studies were limited to bulk wave and Lamb wave only. There were only few studies investigated the guided-wave mixing in circular waveguide, e.g. pipes [39]. Despite that, very limited studies focused on nonlinear guided-wave mixing in buried pipes. Pipes, in practice, are installed underground or covered by insulated materials for working in high temperature areas. It would be valuable and essential for carrying out a research on the application of wave mixing technique in buried pipes. The objective of this paper is to gain fundamental insights into the nonlinear features (i.e. combinational harmonics and second harmonics) of guided-wave mixing in pipes embedded in soil.

The paper is organised as follows. The theory of weakly nonlinear elasticity describes the material nonlinearity of the embedded pipes and the choice of frequency range is explained in Section 4.2. The three-dimensional (3D) scanning laser vibrometer setup is presented, and the experimental results regarding to the combinational harmonic and the second harmonics are analysed in Section 4.3. A 3D finite element (FE) model of a pipe buried in soil is established in Section 4.4. Meanwhile, the experimentally observed nonlinear guided wave phenomenon in guided-wave mixing and single frequency excitation are endorsed by the FE simulation results. In Section 4.5, parametric studies are carried out to analyse the change in the combinational harmonic at the sum of the excitation frequencies and the second harmonics from two single frequencies under different stages of thermal fatigue damage. Finally, conclusions are given in Section 4.6.

4.2 Theoretical background

4.2.1 Weakly nonlinear elasticity theory

A set of constitutive equations in the basis of continuum mechanics is employed to simulate the behaviour of material nonlinearity in guided wave propagation. The definition of nonlinear strain energy function is from deformation gradient **F** which is expressed as [40-41]

$$\mathbf{F} = \frac{\partial \mathbf{y}}{\partial \mathbf{Y}} \tag{4.1}$$

where **y** and **Y** are the positions for material particle in the current and reference configuration, respectively. The rotation tensor **R** and the right stretch tensor **U** can constitute **F** from polar decomposition.

$$\mathbf{F} = \mathbf{RU} \tag{4.2}$$

where **R** is orthogonal and det **R**=1. The elastic strain energy function *W* can be interpreted by Cauchy stress tensor.

$$\boldsymbol{\sigma} = \mathrm{J}^{-1}\mathbf{F}\frac{\partial \mathrm{W}}{\partial \mathbf{F}} \tag{4.3}$$

where J^{-1} is the inverse of Jacobian function.

The right Cauchy-Green strain tensor **C** can be decomposed by **F**. It can also use to express the term Green-Lagrange deformation tensor **E**.

$$\mathbf{C} = \mathbf{F}^{\mathrm{T}}\mathbf{F} \tag{4.4}$$

$$\mathbf{C} = 2\mathbf{E} + \mathbf{I} \tag{4.5}$$

where **I** is the identical matrix.

By using Murnaghan model [42], the governing equation for weakly nonlinear elasticity is employed. The strain energy function *W* is a function of **E** and is defined in Equation 4.6. The Murnaghan's third order elastic coefficients (*l*, *m* and *n*) in the equation describe the nonlinear response of materials.

$$W(\mathbf{E}) = \frac{1}{2}(\lambda + 2\mu)i_1^2 + \frac{1}{3}(l + m)i_1^2 - 2mi_1i_2 - 2\mu i_2 + ni_3 \tag{4.6}$$

where $i_1 = tr\mathbf{E}$, $i_2 = 0.5[i_1^2 - tr(\mathbf{E})^2]$ and $i_3 = det\mathbf{E}$ are the principal invariants; λ and μ are the Lamé elastic constants.

4.2.2 Excitation signals used in FE simulations and experiments

Two different types of excitation signals were used in the FE simulations and experiments, (i) excitation signal combined two signals at different central frequencies (f_1 & f_2) (Figure 4.1c), and (ii) two excitations with different single central frequency f_1 and f_2 (Figures 4.1a and 4.1b), respectively. Figure 4.1c shows the excitation signal generated by combining two sinusoidal tone burst pulses modulated by a Hann window. These two tone burst pulses have 15 cycles

and 10 cycles and are at different frequencies f_1 (110 kHz) and f_2 (70 kHz), respectively (Figures 4.1a and 4.1b). The use of low frequency excitation is to avoid generating undesired wave modes for practical applications, and hence, the cumulative effect is not considered since the condition of phase matched is not applicable to the choice at low frequency range in this study. In the time-domain, there is no time delay between excitation signals with central frequencies f_1 and f_2. In the guided-wave mixing, the second harmonics and the combinational harmonics can be generated due to material nonlinearity. The focus of the present study is to investigate and compare the combinational harmonic generation due to torsional guided wave mixing at the sum of the excitation frequency and the second harmonic generation due to the torsional guided wave at single central frequency.

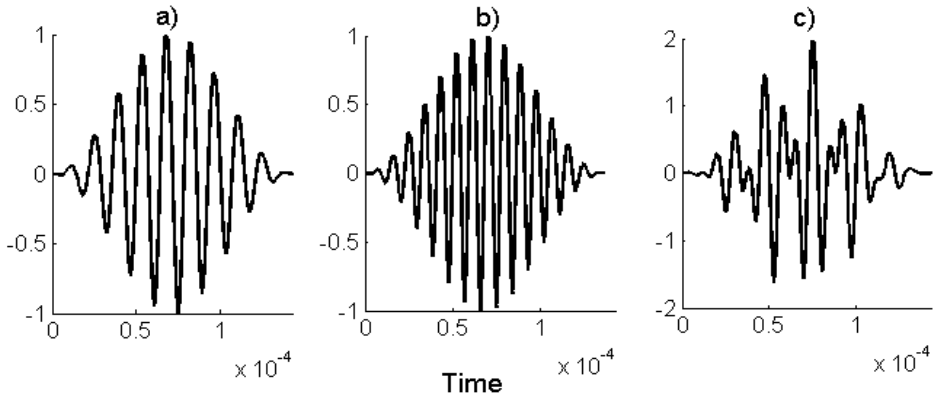

Figure 4.1 The excitation signal with central frequency at a) f_2 and b) f_1, and c) combined excitation signal (f_1 & f_2)

4.3 Experimental study of nonlinear features of guided wave in pipes embedded in soils

4.3.1 Experimental setup

A pipe of 1m long was embedded into the soil to replicate the embedment condition for experimental study. The pipe was placed in a rectangular wooden box with dimensions of 230×220×250mm^3 (Figure 4.2). The container walls were fabricated by 20mm thick plywood plates. The wall thickness of the pipe is 3mm and the outer diameter is 25mm. Circular apertures were created at the container walls located at both sides. The circular apertures are slightly bigger than the pipe diameter so that the pipe can be inserted into the wooden box.

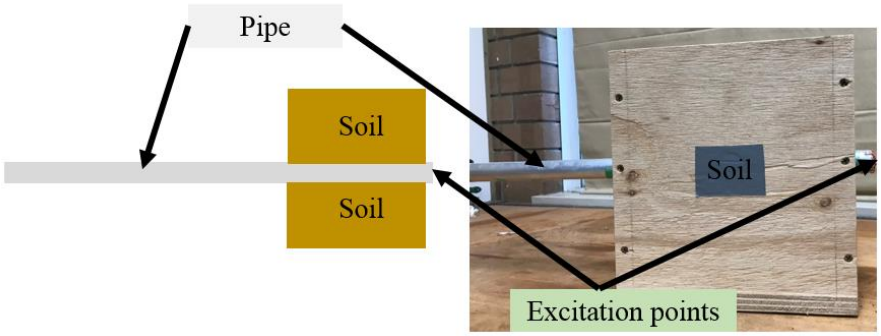

Figure 4.2 Schematic diagram (left) and experimental setup (right) of pipe embedded in soil

The selected cohesionless soils were then backfilled into the wooden box. The soils are clean sands (well-graded and dry) [9] with less than 5% fine soils (i.e. finer than 75μm). The sand for an experimental test was prepared by a sieving test with the use of the mechanical sieve shaker. The soil distribution grading is plotted in Figure 4.3. The particle size was controlled not to be coarser than 1.18mm. The major sizes of the sand particles are between 0.6mm to 1.18mm. Clay and slit were filtered out in the sieving process.

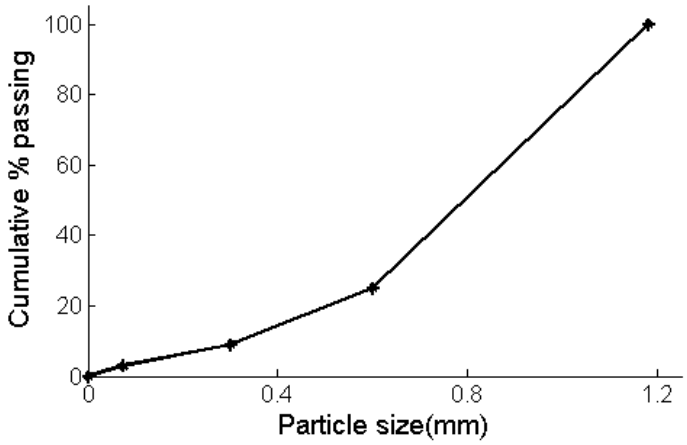

Figure 4.3 Grain size distribution chart for soil used in the experimental study

Four equally spaced shear piezoceramic transducers (shear plates) with thickness of 1mm were bonded at the end of the pipe and they are actuated at the same time using identical excitation signal to generate fundamental torsional guided waves. The cross-section of the shear piezoceramic transducers is $6\times6mm^2$. The signal was generated by a function generator and then amplified to 120V through an amplifier (KROHN-HITE 7500) before it was transmitted to the shear piezoceramic transducers. 3D scanning laser vibrometer was used to measured guided wave signals at 350mm from the left end of the pipe. The measurement was carried out in the pipes with and without soil. To improve the signal quality, reflective coating was sprayed on the surface of the specimen. Low-pass filter and an averaging of 1500 times were adopted to improve the signal-to-noise ratio. Velocity signals were recorded in *y*- and *z*-direction (Figure 4.4), which represent tangential and longitudinal directions, respectively. The measured time-domain signals are normalised by their maximum amplitude and transformed to frequency-domain for analysis using Fast Fourier Transform (FFT). This allows comparison between the data in bare pipe and embedded pipe. The schematic diagram in Figure 4.4 indicates the laser vibrometer and pipe embedment experimental setup.

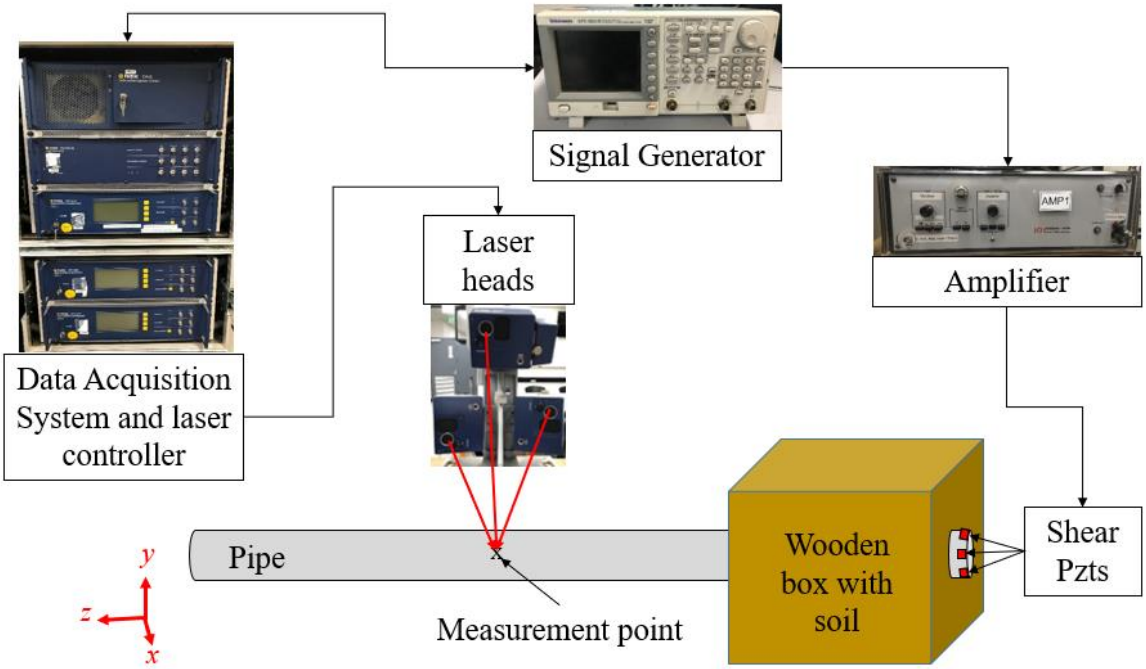

Figure 4.4 Experimental setup for measurement using laser Doppler vibrometer

4.3.2 Combinational harmonic generation due to guided-wave mixing

Figure 4.5 shows the time-domain and frequency-domain signals measured at the location of 350mm in tangential and longitudinal directions, which capture the torsional guided wave and longitudinal guided wave, respectively. The mixed frequency response in the absence of soil is indicated by grey dotted line, while the response of the pipe embedded in soil is indicated by black solid line. Figures 4.5a and 4.5b indicate an obvious decrease of the signals when soils were added to the pipe. To have a substantial analysis, frequency spectra are plotted in Figure 4.5c and 4.5d in which vertical dashed lines are used to indicate the excitation frequencies f_1 and f_2, and combinational harmonic at sum frequency ($f_1 + f_2$). Aside from the fundamental frequencies at f_1 and f_2, the sum frequency component ($f_1 + f_2$ = 180 kHz) is significantly indicated in longitudinal direction (Figure 4.5d). But no harmonics are induced in tangential direction, which means torsional guided wave does not contain these nonlinear features (Figure

4.5c). The results in Figure 4.5 also indicate that the energy of the guided wave radiates to the surrounding soil when the guided waves propagate along the pipe. The amplitudes of components at the excitation frequencies f_1 and f_2, and combinational harmonic at the sum frequency ($f_1 + f_2$) for the specimen buried in soil are reduced because a portion of the wave energy leaks to the surrounding soil. The phenomenon of amplitude reduction at the excitation frequencies is consistent with the findings from the study carried out by Leinov *et al.* [9], who showed that guided wave leakage can be caused by surrounding soil.

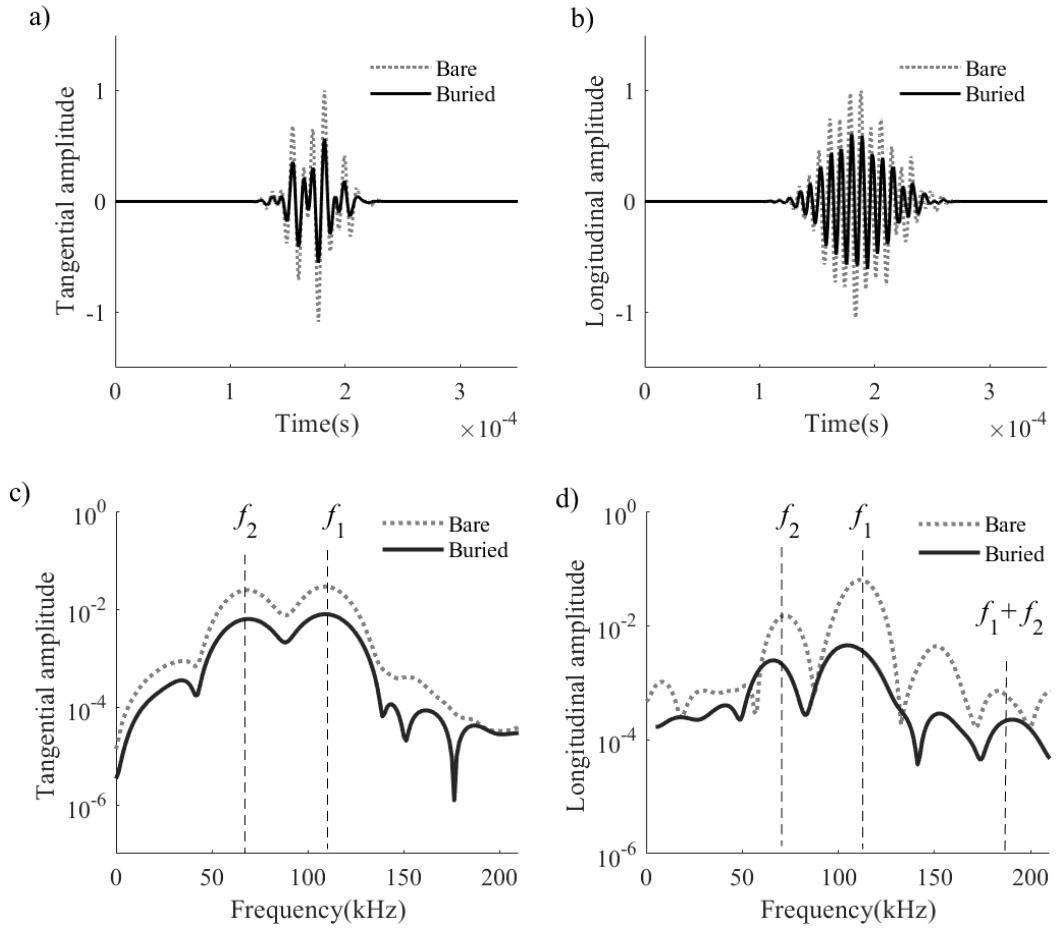

Figure 4.5 a) & b) Time-domain and c) & d) Frequency-domain velocity responses measured by 3D scanning laser in bare pipe and buried pipe in tangential and longitudinal directions

4.3.3 Second harmonic generation due to single central frequency guided wave

The generation of second harmonic due to single frequency torsional guided wave has been researched in the literature [25]. The study showed that the fundamental mode of torsional guided wave T(0,1) propagation in a pipe with material nonlinearity can induce second harmonic of longitudinal wave due to shear coupling, which can be measured from velocity in longitudinal direction using laser vibrometer.

Similar experiments were carried out in the same bare pipe and buried pipe specimen using excitation signal with a single frequency. Figures 4.6a and 4.6b show the results obtained using excitation with a single central frequency at f_1 = 110kHz and f_2 = 70kHz, respectively. The results in Figures 4.6a and 4.6b indicate that the measured signals also contain second harmonic ($2f_1$ or $2f_2$). These results are consistent with results reported in the literature [24]. Compared the results in Figures 4.6a and 4.6b, the amplitude at excitation frequencies and second harmonic frequencies in the buried pipe are smaller than those in bare pipe.

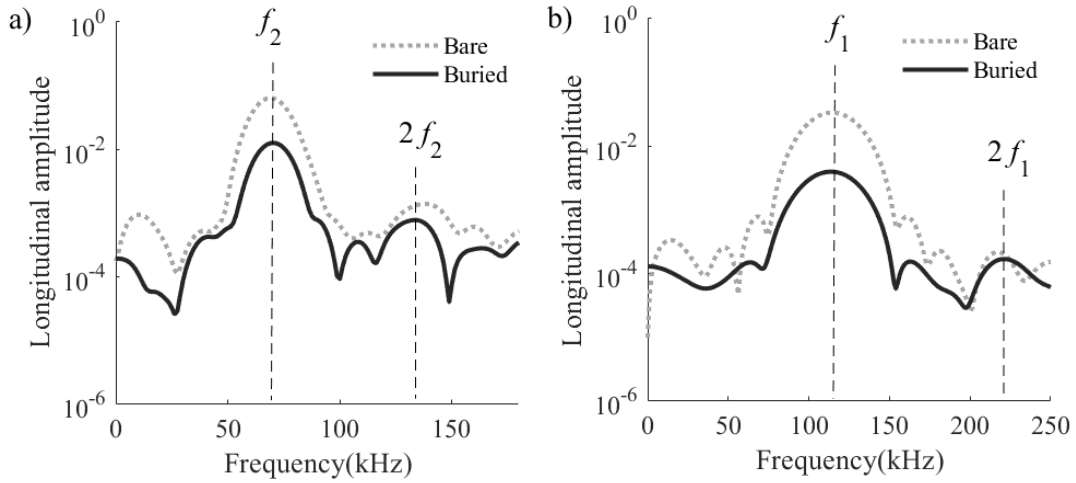

Figure 4.6 Experimental data with and without soil at a) 70kHz and b) 110kHz

4.4 3D FE simulations of pipe with material nonlinearity

4.4.1 Modelling of pipe embedded in soil

The combinational harmonic generation due to guided-wave mixing and the second harmonic generation due to single central frequency torsional guided wave in pipes with embedding soil are simulated using 3D FE models in this section. The Murnaghan model is implementable with the aid of a user defined subroutine in some commercial FE packages, for example ABAQUS. The third order constants in the equation can apply to the three-dimensional FE model. The stress $\hat{\boldsymbol{\sigma}}$ used in ABAQUS is represented as Green-Naghdi rate of Cauchy stress $\boldsymbol{\sigma}$ [40,43].

$$\hat{\boldsymbol{\sigma}} = \mathbf{R}^{\mathrm{T}}\boldsymbol{\sigma}\mathbf{R} \tag{4.7}$$

$$\boldsymbol{\sigma} = \mathrm{J}^{-1}\mathbf{F}\mathbf{Q}\mathbf{F}^{\mathrm{T}} \tag{4.8}$$

where $\mathbf{Q} = \frac{\partial \mathrm{W}(\mathbf{E})}{\partial \mathbf{E}}$ is the second Piola-Kirchhoff stress and $\mathrm{J}^{-1} = \det(\mathbf{F})$. Equation 4.7 can transform to

$$\hat{\boldsymbol{\sigma}} = \mathrm{J}^{-1}\mathbf{U}\mathbf{Q}\mathbf{U}^{\mathrm{T}} \tag{4.9}$$

This theory is applied to ABAQUS/Explicit through the user material subroutine VUMAT to model the influence of intrinsic material nonlinearity on guided wave simulation. The variables, which are material properties, are adopted to define the mechanical constitutive behaviour from the strain energy function. The self-defined parameters **F** and **U** are replaced by the new calculations in each time step. The subroutine updates the stress at the end of each time step and carries on proceeding to the following integration step.

An aluminium pipe embedded in a medium of cylindrical sand layer was modelled using ABAQUS. The cross-section of the pipe and the cylindrical sand layer with FE mesh are

shown in Figure 4.7. Tie constraint with surface-to-surface option was assigned between the nodes located at the external surface of the pipe and the internal surface of the cylindrical sand layer. The dimensions of the modelled pipe are the same as the pipe used in the experiment described in the previous experimental section. The thickness of the sand layer is 27.5mm. The properties of aluminium and sand are listed in Tables 4.1 and 4.2. The VUMAT subroutine of the weakly nonlinear elasticity theory was implemented to simulate the nonlinear features of guided wave in ABAQUS. Linear and reduced integration elements (C3D8R) were used in the FE model. To ensure the accuracy of the FE simulations, there are at least 20 FE elements in the smallest wavelength considered in this study. The element sizes used in the pipe and the cylindrical sand layer are approximately equal to $0.5\times0.5\times0.5mm^3$. The duration of simulation was selected to be 0.5ms.

Lamé constants (GPa)	λ	56.68
	μ	27.13
3rd order elastic constants (GPa)	l	-277.74
	m	-351.7
	n	-573.94
Density (kg/m^3)	ρ	2700

Table 4.1 Material properties of aluminium pipe used in the FE simulation

Density, ρ (kg/m^3)	1620
Torsional velocity, v_T (m/s)	150
Longitudinal velocity, v_L (m/s)	800

Table 4.2 Sand properties used in the FE simulation

The excitation force was applied tangentially at the circumference of the pipe. The signal in longitudinal way was captured in z-direction. It is notable that the signal in torsional

position was collected at point X (Figure 4.7) since it has the largest signal magnitude of the torsional wave in *y*-direction. An excitation of mixed frequency and single frequencies at f_1=110kHz and f_2=70kHz, with 15 cycles and 10 cycles respectively, were applied for verification. Figure 4.8 is the snapshot of the time-domain signal to visualise the wave propagation and it is simulated by the FE pipe model embedded in soil. As shown in the figure, a portion of energy is absorbed by the soil media when the wave travels out of the soil zone.

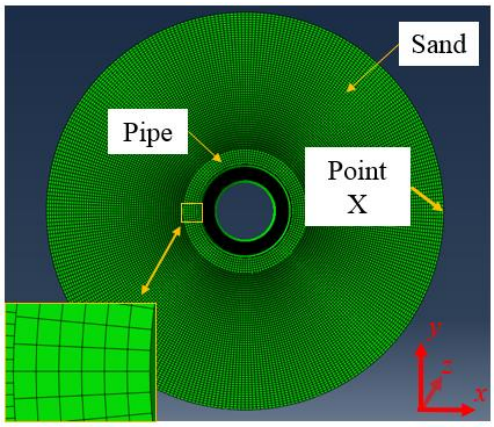

Figure 4.7 Cross-section of the 3D FE model of the pipe embedded in soil

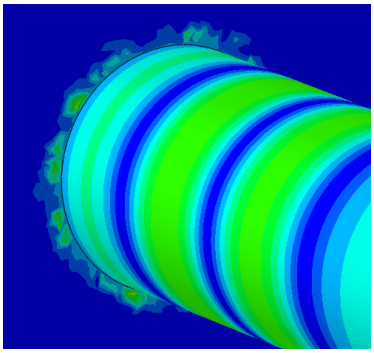

Figure 4.8 A snapshot of FE simulated displacements when the wave is propagating from soil to the pipe

4.4.2 Validation of 3D FE Model

4.4.2.1 Group velocity

The group velocity dispersion curves shown in Figure 4.9 are the fundamental torsional mode T(0,1) (circle markers) and the longitudinal mode L(0,1) (square markers), respectively. The velocity signals were recorded at five measurement points and the excitation frequencies considered were from 70kHz to 430kHz in steps of 40kHz. The velocities were calculated using the data measured at the five measurement points and they were then averaged. Two consecutive measuring points have a distance of 50mm. There is good agreement between the theoretical calculations in DISPERSE [44] (lines) and the numerical results in the 3D FE model (markers) for both torsional and longitudinal waves.

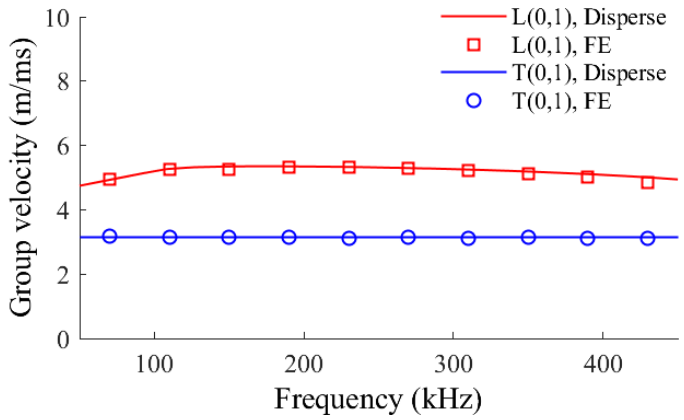

Figure 4.9 Group velocity dispersion curves calculated by DISPERSE and 3D FE simulations

4.4.2.2 Combinational harmonic

The pre-mixed incident torsional waves were excited at the one end of the pipe. It propagates and then enters the sand region. In the numerical study, the excitation signal with combined frequency f_1 = 110kHz and f_2 = 70kHz, was adopted as in the section describing experimental setup. Experimentally measured and FE simulated time-domain signals were obtained at 500mm from the excitation location. The signals were normalised by the maximum amplitude to allow direct comparison and were then transformed to frequency-domain using FFT. Figure 4.10a and Figure 4.10b are the frequency-domain signals in tangential direction and longitudinal direction, respectively. As shown in Figure 4.10b, the combinational harmonic at

the sum frequency ($f_1 + f_2$) is highlighted by dashed lines. As shown in the interested bandwidth, both FE and experimental results have no combinational harmonic in the signals obtained in tangential direction. In longitudinal direction, the combinational harmonic at the sum frequency can be observed due to the shear coupling effect [25]. The wave energy leakage from the pipe to the sand is observed in Figure 4.10. The FE model with embedded sand validates the experimental work. The amplitudes of buried pipe are always lower than that of bare pipe in both FE and experimental data.

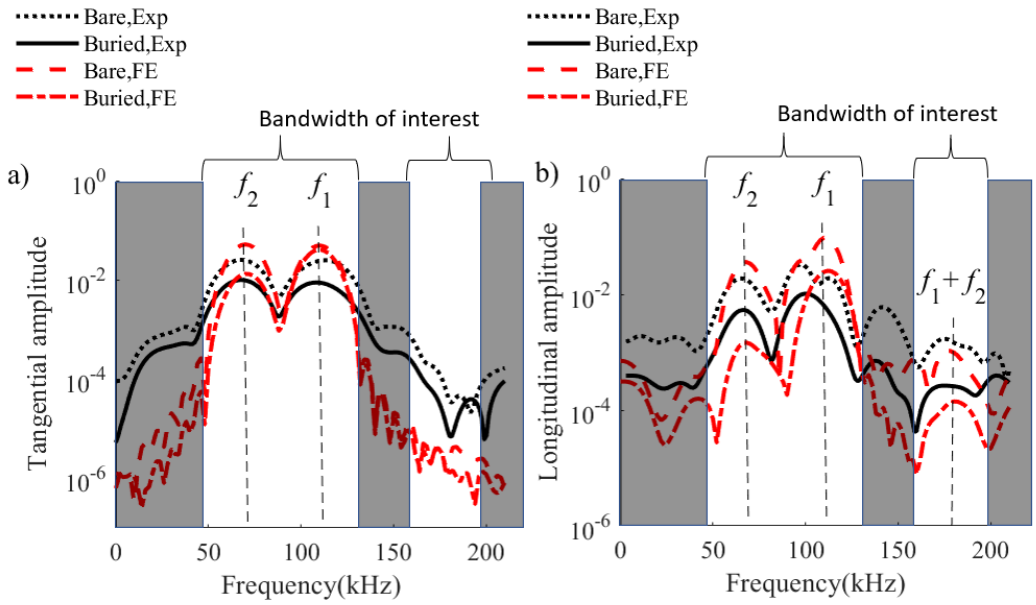

Figure 4.10 Frequency-domain signals of bare and buried pipes obtained from FE simulations and experiments in a) tangential and b) longitudinal directions

4.4.2.3 Second harmonic

Figure 4.11 shows the frequency-domain signals in longitudinal direction using excitation signals with single central frequency f_1 = 110kHz and f_2 = 70kHz, respectively. The results in Figure 4.11 indicate that the amplitudes at f_1 f_2, $2f_1$ and $2f_2$ drop significantly in the experimental measured data and the FE simulated outcome in the presence of soil. It should be noted that the combinational harmonic at sum frequency is absent since the excitation signals are single

central frequency wave. Therefore, there is no guided-wave mixing effect and only the second harmonics are induced in the longitudinal direction.

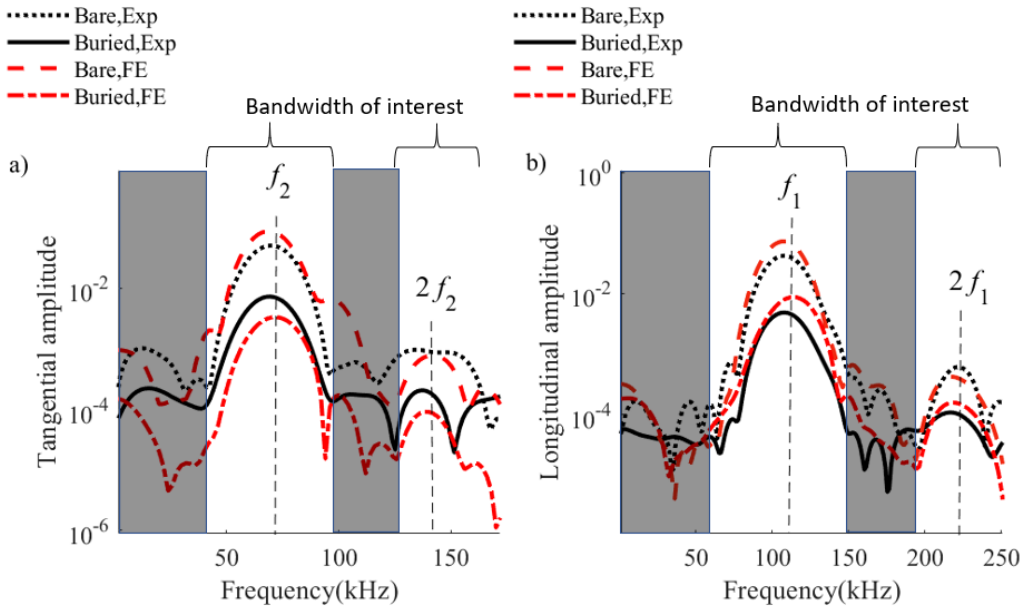

Figure 4.11 Experimental and FE simulated signals at single frequencies a) 70kHz and b) 110kHz in in longitudinal direction

Figure 4.12 is the extraction of percentage reduction at the interested peaks from Figure 4.10 and 4.11. By comparing the amplitudes between the bare and buried pipe, the percentage reductions of longitudinal guided wave amplitude due to the pipe embedded in soil were calculated for both FE and experimental results. The figure calculates the reduction for both the combinational harmonic at sum frequency using wave mixing excitation signal and the second harmonic using single frequency excitation signals. The analysis quantifies the amount of energy leakage in percentage for damage assessment which shows very good agreement between FE and experimental results. The wave energy in the pipe is radiated when the pipe is embedded into the other medium, such as sand. Therefore, the amplitudes of the wave decrease significantly.

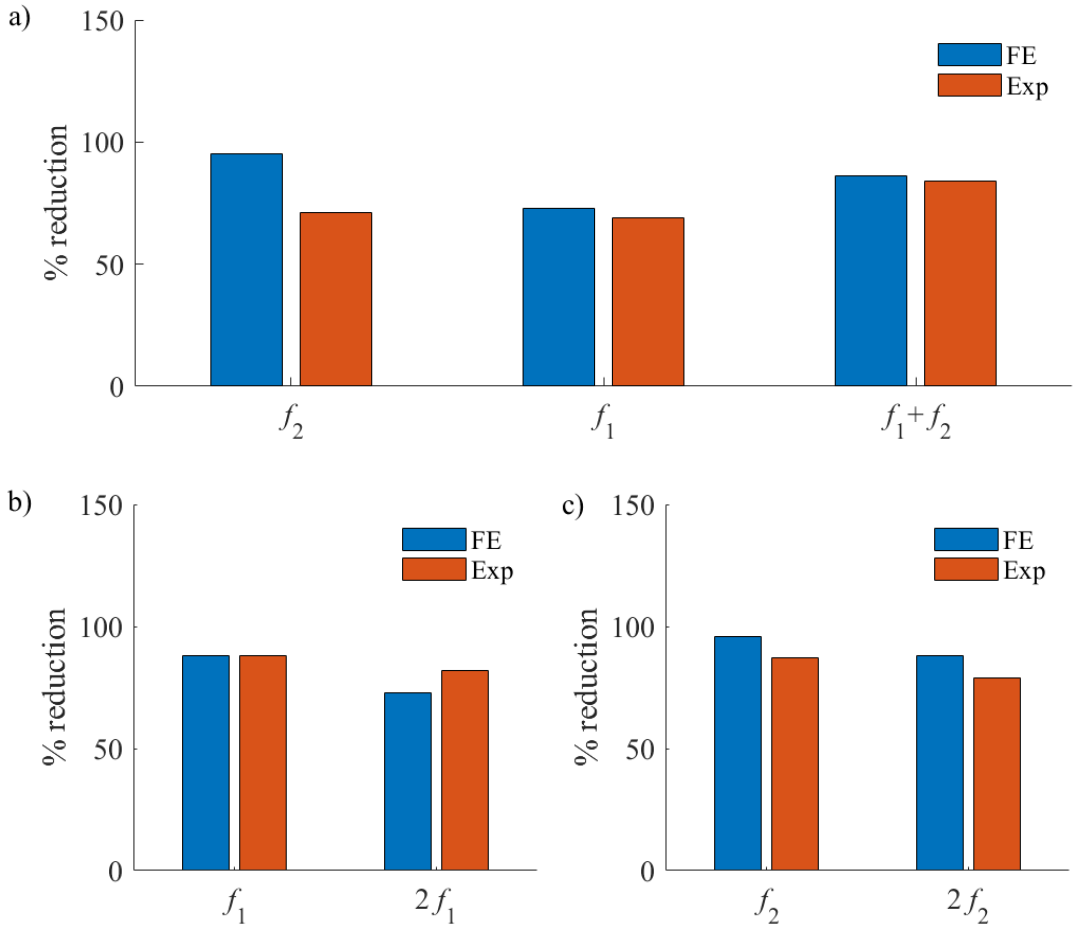

Figure 4.12 Percentage reduction of longitudinal wave amplitude due to the pipe embedded in soil using a) wave mixing at f_1 & f_2, b) single frequency at f_1, and c) single frequency at f_2 as the excitation signal

4.5 Influence of thermal aging on nonlinear features in buried pipe

Thermal aging in pipes has the possibility to result in material degradation [45]. One of the investigation methods is to implement nonlinear guided wave mixing which can determine the conditions of aging stage at different damage levels [38]. The level of material degradation is varied with aging times. Thus, the combinational harmonic and the second harmonic are sensitive to different stages of thermal aging. The nonlinear parameters β'_{comb} and β'_{second} can

describe the combinational harmonic at sum frequency and second harmonic at single frequency [40] which are defined as

$$\beta'_{comb} = \frac{A_{f_1+f_2}}{A_{f_1}A_{f_2}} \tag{4.10}$$

$$\beta'_{second} = \frac{A_2}{A_1^2} \tag{4.11}$$

where A_{f_1}, A_{f_2}, $A_{f_1+f_2}$, A_1 and A_2 represent the magnitude of the incident waves at f_1 and f_2, the combinational harmonic at sum frequency, the fundamental frequency and the corresponding second harmonic, respectively.

The nonlinear parameters vary with the increase of thermal aging cycle. A set of experimental data contributed from a recent research [46] is used in this section and is summarised in Table 4.3. The authors introduced heat treatment on the specimens at a temperature of 220°C for different time period, which were 0, 20, 40, 60, 120, 600 and 6000 minutes. The data precisely recorded the change of the third-order elastic constants of aluminium at different level of thermal aging.

		Thermal aging time						
		0 min	20 min	40 min	60 min	120 min	600 min	6000 min
Third-order elastic constants (GPa)	*l*	-277.74	-311.84	-335.04	-292.79	-298.73	-318.1	-264.67
	m	-351.7	-381.54	-381.28	-357.23	-338.61	-366.92	-360.23
	n	-573.94	-380.15	-524.92	-916.65	-441.99	-379.99	-571.76

Table 4.3 Material properties of aluminium at different level of thermal aging cycle [46]

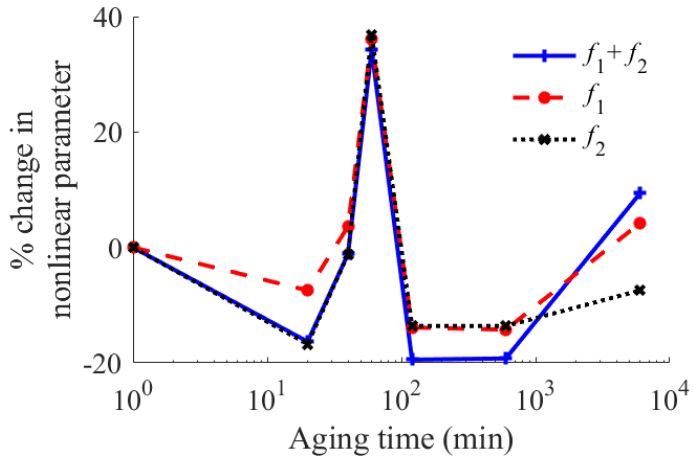

Figure 4.13 Relationship between the percentage change of nonlinear parameters and thermal aging time

Figure 4.13 is the percent change of nonlinear parameter as a function of thermal aging time for the combinational harmonic at sum frequency and the second harmonics from the respective single frequencies. Under the thermal effect, the variations of all three curves (percentage of change of nonlinear parameter) have similar trend but different values. Comparing the results with Kim *et al.* [46], they have the same tendency in the nonlinear parameters as a function of thermal aging time. The percentage of change of nonlinear parameter initially drop in the first 20 minutes. They then increase more than 30% and reach sharp peaks at 60 minutes. The curves indicate that the percentage change of the nonlinear parameter for the combinational harmonic at sum frequency and the second harmonics gradually decrease in 2 hours. They eventually grow slowly to the final stage approximately after 4 days. By comparing the percentage change of the nonlinear parameters, the combinational harmonic has a higher value than or nearly the same value as the second harmonics among the seven aging times. Thus, the percentage change of β'_{comb} is more sensitive to that of β'_{second} in most of the cases. As discussed before, the guide-wave mixing can avoid the unwanted instrumentation nonlinearity. This makes the combination harmonic attractive to be used for damage detection.

4.6 Conclusions

The phenomenon of guided-wave mixing in pipes in the presence and absence of embedded soil has been investigated numerically and experimentally in this paper. The energy leakage of guided wave propagation is due to surrounding materials. The existence of combinational harmonic at sum frequency in longitudinal direction is generated by mixing two fundamental torsional waves. The energy leakage causes reduction in the amplitudes of the frequency-domain signals, especially amplitude at the excitation frequencies, the second harmonics at single central frequencies, and the combinational harmonic at sum frequency. The data collected in the experiment is in good agreement with the results of FE simulations. In the experiments, the guided wave signals were measured by the 3D scanning laser Doppler vibrometer. The results of the 3D FE model of a pipe embedded in sand have shown that the loss in energy is led by the interaction between the pipe and the sand. A study of the effect of thermal aging on the combinational harmonic at sum frequency and the second harmonics have shown that the change in β'_{comb} is relatively sensitive to that in β'_{second}. The findings presented in this study provide improved physical insight into the nonlinear features of guided wave mixing due to material nonlinearity in buried pipes.

Acknowledgement

This work was supported by the Australian Research Council through DP200102300. The support is greatly appreciated.

4.7 References

1. Mariani, S., Nguyen, T., Phillips, R. R., Kijanka, P., Lanza di Scalea, F., Staszewski, W. J., ... & Carr, G. (2013). Noncontact ultrasonic guided wave inspection of rails. *Structural Health Monitoring*, *12*(5-6), 539-548.
2. Mitra, M., & Gopalakrishnan, S. (2016). Guided wave based structural health monitoring: A review. *Smart Materials and Structures*, *25*(5), 053001.
3. Su, Z., Cheng, L., Wang, X., Yu, L., & Zhou, C. (2009). Predicting delamination of composite laminates using an imaging approach. *Smart Materials and Structures*, *18*(7), 074002.
4. Ng, C. T., Mohseni, H., & Lam, H. F. (2019). Debonding detection in CFRP-retrofitted reinforced concrete structures using nonlinear Rayleigh wave. *Mechanical Systems and Signal Processing*, *125*, 245-256.
5. Hu, X., Ng, C. T., & Kotousov, A. Scattering characteristics of quasi-Scholte waves at blind holes in metallic plates with one side exposed to water. *NDT & E International*, *117*, 102379.
6. Nasedkina, A. A., Alexiev, A., & Malachowski, J. (2016). Numerical simulation of ultrasonic torsional guided wave propagation for pipes with defects. In *Advanced Materials* (pp. 475-488). Springer, Cham.
7. Pavlakovic, B. N., Lowe, M. J. S., & Cawley, P. (2001). High-frequency low-loss ultrasonic modes in imbedded bars. *J. Appl. Mech.*, *68*(1), 67-75.
8. Kwun, H., Kim, S. Y., Choi, M. S., & Walker, S. M. (2004). Torsional guided-wave attenuation in coal-tar-enamel-coated, buried piping. *Ndt & E International*, *37*(8), 663-665.
9. Leinov, E., Lowe, M. J., & Cawley, P. (2016). Ultrasonic isolation of buried pipes. *Journal of Sound and Vibration*, *363*, 225-239.

10. Ahmad, R., Banerjee, S., & Kundu, T. (2009). Pipe wall damage detection in buried pipes using guided waves. *Journal of pressure vessel technology*, *131*(1).
11. Muggleton, J. M., Kalkowski, M., Gao, Y., & Rustighi, E. (2016). A theoretical study of the fundamental torsional wave in buried pipes for pipeline condition assessment and monitoring. *Journal of Sound and Vibration*, *374*, 155-171.
12. Leinov, E., Lowe, M. J., & Cawley, P. (2015). Investigation of guided wave propagation and attenuation in pipe buried in sand. *Journal of Sound and Vibration*, *347*, 96-114.
13. Valle, C., Qu, J., & Jacobs, L. J. (1999). Guided circumferential waves in layered cylinders. *International Journal of Engineering Science*, *37*(11), 1369-1387.
14. Coccia, S., Bartoli, I., Marzani, A., di Scalea, F. L., Salamone, S., & Fateh, M. (2011). Numerical and experimental study of guided waves for detection of defects in the rail head. *NDT & E International*, *44*(1), 93-100.
15. Sun, Z., Zhang, L., Gavigan, B., Hayashi, T., & Rose, J. L. (2003, January). Ultrasonic flexural torsional guided wave pipe inspection potential. In *ASME Pressure Vessels and Piping Conference* (Vol. 16974, pp. 29-34).
16. Dobson, J., & Cawley, P. (2017). The scattering of torsional guided waves from Gaussian rough surfaces in pipework. *The Journal of the Acoustical Society of America*, *141*(3), 1852-1861.
17. Carandente, R., & Cawley, P. (2012). The effect of complex defect profiles on the reflection of the fundamental torsional mode in pipes. *NDT & E International*, *46*, 41-47.
18. Lee, J. H., & Lee, S. J. (2009). Application of laser-generated guided wave for evaluation of corrosion in carbon steel pipe. *Ndt & E International*, *42*(3), 222-227.
19. Bingham, J., & Hinders, M. (2009). Lamb wave detection of delaminations in large diameter pipe coatings. *The Open Acoustics Journal*, *2*(1).
20. Pau, A., & Lanza di Scalea, F. (2015). Nonlinear guided wave propagation in prestressed plates. *The Journal of the Acoustical Society of America*, *137*(3), 1529-1540.
21. Sohn, H., Lim, H. J., DeSimio, M. P., Brown, K., & Derriso, M. (2014). Nonlinear ultrasonic wave modulation for online fatigue crack detection. *Journal of Sound and Vibration*, *333*(5), 1473-1484.
22. Deng, M. (2003). Analysis of second-harmonic generation of Lamb modes using a modal analysis approach. *Journal of applied physics*, *94*(6), 4152-4159.
23. Müller, M. F., Kim, J. Y., Qu, J., & Jacobs, L. J. (2010). Characteristics of second harmonic generation of Lamb waves in nonlinear elastic plates. *The Journal of the Acoustical Society of America*, *127*(4), 2141-2152.

24. Chillara, V. K., & Lissenden, C. J. (2013). Analysis of second harmonic guided waves in pipes using a large-radius asymptotic approximation for axis-symmetric longitudinal modes. *Ultrasonics*, *53*(4), 862-869.
25. Liu, Y., Khajeh, E., Lissenden, C. J., & Rose, J. L. (2013). Interaction of torsional and longitudinal guided waves in weakly nonlinear circular cylinders. *The Journal of the Acoustical Society of America*, *133*(5), 2541-2553.
26. Li, W., & Cho, Y. (2014). Thermal fatigue damage assessment in an isotropic pipe using nonlinear ultrasonic guided waves. *Experimental Mechanics*, *54*(8), 1309-1318.
27. Jingpin, J., Xiangji, M., Cunfu, H., & Bin, W. (2017). Nonlinear Lamb wave-mixing technique for micro-crack detection in plates. *Ndt & E International*, *85*, 63-71.
28. Ishii, Y., Biwa, S., & Adachi, T. (2018). Non-collinear interaction of guided elastic waves in an isotropic plate. *Journal of Sound and Vibration*, *419*, 390-404.
29. Hasanian, M., & Lissenden, C. J. (2018). Second order ultrasonic guided wave mutual interactions in plate: Arbitrary angles, internal resonance, and finite interaction region. *Journal of Applied Physics*, *124*(16), 164904.
30. Liu, M., Tang, G., Jacobs, L. J., & Qu, J. (2012). Measuring acoustic nonlinearity parameter using collinear wave mixing. *Journal of applied physics*, *112*(2), 024908.
31. Demčenko, A., Koissin, V., & Korneev, V. A. (2014). Noncollinear wave mixing for measurement of dynamic processes in polymers: Physical ageing in thermoplastics and epoxy cure. *Ultrasonics*, *54*(2), 684-693.
32. McGovern, M. E., Buttlar, W. G., & Reis, H. (2014). Characterisation of oxidative ageing in asphalt concrete using a non-collinear ultrasonic wave mixing approach. *Insight-Non-Destructive Testing and Condition Monitoring*, *56*(7), 367-374.
33. Jiao, J., Lv, H., He, C., & Wu, B. (2017). Fatigue crack evaluation using the non-collinear wave mixing technique. *Smart Materials and Structures*, *26*(6), 065005.
34. Alston, J., Croxford, A., Potter, J., & Blanloeuil, P. (2018). Nonlinear non-collinear ultrasonic detection and characterisation of kissing bonds. *NDT & E International*, *99*, 105-116.
35. Li, F., Zhao, Y., Cao, P., & Hu, N. (2018). Mixing of ultrasonic Lamb waves in thin plates with quadratic nonlinearity. *Ultrasonics*, *87*, 33-43.
36. Metya, A. K., Tarafder, S., & Balasubramaniam, K. (2018). Nonlinear Lamb wave mixing for assessing localized deformation during creep. *NDT & E International*, *98*, 89-94.

37. Shan, S., Hasanian, M., Cho, H., Lissenden, C. J., & Cheng, L. (2019). New nonlinear ultrasonic method for material characterization: Codirectional shear horizontal guided wave mixing in plate. *Ultrasonics*, *96*, 64-74.
38. Ju, T., Achenbach, J. D., Jacobs, L. J., & Qu, J. (2019). Nondestructive evaluation of thermal aging of adhesive joints by using a nonlinear wave mixing technique. *NDT & E International*, *103*, 62-67.
39. Yeung, C., & Ng, C. T. (2020). Nonlinear guided wave mixing in pipes for detection of material nonlinearity. *Journal of Sound and Vibration*, *485*, 115541.
40. Yang, Y., Ng, C. T., & Kotousov, A. (2019). Second-order harmonic generation of Lamb wave in prestressed plates. *Journal of Sound and Vibration*, *460*, 114903.
41. He, S., Ng, C. T., & Yeung, C. (2020). Time-domain spectral finite element method for modeling second harmonic generation of guided waves induced by material, geometric and contact nonlinearities in beams. *International Journal of Structural Stability and Dynamics*, *20*(10), 2042005.
42. Murnaghan, F. D. (1937). Finite deformations of an elastic solid. *American Journal of Mathematics*, *59*(2), 235-260.
43. Yang, Y., Ng, C. T., Mohabuth, M., & Kotousov, A. (2019). Finite element prediction of acoustoelastic effect associated with Lamb wave propagation in pre-stressed plates. *Smart Materials and Structures*, *28*(9), 095007.
44. Pavlakovic, B., & Lowe, M. J. S. (2000). DISPERSE: A system for generating dispersion curves, User's Manual. *Imperial College London*.
45. Yan-Xun, X., Fu-Zhen, X., & Ming-Xi, D. (2010). Evaluation of thermal degradation induced material damage using nonlinear Lamb waves. *Chinese Physics Letters*, *27*(1), 016202.
46. Kim, J., Kim, C. S., Song, D. G., & Jhang, K. Y. (2020). Ultrasonic nonlinearity parameter in uniaxial stress condition. *Ultrasonics*, *102*, 105914.

Chapter 5

Torsional Guided Wave Mixing with Acoustoelastic Effect in Tubular Structures with Weakly Material Nonlinearity

(Paper 4, Manuscript)

Carman Yeung and Ching Tai Ng,

School of Civil, Environmental and Mining Engineering

The University of Adelaide, SA 5005, Australia

Publication:

Yeung, C. & Ng, C. T. (2020). Torsional guided wave mixing with acoustoelastic effect in tubular structures with weakly material nonlinearity.

Statement of Authorship

Title of Paper	Torsional guided wave mixing with acoustoelastic effect in tubular structures with weakly material nonlinearity.
Publication Status	☐ Published ☐ Accepted for Publication ☐ Submitted for Publication ☑ Unpublished and Unsubmitted w ork w ritten in manuscript style
Publication Details	Yeung, C. & Ng, C. T. (2020). Torsional guided wave mixing with acoustoelastic effect in tubular structures with weakly material nonlinearity.

Principal Author

Name of Principal Author (Candidate)	Carman Yeung		
Contribution to the Paper	Undertook literature review, developed numerical models, designed experimental tests, performed data analysis and prepared manuscript		
Overall percentage (%)	80%		
Certification:	This paper reports on original research I conducted during the period of my Higher Degree by Research candidature and is not subject to any obligations or contractual agreements with a third party that would constrain its inclusion in this thesis. I am the primary author of this paper.		
Signature		Date	10 Sep 2020

Co-Author Contributions

By signing the Statement of Authorship, each author certifies that:

i. the candidate's stated contribution to the publication is accurate (as detailed above);

ii. permission is granted for the candidate in include the publication in the thesis; and

iii. the sum of all co-author contributions is equal to 100% less the candidate's stated contribution.

Name of Co-Author	Ching-Tai Ng		
Contribution to the Paper	Supervised development of numerical model, reviewed manuscript and prepared for submission		
Signature		Date	9 Sep 2020

Abstract

Acoustoelastic effect of single frequency guided wave propagation in structures has been well-established. However, this effect on guided wave mixing has not been fully explored. This study carries out a numerical and experimental study of torsional guided wave mixing with consideration of acoustoelastic effect in tubular structures and weakly material nonlinearity. A three-dimensional (3D) finite element (FE) model is proposed to simulate the effect of stress on guided wave mixing in tubular structures. The FE model takes into account the nonlinear strain energy function and the theory of incremental deformation. A series of numerical case studies are carried out to investigate the change of group velocity in the pre-stressed tubular structures subjected to different levels of loading. Experiments are also carried out to measure and compare the nonlinear features, such as combinational harmonics and second harmonics. The results show that the generation of combinational harmonic at sum frequency due to material nonlinearity provides valuable stress information for tubular structures, which is also useful for damage diagnosis.

Keywords: Acoustoelasticity, guided wave, wave mixing, torsional wave, circular hollow section

5.1 Introduction

Cylindrical hollow section has many applications in engineering structures, such as truss members. Stress is developed when the members are subjected to operational loading, such as tensile and compressive forces. The effect of stress is unavoidable in these tubular structures. The non-destructive evaluation (NDE) of the applied, residual and thermally-induced stresses, along with the non-destructive detection of damage plays an important role in ensuring the integrity of structures.

Ultrasonic guided wave has been used for NDE and to interrogate the life expectancy of a structure. It has the capability of long-distance inspection [1] and provides in-situ online monitoring for inaccessible locations [2]. The techniques using guided wave have been evolved from linear guided wave to nonlinear guided wave in recent years. In the literature, studies on linear guided wave mainly focused on the analysis of wave scattering and mode conversion effect at defect [3]-[4]. The low frequency excitation of guided wave signal, below 250 kHz, in tubular structures is more practical in real applications [5] since less wave modes are induced in the low frequency range. For nonlinear guided wave, the studies emphasised on the investigation of higher harmonic generation in frequency-domain at early stage of damage [6]-[8]. Higher harmonic generation in cylindrical-like structures has been the major focus in area of nonlinear guided waves [9]-[10]. An analytical study carried out by Liu *et al.* [11] showed that only secondary harmonic in longitudinal direction due to shear coupling is generated when the primary wave mode is torsional wave.

5.1.1 Acoustoelasticity on guided waves

Guided wave can potentially be used in structures under pre-stressed conditions, which has acoustoelastic effect influencing the wave speeds. The study of acoustoelastic guided waves has been the subject of research over the last decade [12]-[16]. Pioneering contributions had Murnaghan [17] who wrote a book on interpreting finite deformation theory and utilising third order elastic modulus. Biot [18] determined the fundamental difference between the stress-free and initially stressed condition, and established wave equations for wave propagation in pre-stressed media. The effect of pre-existing stress has focused on measuring the velocity change of ultrasonic wave in different structures, such as wire strands [19] and pipes [20]. Hirao *et al.* [21] studied the acoustoelastic effect on Rayleigh wave. They reported that Rayleigh wave was no longer non-dispersive in the presence of non-uniform stress loading. Lu *et al.* [22] presented a comprehensive study on applied and residual stresses. They took into account the stress effect in the wave propagation and velocity calculation. Pau and Di Scalea [23] developed an analytical model for nonlinear guided wave to monitor the stress condition in structures.

There has been increasing research interests on nonlinear guided wave due to its high sensitivity to micro defects. Some recent works (Mohabuth *et al.* [24] and Yang *et al.* [25]) applied the theory of incremental deformation to study the change of Lamb wave speed in a pre-stressed plate. Yang *et al.* [26] also carried out an investigation on the nonlinear features of Lamb wave (i.e. the generation of second harmonic) under acoustoelastic effect in pre-stressed plates.

5.1.2 Guided wave mixing

Guided wave mixing is known as the interaction of more than one guided wave with different central frequencies in a structure. The combinational harmonics, which are the sum and

difference of the fundamental excitation frequencies, are generated due to the interaction of the waves. The study of guided wave with single central frequency encounters an obstacle in differentiating material nonlinearity from other unwanted nonlinearities, such as nonlinearities from coupling media and data acquisition system [27]. This problem can be overcome by guided wave mixing since the combinational harmonics are not affected by the instrumentation.

Guided wave mixing has been studied for different types of structures, such as plates [28] and concretes [29]. Some pioneer works in this field are Liu *et al.* [30], who generated a longitudinal wave and a shear wave in elastic solids and measure the acoustic nonlinearity parameter. McGovern *et al.* [31] used bulk wave mixing in non-collinear direction to study the nonlinear response in concrete. Research on mixing of Lamb waves in plates has been conducted for some time. To study microscopic imperfections, Hasanian and Lissenden [32] derived an analytical solution for Lamb wave mixing phenomenon. Li *et al.* [33] introduced one-way mixing approach in thin plates to study the interaction between symmetric and anti-symmetric Lamb waves. Shan *et al.* [34] used two shear horizontal waves with collinear interaction approach to interrogate the effect of material nonlinearity in plates. A recent research conducted by Yeung and Ng [35] has experimentally demonstrated the generation of the combinational harmonic at sum and difference frequencies in pipes. Despite the literature have shown the benefits of using wave mixing for damage detection, the acoustoelastic effect on guided wave mixing has not been investigated. The objective of this paper is to carry out numerically and experimentally studies on torsional guided wave mixing in tubular structures under pre-stressed conditions.

The organisation of this paper begins with the theoretical background of acoustoelasticity with the consideration of material nonlinearity in Section 5.2. The three-dimensional (3D) finite element (FE) tubular model with the implementation of pre-loading effect at both ends is described in Section 5.3. This study investigates the selected frequency

range and the application of the nonlinear strain function in the FE model. Verification for acoustoelastic effect in the change of speed is provided. The effect of material nonlinearity with acoustoelasticity on linear and nonlinear features of guided wave are also compared in this section. Section 5.4 is the experimental investigation for validating the FE model. Section 5.5 presents a series of numerical case studies considering different levels of loading. Finally, conclusions are drawn in Section 5.6.

5.2 Theory of nonlinear guided waves under acoustoelastic effect

This section consists of two parts describing the generation of second harmonic and combinational harmonic in structures under pre-stressed condition. The concept of finite deformation in a structure with weakly nonlinear elasticity is based on based continuum mechanics.

5.2.1 Acoustoelastic effect

The superimposition of incremental motions on a finite homogeneous deformation is expressed by a set of governing equations for pre-stressed elastic solids [36]. By considering a hyperelastic material in an isotropic medium, we define α_r as free-of-stress configuration (reference) and α_c stressed configuration (current). The Cartesian coordinates $\boldsymbol{X}$ and $\boldsymbol{x}$ are the respective material points in the initial stage and finial stage, respectively. The deformation gradient from α_r to α_c is expressed by $\mathbf{F} = \mathrm{Grad}\,\boldsymbol{x}$. The local measure ($J$ = det $\mathbf{F}$ > 0) represents the volume change in the material. The other expressions for the deformation gradient tensor **F** and the local measure J are

$$\mathbf{F} = \mathbf{VR} = \mathbf{RU} \tag{5.1}$$

where **V**, **U** and **R** denote as left stretch, right stretch and orthogonal tensors.

The strain energy function *W* can be co-related to **F** via the principal invariants of the right Cauchy-Green deformation tensor **C**

$$\mathbf{C} = \mathbf{F}^{\boldsymbol{T}}\mathbf{F} = \mathbf{U}^{\mathbf{2}} \tag{5.2}$$

$$I_1 = tr\mathbf{C},\ I_2 = \tfrac{1}{2}[(tr\mathbf{C})^2 - tr(\mathbf{C})^2] \text{ and } I_3 = det\mathbf{C} \tag{5.3}$$

$$\boldsymbol{S} = \frac{\partial W}{\partial \mathbf{F}} = \sum_{i=1}^{3} W_i \frac{\partial I_i}{\partial \mathbf{F}} \tag{5.4}$$

$$\boldsymbol{A} = \frac{\partial^2 W}{\partial \mathbf{F}\partial \mathbf{F}} = \sum_{i=1}^{3} W_i \frac{\partial^2 I_i}{\partial \mathbf{F}\partial \mathbf{F}} + \sum_{i=1}^{3}\sum_{j=1}^{3} W_{ij} \frac{\partial I_i}{\partial \mathbf{F}} \otimes \frac{\partial I_j}{\partial \mathbf{F}} \tag{5.5}$$

where $I_i, i \in \{1,2,3\}$ are the principal invariants of **C**. $\boldsymbol{S}$ and $\boldsymbol{A}$ are the nominal stress tensor and elasticity tensor, respectively. The derivations in Equations (5.4) and (5.5) can refer to [37].

The symmetric Cauchy stress tensors is defined as

$$\boldsymbol{\sigma} = J^{-1}\mathbf{F}\frac{\partial W}{\partial \mathbf{F}} \tag{5.6}$$

By defining $\boldsymbol{u}(\boldsymbol{x}, t)$ to be the displacement of the material point $\boldsymbol{x}$. The incremental governing equation in a pre-stressed structure is given by

$$A_{0_{piqj}} \frac{\partial^2 u_j}{\partial x_p \partial x_p} = \rho \frac{\partial^2 u_i}{\partial t^2} \tag{5.7}$$

where $A_{0_{piqj}}$ is the Eulerian elasticity tensor in the fourth order and ρ is the mass density of the material in α_c.

5.2.2 Material nonlinearity

The change of microstructure due to material nonlinearity is for the detection of material imperfections. It describes the nonlinear behaviour of the material. The third-order strain

energy function for nonlinear guided waves is defined based on the study of Murnaghan [38]. The nonlinear strain energy function *W* can be expressed in a power series

$$W = \frac{1}{2}(\lambda + 2\mu)i_1^2 - 2mi_1i_2 - 2\mu i_2 + \frac{1}{3}(l + 2m)i_1^3 + ni_3 \tag{5.8}$$

where *l*, *m* and *n* are the third order elastic constants; λ and μ are the Lamé elastic coefficients; i_1, i_2 and i_3 are the principal invariants of the Green-Lagrange strain tensor **E**. This strain tensor is composed of the Cauchy-Green deformation tensor and the identity tensor, which is shown in Eq (5.10).

$$i_1 = tr\mathbf{E},\ i_2 = \tfrac{1}{2}[(tr\mathbf{E})^2 - tr(\mathbf{E})^2] \text{ and } i_3 = det\mathbf{E} \tag{5.9}$$

$$\mathbf{E} = \frac{1}{2}(\mathbf{C} - \mathbf{I}) \tag{5.10}$$

5.3 Three-dimensional finite element simulation

A 1m long aluminium tube was modelled by a commercial software, ABAQUS, to simulate the wave propagation and the simulated signals were analysed using different strategies. Table 5.1 shows the material properties of aluminium used in this study. The inner radius of the hollow cross-section is 9.5 mm with wall thickness of 3 mm. C3D8R elements were used to model the aluminium tube, which is a solid element with three translational degrees-of-freedom at each node. The dynamic simulation was solved by explicit integration approach [39]. The mesh size was approximately 0.6 mm × 0.6 mm × 0.6 mm. This ensures more than 20 nodes existed for the shortest wavelength of the wave considered in this study. There were five layers of elements across the wall thickness of the tube to ensure the accuracy of the wave simulation. The torsional guided waves were generated by applying tangential force at eight nodes in circumferential direction. These nodes were evenly distributed at the circumference of the left end of the tube.

Table 5.1 Material properties of aluminium used in the FE simulations

Density (kg/m^3)	ρ	2700
Lamé constants (GPa)	λ	56.68
	μ	27.13
Third order elastic constants (GPa)	l	-277.74
	m	-351.7
	n	-573.94

5.3.1 Frequency selection for guided wave mixing

The benefit of using low frequency excitation is to avoid the generation of higher order wave modes [5]. In this study, the wave mixing frequencies were selected to be f_1=70 kHz and f_2=110 kHz, respectively. The two narrow-band sinusoidal tone burst pulses at f_1 with 15 cycles and f_2 with 10 cycles were first modulated by Hann window individually. They were then added together without time delay to form a combined excitation signal for the wave mixing. Although this frequency combination does not satisfy with the phase matching condition of cumulative effect, this is not the focus in the current study. In addition to second harmonic of the individual excitation frequencies, $2f_1$ and $2f_2$, combinational harmonics at sum and difference frequencies (i.e.$f_2 \pm f_1$) were also induced due to material nonlinearity.

5.3.2 Modelling of material nonlinearity

The generation of harmonics from torsional guided wave mixing, such as second harmonics and combinational harmonics, can be simulated using the constitutive model described in the theoretical section. In this study, ABAQUS/Explicit was used for 3D FE simulations. The FE model implements a material subroutine VUMAT to simulate the effect of material nonlinearity. The stress $\hat{\boldsymbol{\sigma}}$ recognised by self-defined subroutine is on Green-Naghdi basis

$$\widehat{\boldsymbol{\sigma}} = \mathbf{R}^{\mathrm{T}}\boldsymbol{\sigma}\mathbf{R} \tag{5.11}$$

Eq (5.11) can also be interpreted in terms of the second Piola-Kirchhoff stress and the right stretch tensor.

$$\widehat{\boldsymbol{\sigma}} = \mathrm{J}^{-1}\mathbf{U}\frac{\partial W}{\partial \mathbf{E}}\mathbf{U}^{\mathrm{T}} \tag{5.12}$$

It is noted that the values in stressNew(i) will be updated at the end of the time $(t + \Delta t)$, depending on the values of the deformation gradient tensor and the right stretch tensor at the end of the last time step (t).

5.3.3 Description of the pre-loading for simulating pre-stressed condition

Quasi-static loading was applied, which allows the tubular structure to pre-stress slowly for studying the acoustoelastic effect in the 3D FE simulation. As shown in Figure 5.1, the quasi-static loading curve was gradually increased to minimize the influence on wave propagation caused by transient effect [25]. Two-stage approach was adapted in the current study as shown in Figure 5.2. In Stage 1, the duration of the simulations is 13 ms. Tensile pressure was first applied on the surface of the two ends of the tubular structure until it reached a steady state. The tensile pressure was indicated by red arrows in Figure 5.2a. In Stage 2, the combined fundamental torsional guided wave signal (f_1 and f_2) was excited at the end of the tubular structure. The yellow arrows indicate the excitation location and direction of the applied loads for generating the incident wave T(0,1) mode (Figure 5.2b).

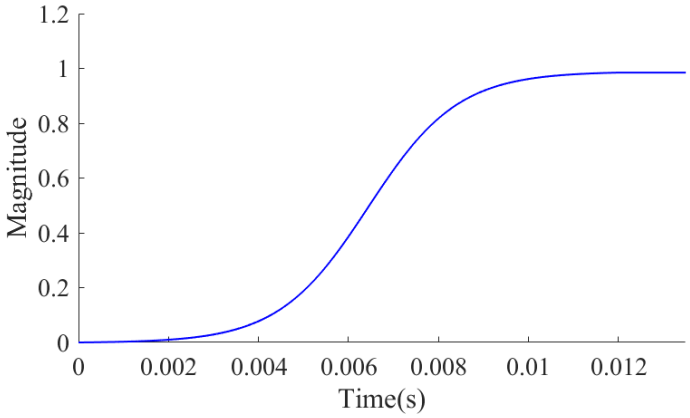

Figure 5.1 Quasi-static loading curve for simulating pre-stressed condition

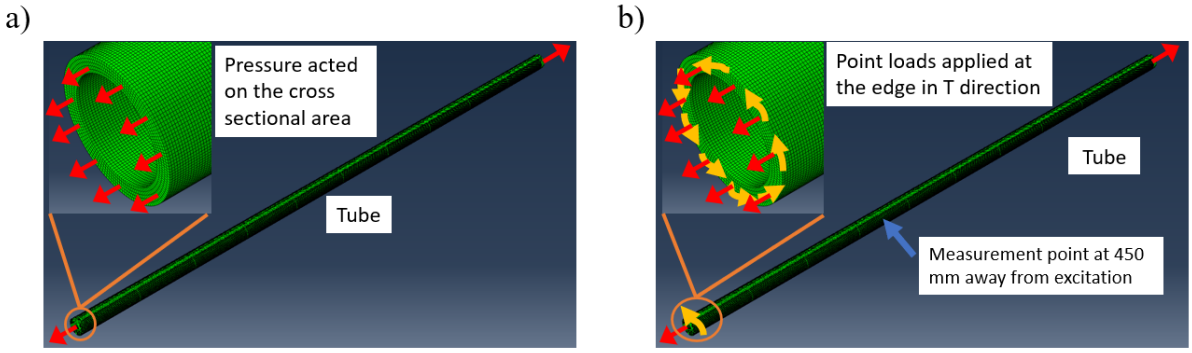

Figure 5.2 Schematic diagram of the two-stage approach, a) applied tensile pressure at both ends of the tubular structure in Stage 1 and b) excitation for generating torsional wave in Stage 2

Velocities of the nodes in tangential and longitudinal directions at 450 mm away from the excitation location were calculated. To have a better understanding of the stress effect on wave propagation in tubular structures, different magnitudes of stresses from 0 MPa to 80 MPa in steps of 20 MPa were considered in this study and the stress-strain condition is below elastic limit in all five cases.

5.3.4 Group velocity change in a pre-stressed tubular structure

The change in group velocity is one of the indications for pre-stressed structures. Figure 5.3 compares the difference of the wave velocity measured in torsional and longitudinal directions

under stress-free state and pre-stressed state at 20 MPa. As shown in Figure 5.3, an obvious shift is presented at the peaks in both torsional and longitudinal directions when a tensile pressure of 20 MPa is applied at the end of the tubular structure. It should be noted that the time-domain signal in longitudinal direction has distortion while it cannot be observed in linear response (Figs 5.4b and 5.4d). A similar distortion response to Figure 5.3 can be found in [34]. Material nonlinearity associated with self-interaction is possibly the cause of the distortion. Figure 5.4 shows the results of the reference FE simulations using linear material properties, in which the peak is not shifted for stress-free and pre-stressed state. It should be noted that the magnitude in the longitudinal motion for nonlinear signal is approximately ten times larger than that for linear signal due to the effect of material nonlinearity.

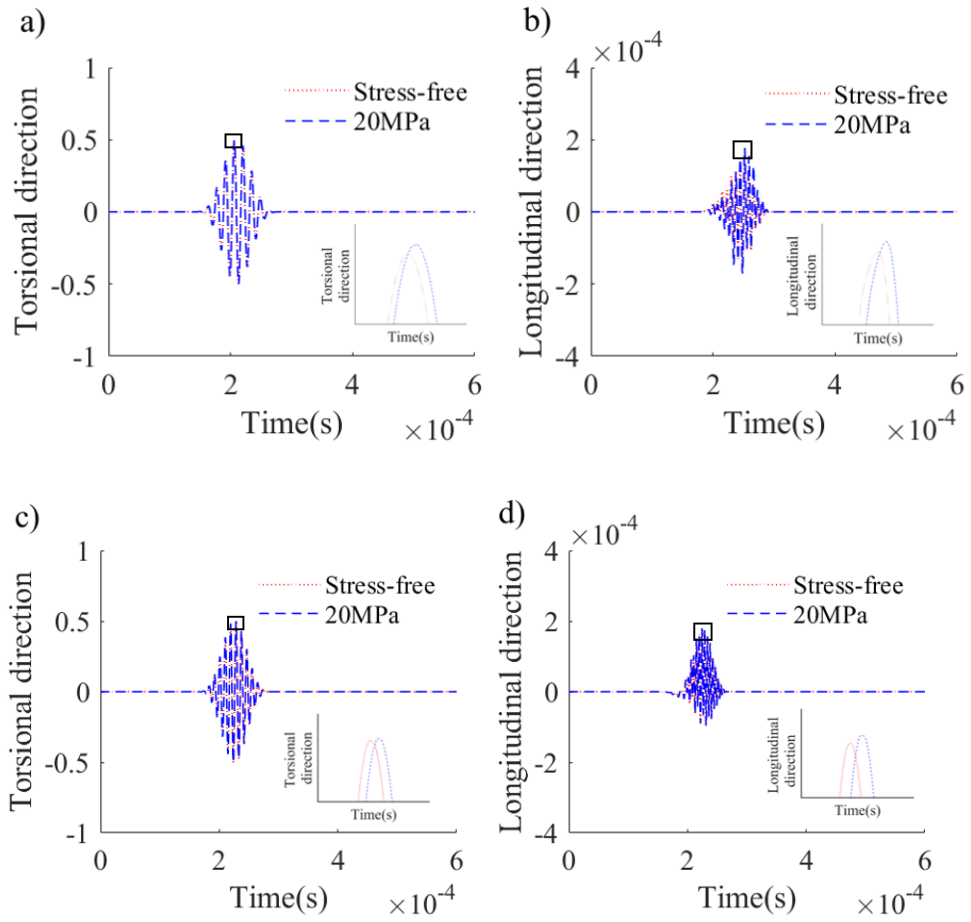

Figure 5.3 FE simulated wave propagation at stress-free and 20 MPa in torsional direction and longitudinal direction at a) & b) f_1 and c) &d) f_2 with nonlinear material properties

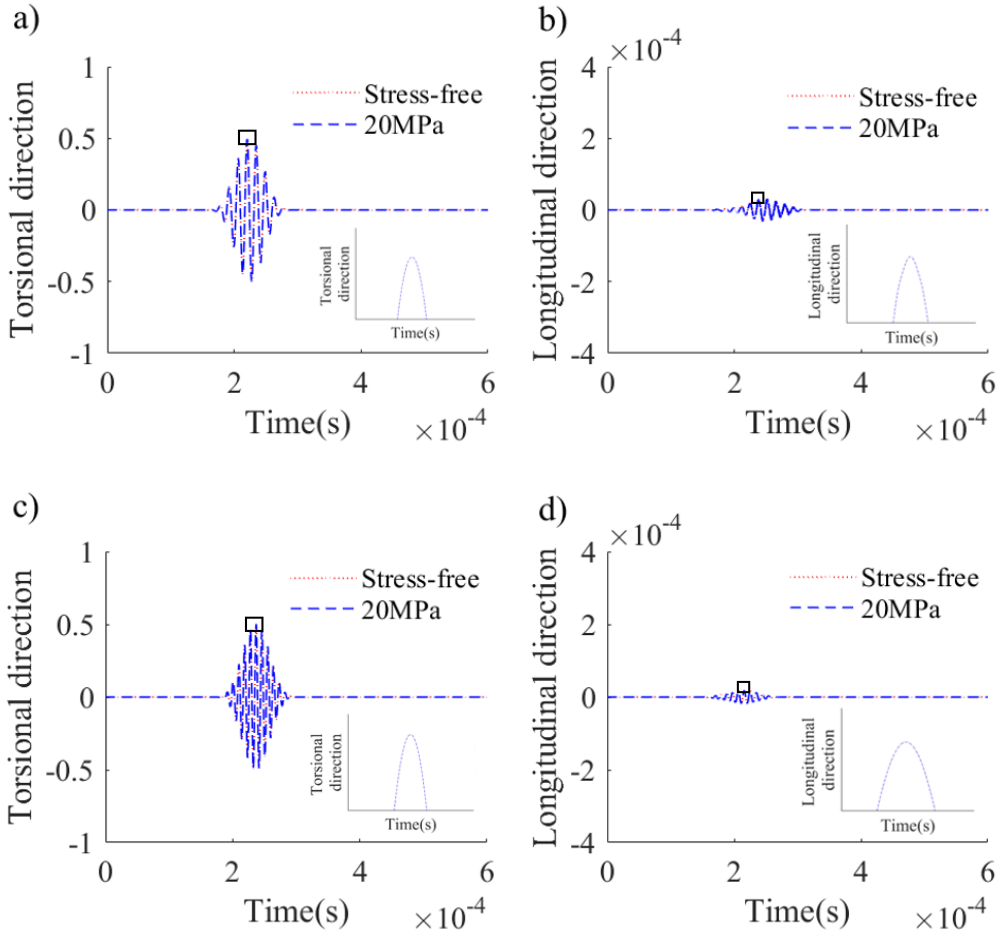

Figure 5.4 FE simulations at stress-free condition and 20 MPa in in torsional direction and longitudinal direction at a) & b) f_1 and c) & d) f_2 with linear material properties

The results of a further analysis of the acoustoelastic effect in tubular structures are shown in Figure 5.5. Since the nonlinear material behaviour with acoustoelasticity distributes along the tube, the group velocities are obtained by averaging the velocities calculated at five consecutive measurement points in the numerical results. Both torsional and longitudinal waves at frequencies f_1 (Figure 5.5a) and f_2 (Figure 5.5b) have a similar decreasing trend in the group velocity changes for the five levels of stresses. Since the change is not significant,

another analysis in frequency-domain is proposed to investigate the pre-loading effect on the combinational harmonics and the second harmonics.

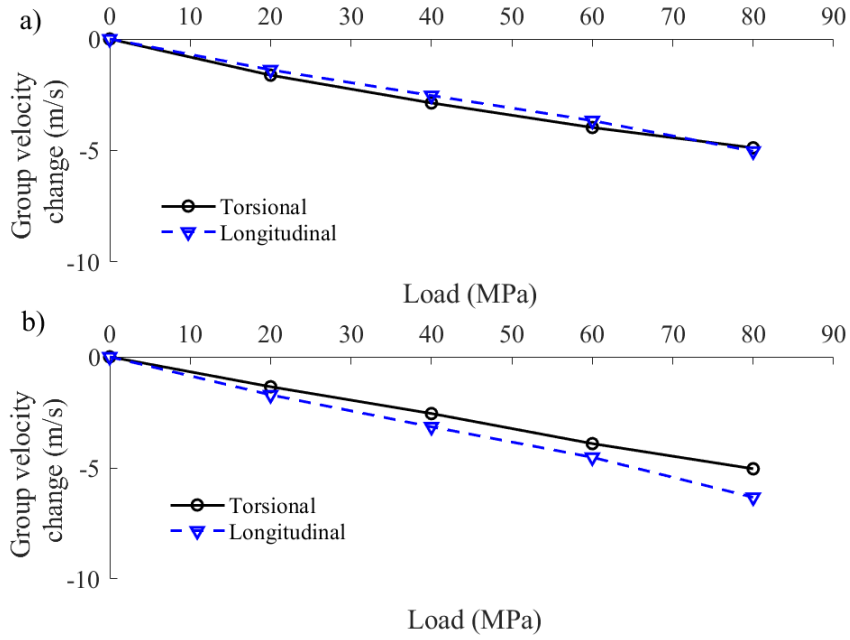

Figure 5.5 Group velocity change due to different levels of pre-stress at frequencies (a) f_1 and (b) f_2

5.3.5 Comparison of linear and nonlinear guided waves

Figure 5.6 shows the time-frequency spectra of the simulated signals using Short Time Fourier Transform (STFT). The excitation was a mixed frequency signal (f_1 and f_2) and the tubular structure was subjected to a tensile pressure of 20 MPa in linear and nonlinear signals. It is noted that nonlinear signals have a greater sensitivity to microstructural changes in a material, which gives frequencies different from the excitation frequencies. They can be second harmonics ($2f_1$ and $2f_2$) and combinational harmonics at sum and difference frequencies (f_2+f_1 and f_2-f_1). In the meantime, linear signals are only received at their primary modes (f_1 and f_2). The data in Figure 5.6 shows a similar result with the findings from the previous study [35]. Except the fundamental frequencies at f_1 and f_2, there is no other harmonics in the tangential

direction (Figures 5.6a and 5.6c) with or without the use of nonlinear strain energy function. Meanwhile, the generation of higher and combinational harmonics at frequencies $2f_1$, $2f_2$, f_2+f_1 and f_2-f_1 are observed in the longitudinal direction due to the shear coupling phenomenon from material nonlinearity (Figure 5.6d).

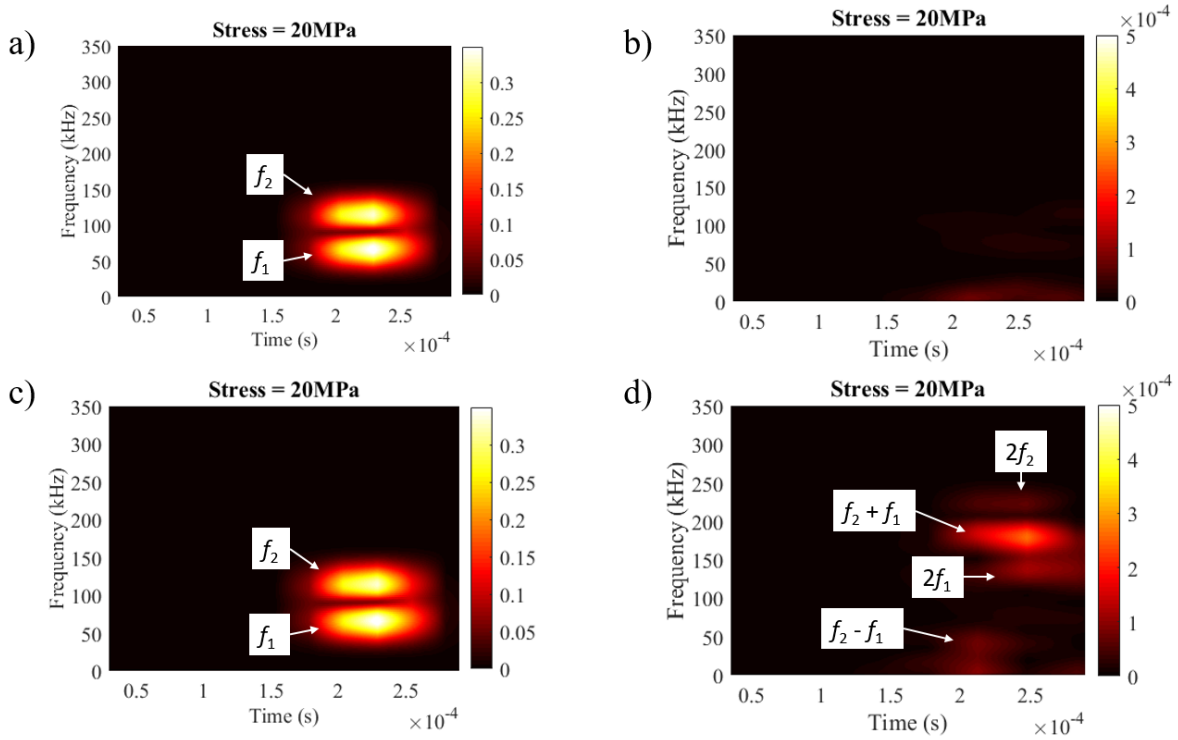

Figure 5.6 Time-frequency spectra of (a) linear torsional, (b) linear longitudinal, (c) nonlinear torsional, and (d) nonlinear longitudinal waves

Numerical simulation of guided wave-mixing in tubular structures allows separating the time-domain signal into torsional and longitudinal directions to gain better understanding in the generation of combinational harmonics. Figure 5.7 is the frequency spectra of the time-domain signals obtained by Fast Fourier Transform (FFT). The frequencies of excitation, second harmonics and combinational harmonics are indicated by vertical dotted lines. In Figure 5.7b for longitudinal motion, red dash-dot line represents linear guided wave signal, which only generates excitation frequencies at f_1 and f_2. Apart from the fundamental frequencies, blue

dashed line indicates the nonlinear guided wave response which generates second order harmonics (i.e. f_2-f_1, $2f_1$, $2f_2$ and f_2+f_1).

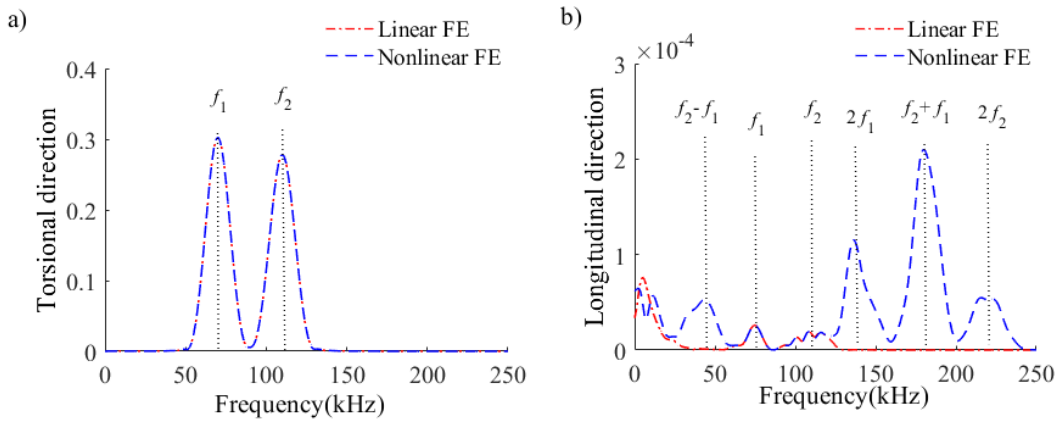

Figure 5.7 FE simulated frequency-domain signals at the mixed frequency (f_1 and f_2) subjected to 20MPa tensile stress in (a) torsional and (b) longitudinal direction

5.4 Experimental validation of acoustoelastic effect

5.4.1 Experimental setup

A 1m long aluminium tube with the same dimensions as the FE model was used in the experimental validation. Four 6 mm × 6 mm × 1 mm piezoceramic shear transducers were bonded on the surface of the tubular structure using conductive epoxy adhesive. The schematic diagram in Figure 5.8 illustrates the experimental setup. The tube was attached to the MTS machine for applying pre-stressed loading of 20 MPa before the data collection. A computer-controlled function generator (NI PIX-5412) creates a pre-mixed frequency signal at f_1 and f_2 with the same number of cycles as in the FE simulations. The selection of the low frequency excitation prevents the generation of high-order wave modes. The signal was amplified by KROHN-HITE 7500 before it was sent to the actuator. The guided wave signal was measured by the other shear transducer, which was located 450 mm away from the excitation location.

The received signal was digitised by NI PIXe-5105. Signal averaging of 500 times and sampling rate of 100 MHz were used for signal improvement.

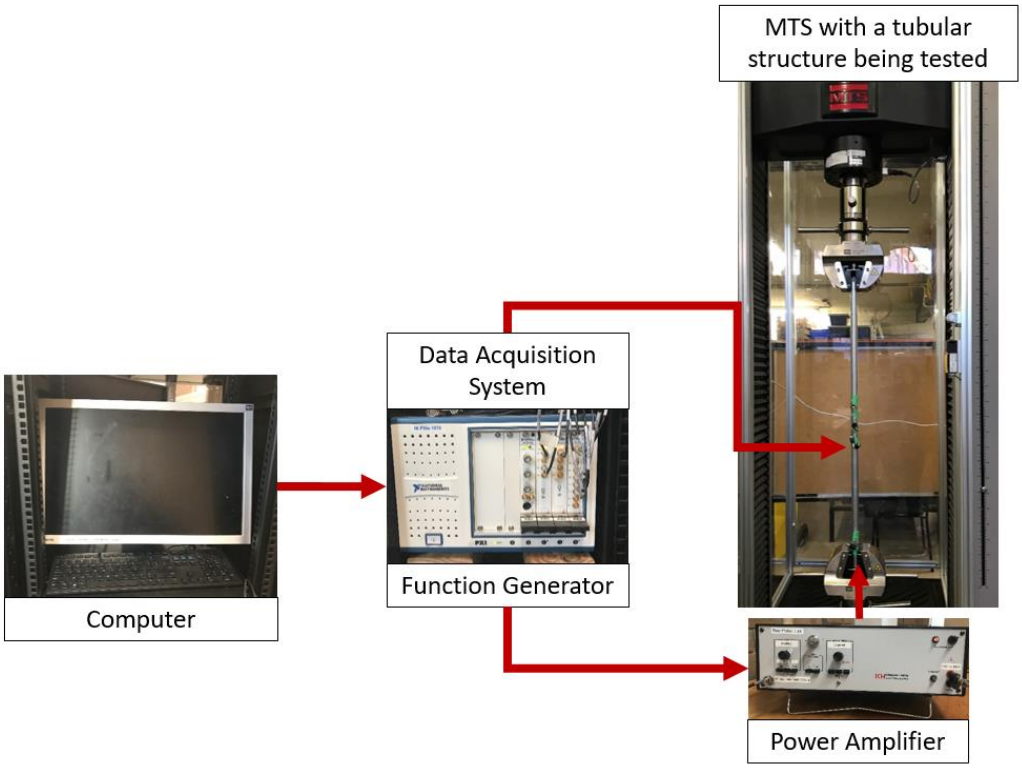

Figure 5.8 Experimental setup for guided wave-mixing with acoustoelastic effect

5.4.2 Generation of harmonics

The mixed frequency signals in both torsional and longitudinal direction were measured by the transducer. Figure 5.9 shows the normalised experimental data (blue dash-dotted line) in both directions and compares it with the FE simulated result (red dashed line). The wave signals in the FE model and the experiment have the same arrival time.

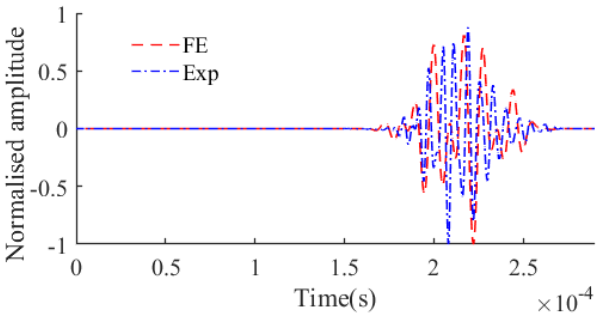

Figure 5.9 Comparison of time-domain signals between FE and experiment in torsional and longitudinal direction

Figure 5.10 compares the signals between the experimental measured data and the FE results by different harmonics (i.e. combinational harmonics at sum and difference frequencies, and second harmonics at $2f_1$ and $2f_2$), which were extracted from STFT. The pulses, which contain torsional and longitudinal motions, have a consistent decreasing trend along the normalised amplitude from the highest value for the difference frequency at f_2 - f_1 to the lowest value for the second harmonic at $2f_2$. The figure shows a good agreement between FE and experiment.

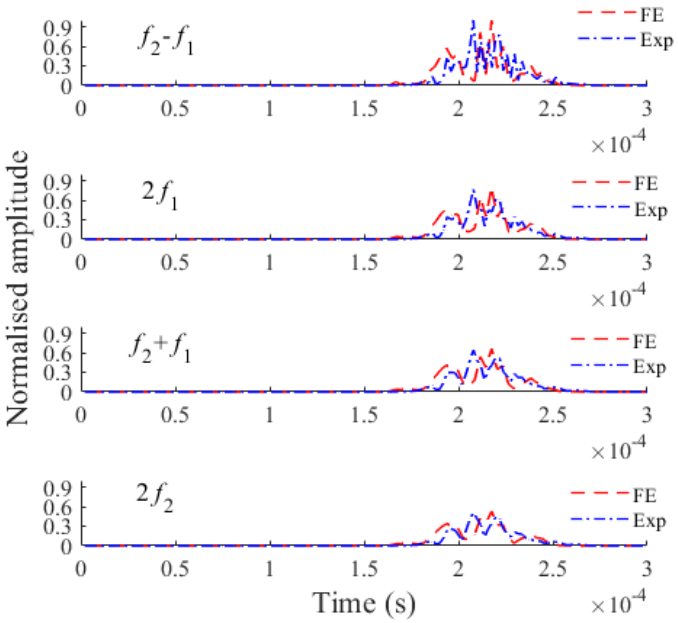

Figure 5.10 Comparison of experimental data and FE results extracted from STFT

Figure 5.11 is another comparison on the second harmonic frequencies at $2f_1$ and $2f_2$ from mixed and single excitation frequencies in longitudinal direction. They are extracted from FE results and processed by STFT. It is noted that both signals for mixed frequency provides a larger response than that for single frequency.

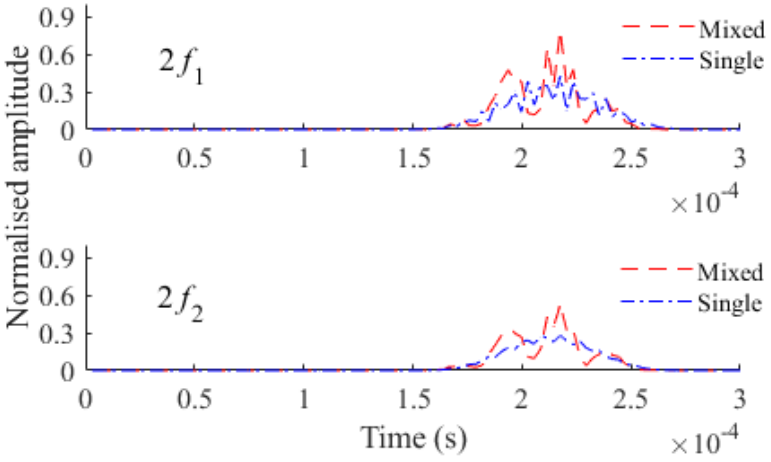

Figure 5.11 Signals of second harmonic generation from FE simulations between mixed frequency and single frequency

5.5 Performance of second and combinational harmonics

The acoustoelastic effect on guided wave mixing in tubular structures has been validated in the experimental validation section. As demonstrated, second and combinational harmonics can only be induced in the longitudinal direction. This section provides additional numerical case studies related to the harmonic generation for the better understanding guided wave-mixing in pre-stressed tubular structures. Nonlinear parameters $\beta'_{comb,mix}$ and $\beta'_{2nd,mix}$ are defined to quantify the generation of combinational and second harmonics in guided wave mixing [40]. The nonlinear parameters are defined as

$$\beta'_{comb,mix} = \frac{A_{f_1 \pm f_2}}{A_{f_1} A_{f_2}} \tag{5.13}$$

$$\beta'_{2nd,mix} = \frac{A_{2,mix}}{A_{f_1} A_{f_2}} \tag{5.14}$$

where $A_{f_1 \pm f_2}$, A_{f_1}, A_{f_2} and $A_{2,mix}$ is the amplitude of the combinational harmonics at sum and difference frequencies, the amplitude of primary frequencies at f_1 and f_2, and the amplitude of second harmonics. Figure 5.12 is the frequency response of the harmonics under different magnitudes of tensile stresses. In general, the combinational harmonic at sum frequency has the largest value throughout the whole trend. The amplitude of the sum frequency increase from stress-free state to pre-stressed state at 80 MPa. Meanwhile, the amplitude at $2f_1$ slightly decreases and the amplitudes at $2f_2$ and f_2-f_1 remain constant from 0 MPa to 80 MPa. The amplitude inconsistency is possibly due to energy re-distribution.

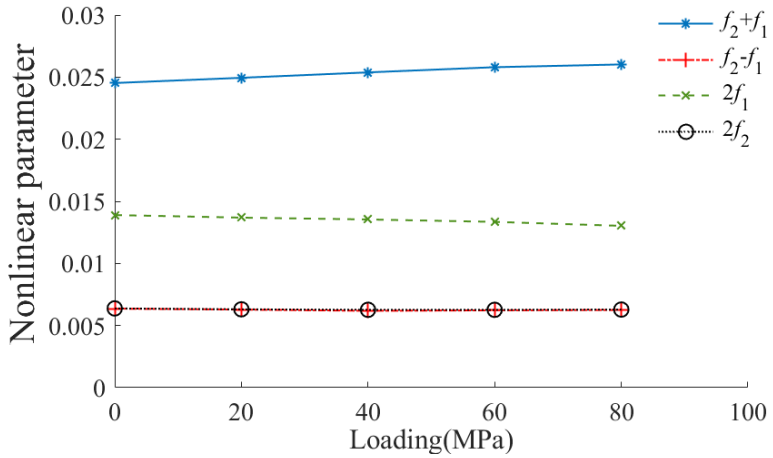

Figure 5.12 Nonlinear parameters of responses in longitudinal direction with different levels of pre-stress

The frequency at f_2 is used for excitation to confirm the energy re-distribution in wave mixing approach. This excitation frequency is one of the primary frequencies used in this study, which is the same as the five pre-stressed cases (Figure 5.13). It aims to compare the trend in terms of nonlinear parameters between the mixed frequency and the single frequency. A nonlinear parameter $\beta'_{2nd,single}$ for single frequency is defined as [40]

$$\beta'_{2nd,single} = \frac{A_{2,single}}{A_1^2} \tag{5.15}$$

where A_1 and $A_{2,single}$ represent the magnitude of the incident frequency and the corresponding second harmonic, respectively. The combinational harmonic at sum frequency (i.e. $f_1 + f_2$) shows an ascending trend line and has the most significant response among the harmonics in Figure 5.12. The frequency response at $f_1 + f_2$ induced by guided wave mixing is compared with the frequency response at $2f_2$ induced by the single frequency. While the effect of stress at single frequency purely accumulates on the second harmonic generation (i.e. $2f_2$), the value of nonlinear parameter $\beta'_{2nd,single}$ increases. Figure 5.13 verifies the claim of energy re-distribution in Figure 5.12 as $2f_2$ ascends gradually with increasing loading. The magnitude for the combinational harmonics at sum frequency is approximately ten times larger than that for the second harmonic. This demonstrates the guided wave mixing is more sensitive and rule out the undesired nonlinear signals from the equipment.

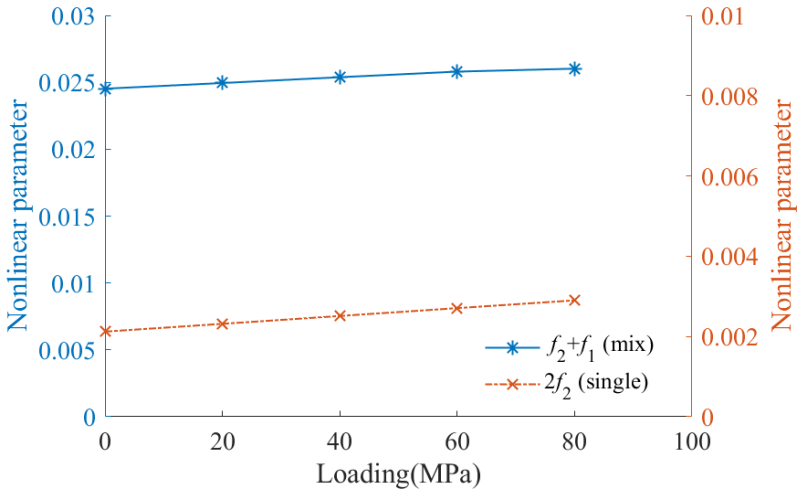

Figure 5.13 Nonlinear parameters of the combinational harmonic at sum frequency using wave mixing and second harmonic using single frequency excitation

5.6 Conclusions

This study has explored the acoustoelastic effect on torsional guided wave mixing in cylindrical structures with the aid of 3D FE models, which implemented the nonlinear strain energy function. The simulations have been carried out using the two-stage approach to model pre-stressing part and wave excitation part. The results have showed that the group velocity change in both tangential and longitudinal directions with the use of nonlinear strain energy function in the models. A series of studies considering different loading cases have been conducted and the results have shown decreasing trend in group velocity.

Linear and nonlinear simulated wave mixing signals in frequency-domain have been compared to demonstrate the generation of combinational and second harmonics in longitudinal direction due to the shear coupling effect using FFT and STFT. Experiment has been conducted to validate the FE simulation with the assigned pre-stressed load. There has been good agreement between the laboratory measurement and the FE simulation in terms of the nonlinear features.

To facilitate the use of guided wave mixing, the analysis of signals in frequency-domain have been included with different level of stresses in this study. The results in terms of nonlinear parameters indicate that the combinational harmonic at sum frequency has the most significant value compared with other induced harmonics in the longitudinal motion. Energy re-distribution happens when the amplitudes of the generation of both combinational harmonics and second harmonics do not consistently increase. While the second order harmonics at f_2-f_1 and $2f_2$ remain stable and the harmonic at $2f_1$ slightly descends, the upward trend is observed at the combinational harmonic at sum frequency. The findings are beneficial to further development on the effect of acoustoelasticity with nonlinear features in guided wave mixing.

Acknowledgement

This work was supported by the Australian Research Council through DP200102300. The support is greatly appreciated.

5.7 References

1. Cawley, P., & Alleyne, D. (1996). The use of Lamb waves for the long range inspection of large structures. *Ultrasonics*, *34*(2-5), 287-290.
2. Hughes, J. M., Vidler, J., Ng, C. T., Khanna, A., Mohabuth, M., Rose, L. F., & Kotousov, A. (2019). Comparative evaluation of in situ stress monitoring with Rayleigh waves. *Structural Health Monitoring*, *18*(1), 205-215.
3. Yeung, C., & Ng, C. T. (2019). Time-domain spectral finite element method for analysis of torsional guided waves scattering and mode conversion by cracks in pipes. *Mechanical Systems and Signal Processing*, *128*, 305-317.
4. Løvstad, A., & Cawley, P. (2011). The reflection of the fundamental torsional guided wave from multiple circular holes in pipes. *NDT & E International*, *44*(7), 553-562.
5. Pattanayak, R. K., Manogharan, P., Balasubramaniam, K., & Rajagopal, P. (2015). Low frequency axisymmetric longitudinal guided waves in eccentric annular cylinders. *The Journal of the Acoustical Society of America*, *137*(6), 3253-3262.
6. He, S., & Ng, C. T. (2017). Modelling and analysis of nonlinear guided waves interaction at a breathing crack using time-domain spectral finite element method. *Smart Materials and Structures*, *26*(8), 085002.
7. Sohn, H., Lim, H. J., DeSimio, M. P., Brown, K., & Derriso, M. (2014). Nonlinear ultrasonic wave modulation for online fatigue crack detection. *Journal of Sound and Vibration*, *333*(5), 1473-1484.
8. Soleimanpour, R., Ng, C. T., & Wang, C. H. (2017). Higher harmonic generation of guided waves at delaminations in laminated composite beams. *Structural Health Monitoring*, *16*(4), 400-417.

9. Liu, Y., Khajeh, E., Lissenden, C. J., & Rose, J. L. (2013). Interaction of torsional and longitudinal guided waves in weakly nonlinear circular cylinders. *The Journal of the Acoustical Society of America*, *133*(5), 2541-2553.
10. Deng, M., Gao, G., Xiang, Y., & Li, M. (2017). Assessment of accumulated damage in circular tubes using nonlinear circumferential guided wave approach: a feasibility study. *Ultrasonics*, *75*, 209-215.
11. Liu, Y., Khajeh, E., Lissenden, C. J., & Rose, J. L. (2013). Interaction of torsional and longitudinal guided waves in weakly nonlinear circular cylinders. *The Journal of the Acoustical Society of America*, *133*(5), 2541-2553.
12. Nikitina, N. Y., Kamyshev, A. V., & Kazachek, S. V. (2009). Application of the acoustoelasticity phenomenon in studying stress states in technological pipelines. *Russian Journal of Nondestructive Testing*, *45*(12), 861-866
13. Kamyshev, A. V., Nikitina, N. E., & Smirnov, V. A. (2010). Measurement of the residual stresses in the treads of railway wheels by the acoustoelasticity method. *Russian Journal of Nondestructive Testing*, *46*(3), 189-193
14. Li, G. Y., He, Q., Mangan, R., Xu, G., Mo, C., Luo, J., ... & Cao, Y. (2017). Guided waves in pre-stressed hyperelastic plates and tubes: Application to the ultrasound elastography of thin-walled soft materials. *Journal of the Mechanics and Physics of Solids*, *102*, 67-79.
15. Bartoli, I., Phillips, R., Coccia, S., Srivastava, A., di Scalea, F. L., Fateh, M., & Carr, G. (2010). Stress dependence of ultrasonic guided waves in rails. *Transportation research record*, *2159*(1), 91-97.
16. Albakri, M. I., Malladi, V. S., & Tarazaga, P. A. (2018). Low-frequency acoustoelastic-based stress state characterization: Theory and experimental validation. *Mechanical Systems and Signal Processing*, *112*, 417-429.
17. Murnaghan, F. D. (1937). Finite deformations of an elastic solid. *American Journal of Mathematics*, *59*(2), 235-260.
18. Biot, M. A. (1940). The influence of initial stress on elastic waves. *Journal of Applied Physics*, *11*(8), 522-530.
19. Chaki, S., & Bourse, G. (2009). Stress level measurement in prestressed steel strands using acoustoelastic effect. *Experimental Mechanics*, *49*(5), 673.
20. Dubuc, B., Ebrahimkhanlou, A., & Salamone, S. (2017). Effect of pressurization on helical guided wave energy velocity in fluid-filled pipes. *Ultrasonics*, *75*, 145-154.
21. Hirao, M., Fukuoka, H., & Hori, K. (1981). Acoustoelastic effect of Rayleigh surface wave in isotropic material. *Journal of Applied Mechanics*, *48*(1), 119-124.

22. Lu, W. Y., Peng, L. W., & Holland, S. (1998). Measurement of acoustoelastic effect of Rayleigh surface waves using laser ultrasonics. In *Review of Progress in Quantitative Nondestructive Evaluation* (pp. 1643-1648). Springer, Boston, MA.
23. Pau, A., & Lanza di Scalea, F. (2015). Nonlinear guided wave propagation in prestressed plates. *The Journal of the Acoustical Society of America*, *137*(3), 1529-1540.
24. Mohabuth, M., Kotousov, A., & Ng, C. T. (2016). Effect of uniaxial stress on the propagation of higher-order Lamb wave modes. *International Journal of Non-Linear Mechanics*, *86*, 104-111.
25. Yang, Y., Ng, C. T., Mohabuth, M., & Kotousov, A. (2019). Finite element prediction of acoustoelastic effect associated with Lamb wave propagation in pre-stressed plates. *Smart Materials and Structures*, *28*(9), 095007.
26. Yang, Y., Ng, C. T., & Kotousov, A. (2019). Second-order harmonic generation of Lamb wave in prestressed plates. *Journal of Sound and Vibration*, *460*, 114903.
27. Hasanian, M., & Lissenden, C. J. (2017). Second order harmonic guided wave mutual interactions in plate: Vector analysis, numerical simulation, and experimental results. *Journal of Applied Physics*, *122*(8), 084901.
28. Cho, H., Hasanian, M., Shan, S., & Lissenden, C. J. (2019). Nonlinear guided wave technique for localized damage detection in plates with surface-bonded sensors to receive Lamb waves generated by shear-horizontal wave mixing. *NDT & E International*, *102*, 35-46.
29. McGovern, M. E., Buttlar, W. G., & Reis, H. (2015). Estimation of oxidative ageing in asphalt concrete pavements using non-collinear wave mixing of critically-refracted longitudinal waves. *Insight-Non-Destructive Testing and Condition Monitoring*, *57*(1), 25-34.
30. Liu, M., Tang, G., Jacobs, L. J., & Qu, J. (2012). Measuring acoustic nonlinearity parameter using collinear wave mixing. *Journal of Applied Physics*, *112*(2), 024908.
31. McGovern, M. E., Buttlar, W. G., & Reis, H. (2014). Characterisation of oxidative ageing in asphalt concrete using a non-collinear ultrasonic wave mixing approach. *Insight-Non-Destructive Testing and Condition Monitoring*, *56*(7), 367-374.
32. Hasanian, M., & Lissenden, C. J. (2018). Second order ultrasonic guided wave mutual interactions in plate: Arbitrary angles, internal resonance, and finite interaction region. *Journal of Applied Physics*, *124*(16), 164904.
33. Li, F., Zhao, Y., Cao, P., & Hu, N. (2018). Mixing of ultrasonic Lamb waves in thin plates with quadratic nonlinearity. *Ultrasonics*, *87*, 33-43.

34. Shan, S., Hasanian, M., Cho, H., Lissenden, C. J., & Cheng, L. (2019). New nonlinear ultrasonic method for material characterization: Codirectional shear horizontal guided wave mixing in plate. *Ultrasonics*, *96*, 64-74.
35. Yeung, C., & Ng, C. T. (2020). Nonlinear guided wave mixing in pipes for detection of material nonlinearity. *Journal of Sound and Vibration*, *485*, 115541
36. Ogden, R. W. (2007). Incremental statics and dynamics of pre-stressed elastic materials. In *Waves in nonlinear pre-stressed materials* (pp. 1-26). Springer, Vienna.
37. Shams, M., Destrade, M., & Ogden, R. W. (2011). Initial stresses in elastic solids: constitutive laws and acoustoelasticity. *Wave Motion*, *48*(7), 552-567.
38. Murnaghan, F. D. (1951). *Finite deformation of an elastic solid*. Wiley.
39. Yang, Y., Ng, C. T., & Kotousov, A. (2018). Influence of crack opening and incident wave angle on second harmonic generation of Lamb waves. *Smart Materials and Structures*, *27*(5), 055013.
40. Croxford, A. J., Wilcox, P. D., Drinkwater, B. W., & Nagy, P. B. (2009). The use of non-collinear mixing for nonlinear ultrasonic detection of plasticity and fatigue. *The Journal of the Acoustical Society of America*, *126*(5), EL117-EL122.

Chapter 6

Conclusions

6.1 Summaries and Contributions of this thesis

This thesis has provided a comprehensive study of the linear and nonlinear phenomena of low-frequency torsional guided waves in pipe-like structures. This research commenced by introducing the importance of SHM, which can identify different types of damage due to material and geometrical changes in structures, in Chapter 1. The advantages of guided wave have been discussed over the other NDT techniques. This chapter also summarises the advantages and disadvantages of linear guided wave, nonlinear guided wave and guided wave mixing.

The first part of this research (Chapter 2) focuses on developing a model associated with macro cracks. A time-domain SFEM model with cracked element has been developed. Torsional and flexural motions are coupled in the basis of the elementary rod theory and the Timoshenko beam theory with three DoF. Guided wave scattering and mode conversion have been accurately simulated. A 3D FE model has been used to verify the model results. Experiments with different crack depth have been conducted which show accurate prediction in the series of parametric studies. The proposed 1D waveguide model significantly reduces the computational cost of simulation compared with 3D FEM modelling.

The second part of this thesis focuses on the nonlinear features of guided wave since they are potentially sensitive to small damage due to material nonlinearity. The generation of

combinational harmonics in guided wave mixing can prevent the signals from contamination by instrumentation nonlinearity. Chapter 3 evaluates the effect of guided wave mixing with two interacting torsional guided waves experimentally and numerically. Experiments using 3D scanning laser Doppler vibrometer have been carried out to measure the combinational harmonic generation at sum and difference frequencies. Murnaghan's strain energy function in nonlinear approach has been applied in a 3D FE model to validate the experimental results, which has good agreement between them.

Chapter 4 is the extension of Chapter 3 using guided wave mixing technique in buried pipes. Energy leakage can be observed from the amplitude of propagating waves. The energy dissipation of the combinational harmonic at sum frequency from mixed frequency and the second harmonic from single frequency have been compared by using experiments and 3D FE simulations. The effect of thermal aging on the corresponding harmonics shows that the combinational harmonic at sum frequency has a higher sensitivity than the others. This outcome encourages the use of guided wave mixing, especially in buried pipes.

Acoustoelastic effect in cylindrical structures is the main focus in Chapter 5. The 3D FE model, which has been utilised for simulating the effect of pre-stressed condition, is based on the development in Chapter 3. Different levels of loading have been selected to create pre-stressed condition in the hollow section. The change in group velocity has been investigated and the results have shown a velocity decreasing trend in both tangential and longitudinal motions. The generation of combinational harmonic at sum frequency has the most obvious rising trend compared with that of combinational harmonic at difference frequency and second harmonics. On the other hand, the magnitude of the frequency response at sum frequency is approximately ten times more than that of the second harmonic from a single frequency.

6.2 Recommendations

This research work has investigated the linear and nonlinear features with fundamental torsional guided wave in cylindrical structures in several scenarios. Below are the possible research directions for further studies

1. The current proposed time-domain SFEM model with a cracked element is only applicable to straight circular waveguide. The SFEM modelling can be extended to bent pipe for studying the complex guided wave effect. It is suggested to investigate the wave propagation phenomenon, particularly the local wave interaction effect at the bend region.
2. The current material nonlinearity model can simulate to second harmonic generation. However, in some situations cumulative more likely occurs in third harmonics than in second harmonics. The material subroutine used in FE model can be extended to the fourth order term in the strain energy function to simulate the generational of higher order combinational harmonics.
3. Underground pipelines usually have several layers, including insulation layer. Defects, such as debonding, can easily be created. Delamination in relation to contact nonlinearity in pipe-like structures can be investigated using wave mixing technique.
4. Water pressure inside a pipe causes the pre-stress condition. Micro cracks can be potentially induced due to hydrostatic pressure. Therefore, acoustoelastic effect with the consideration of material nonlinearity caused by fluid pressure in the pipe can be a further study.